Michigan Technological University

Michigan Technological University
Digital Commons @ Michigan Tech

Dissertations, Master's Theses and Master's Reports

2018

GENERALIZABLE MODELING OF CHARGE TRANSPORT IN SINGLE ELECTRON TRANSISTOR DEVICES: APPLICATION TO THERMAL SENSITIVITY IN SEMICONDUCTING ISLAND SYSTEMS

Paniz Khanmohammadi Hazaveh
Michigan Technological University, pkhanmoh@mtu.edu

Copyright 2018 Paniz Khanmohammadi Hazaveh

Recommended Citation

Khanmohammadi Hazaveh, Paniz, "GENERALIZABLE MODELING OF CHARGE TRANSPORT IN SINGLE ELECTRON TRANSISTOR DEVICES: APPLICATION TO THERMAL SENSITIVITY IN SEMICONDUCTING ISLAND SYSTEMS", Open Access Dissertation, Michigan Technological University, 2018.
https://digitalcommons.mtu.edu/etdr/736

Follow this and additional works at: https://digitalcommons.mtu.edu/etdr

 Part of the Electrical and Computer Engineering Commons, Engineering Physics Commons, and the Quantum Physics Commons

GENERALIZABLE MODELING OF CHARGE TRANSPORT IN SINGLE ELECTRON TRANSISTOR DEVICES: APPLICATION TO THERMAL SENSITIVITY IN SEMICONDUCTING ISLAND SYSTEMS

By

Paniz Hazaveh

A DISSERTATION

Submitted in partial fulfillment of the requirements for the degree of

DOCTOR OF PHILOSOPHY

In Electrical Engineering

MICHIGAN TECHNOLOGICAL UNIVERSITY

2018

© 2018 Paniz Hazaveh

This dissertation has been approved in partial fulfillment of the requirements for the Degree of DOCTOR OF PHILOSOPHY in Electrical Engineering.

Department of Electrical and Computer Engineering

Dissertation Co-Advisor:	*Paul L. Bergstrom*
Dissertation Co-Advisor:	*John A. Jaszczak*
Committee Member:	*Warren F. Perger*
Committee Member:	*Elena Semouchkina*
Committee Member:	*Yoke Khin Yap*
Department Chair:	*Daniel R. Fuhrmann*

Table of Contents

Acknowledgements

This work would not be completed without help of people who supported me throughout the years. First of all, I would like to my parents, Ali and Samira. And my grandparents for their tremendous support and encouragement.

My advisors Dr. Paul Bergstrom and Dr. John Jaszczak for their patience, their guidance and moral support, throughout my Ph.D. work. I would like to express my gratitude to my committee members for their guidance and technical instructions. I would like to thank the ECE department chair, Dr. Daniel Fuhrmann who supported me throughout my study at Michigan Technological University.

I would like to thank Dr. Madhusudan Savaikar and Dr. Douglas Banyai for their assistance and valuable guidance. I also would like to acknowledge the computational resources and support from the Michigan Tech's High-Performance Computing Facility (https://hpc.mtu.edu) to complete the simulations performed in this work. Superior and Portage, components of high-performance computing infrastructure at Michigan Technological University, were used in obtaining results presented in this publication.

Preface

This dissertation presents algorithm development and modeling of electron transport in different semiconducting single electron transistor (SET) devices with different material properties and geometries. The current-voltage (*IV*) characteristics of the SET models are calculated using a semi-classical approach for electron tunneling and Kinetic Monte Carlo (KMC) simulation for the dynamics. A summary of highlights of what has been done in each chapter is listed below:

Chapter 1: Introduction.

This chapter motivates the study by briefly discussing the current landscape of the development in fundamental electronics devices. The single electron transistor (SET) is introduced, and the background physics underlying its operation and simulation are reviewed.

Chapter 2: Physics-based modeling of IV characteristics of a single-island tunneling device with a semiconducting island.

- A generalizable model for calculating tunneling rates between semiconductor or metallic elements of a SET device is presented and the KMC simulation utilized is summarized.
- The transition probability between metallic and semiconducting islands is dynamically calculated depending on the initial energy of the electron and the barrier height.
- A model density of states (DOS) of a semiconducting quantum dot, including a modified-parabolic band model and a band gap is introduced.

- Island size and energy scales, in which the continuous band model for the semiconducting island can be used, are explored. In particular, the appropriateness of discrete versus continuous DOS models is discussed based on island size.
- Using relevant approximations, tunneling rates between a semiconductor quantum dot and metallic or semiconducting electrodes, considering the energy gap in semiconductor, are calculated, and *IV* characteristics are explored for the following types of systems, including several test cases:
    - Test Case I: Coulomb staircase of a SET device with metallic electrodes and a semiconducting island
    - Test Case II: Impact of gate capacitance on IV_g characteristics on a SET device with metallic electrodes and a semiconducting island
    - Test Case III: Impact of junction widths on IV_g Characteristics on a SET device with metallic electrodes and as semiconducting Island
    - Temperature dependence: metallic electrodes and a semiconducting island
    - Semiconducting electrodes and semiconducting island
    - Temperature dependence: semiconducting electrodes and a semiconducting island
    - Impact of band gap

Chapter 3: Efficient Physics-based Modeling of a Representative Semiconducting Quantum Dot Single Electron Device

The content of this chapter has been published as a conference proceedings paper and is used with permission: P. Hazaveh, P. L. Bergstrom, and J. A. Jaszczak. "Efficient physics-based modeling of a representative semiconducting quantum dot single electron device," *IEEE 17th International Conference on Nanotechnology (IEEE NANO 2017)*, pp. 739 – 744, 2017.

- In this model, the band gap is utilized to control the temperature sensitivity of the SET devices by applying appropriate bias to the gate electrode.
- Simulation results are compared to results for an experimental device. The device appears to be a nanometer-scaled MOSFET with quantum dots formed in the channel. An explanation is proposed for the experimentally observed baseline current increase along with Coulomb oscillations in the *IV* characteristic of the experimentally realized nanometer-scale MOSFET.

Chapter 4: is focused on physics based modeling of IV characteristic for a single-island tunneling device with semiconducting island with discrete energy levels.

- This SET model has an island small enough that the discrete energy-level spacings are comparable to other energy scales of the system and cannot be ignored.
- The tunneling rate between a semiconductor quantum dot island with discrete energy levels and a band gap coupled to metallic or semiconducting electrodes is calculated.
- The transition probability between metallic/semiconducting islands is dynamically calculated depending on the initial energy of the electron and the barrier height.
- The density of states (DOS) of a semiconducting quantum dot used as an island is more complicated than a metallic nanometer-sized island, especially in higher energy levels. Here, a proper modified-parabolic approximation is introduced. Island size and energy scales, in which the energy spacing between discrete levels cannot be ignored, is explored.

Chapter 5: Modeling of IV characteristics of a double-island tunneling device with semiconductor islands.

Some figures and text in this chapter are reprinted, with permission from: P. K. Hazaveh, P. L. Bergstrom, and J. A. Jaszczak, "Modeling of gate effects on electron transport in a single-electron transistor with two semiconducting islands between two semiconducting electrodes," *Proceedings of the IEEE 13th Nano Materials and Devices Conference (IEEE NMDC 2018),* pp. 459 – 462, 2018.

- A modified-parabolic approximation is utilized in the DOS. It is discussed that in consideration of all the relevant energy scales in our model, if the island size is larger than ~3 nm, it is appropriate to neglect the discrete energy levels, whereas if the island size is smaller than ~3 nm, the discrete nature of energy levels should be accounted for. Two different simple band models are explored:
    1. SET device with semiconducting islands large enough that the discrete energy levels can be ignored compared to other energy scales of the system. The continuous band model is used for such a device.
    2. SET device, where one of the islands is small enough that the energy spacing between energy levels is comparable to other energy scales of the model and cannot be ignored.
- The transition probability between two semiconducting materials is dynamically calculated depending on the initial energy of the electron and the barrier height.
- The tunneling rated between two semiconducting islands and electrodes are calculated, considering the energy gap in the semiconductors.

- The impact of discrete energy levels in smaller semiconducting islands on the *IV* characteristics of semiconducting SET devices is explored.
- The effect of gate capacitance and gate potential on *IV* characteristic of semiconducting SET devices is studied.
- The band gap and discrete energy levels are utilized to control the degree of temperature sensitivity of the SET devices by applying appropriate biases to the gate electrode.

Abstract

Electronic devices, especially MOSFETs, have been dimensionally scaled down to enhance operation of integrated circuits, addressing challenges such as current leakage, fluctuation of intrinsic semiconductor properties, and power dissipation. Reaching dimensions below 20 nm, there are fundamental limitations that are difficult to overcome, driving alternative device paradigms to be sought utilizing the quantum mechanical behavior of electrons. Single electron transistor (SET) devices are examples of a new generation of low-power transistors designed to transport information via single electron tunneling through one or more islands separated by tunnel junctions. Experimentally explored SET devices have shown that there are advantages to using semiconductors for the islands as compared to using metallic islands. Although semiconducting SET devices have been experimentally explored, the simulation of the transport characteristics of such devices remains an area requiring further development for gaining deeper insights into the device behavior. Progress has been limited due to the complexity of the underlying physics of electron tunneling to and from a semiconducting nanometer-scale island. Ab initio calculations are capable of accurate modeling of the physics, but are computationally prohibitive given the nanometer scales represented in the system.

This work is dedicated to understanding the behavior of electron transport involving semiconducting islands and has led to development of a kinetic Monte Carlo (KMC)-based algorithm to simulate the current-voltage characteristics of single electron transistor (SET) devices comprised of one or two semiconducting nanometer-scale islands and three electrodes (source, drain and gate) with regard to the terminal potentials, temperature. The

impact of the band gap, the more complex density of states, charging energy, and island-size-dependent discreteness of energy levels in a semiconducting island on the tunneling rate are also examined.

Semiconducting islands provide parameters that can be utilized to control the SET characteristics. The alignment of the semiconducting island's band gap with the Fermi energy of the electrodes can be tuned to control the degree of temperature's impact on the currant-voltage characteristics of the device. It is confirmed in this work that our model is generalizable to predict electron tunneling in materials with different band structure.

1 Introduction

Improvement of electronic device technology depends on portability, power consumption, system complexity, and cost efficiency of integrated circuits (ICs). As the size of the transistors decreases, the number of transistors that can be fit on ICs increases (see, for example [1]) . As the ICs get smaller and more energy efficient, and the technologies becomes more powerful and inexpensive, innovative and energy-efficient technologies have increasingly been entering peoples' everyday lives [2].

Moore's law was "discovered" by Gordon Moore, co-founder of Intel in 1965, by observing the trend every year the number of transistors in an integrated circuit doubles [3]. He revisited this law in 1975 and revised the statement that roughly every 18 months the transistor density doubles in integrated circuits. This has proven to predict the advancement of technology in microelectronics for many years, nearly up to the present; perhaps longer than many expected that it could be sustained [4]. More recently, the rate of increase in transistor density has slowed, starting when the minimum features of the transistors reached 20 nm [4].

Metal Oxide Semiconductor Field Effect Transistors (MOSFETs) are the main components used in the IC industry [5]. For decades now, electronic devices, especially MOSFETs, have been dimensionally scaled to enhance the speed and optimize power consumption of ICs [6]. Scaling down MOSFETs to nanometer-scale dimensions has faced some major problems and limitations over the years. Some of these limitations have been solved by materials engineering and new fabrication techniques. Reaching the scale of 20 nm, there are fundamental limitations, which are extraordinarily expensive or reaching fundamental limits to solve [7, 8], such as current leakage, electron tunneling between

different layers of MOSFET, fluctuation of intrinsic semiconductor properties and power dissipation. In small dimensions where quantum mechanical behavior begins to dominate device characteristics near room temperature, the understanding of the transport of carriers across junctions in quantum-electronic tunneling-based structures becomes yet more important to the ongoing development of the electronics industry. This has caused engineers to think of alternative devices that explicitly utilize the quantum-mechanical behavior of small devices, as opposed to trying to mitigate such behavior. Engineers and experimental physicists have been exploring small junction devices where adding and removing one single electron to or from the system can be detected and controlled. Single-electron devices and single-electron transistor (SET) are in this category of devices, and are candidates for a new generation of low power transistors designed to transport information via single electron tunneling through insulating junctions [9, 10].

There are several practical applications of SET devices, for example they can be used for switching in multiple level logic gates. The Coulomb blockade region is larger in SET devices with multiple islands compares to single island devices (larger source drain threshold), which makes them a great candidate for switching components. Karre et al. [11] demonstrated a Coulomb blockade effect and Coulomb oscillations at room temperature in a multi-island transport device using nanometer-size tungsten dots with a mean diameter of 8 nm. Extra charge present on the quantum-dot island in a SET has a strong impact on $I_d V_g$ characteristics of the SET, therefore these devices can be used as sensitive electrometer devices [10]. Other examples of what can be designed using SET devices include single electron memory devices [12], charge-state logic and programmable single-

electron transistor logic [13], photon sensors [14], and chemical and gas sensors [15]. Some of the more recent applications of SET devices as biosensors are:

1- **pH sensor**: Because SET devices are highly sensitive to small changes in the potential energy state of the control gate, changing the surface charge state through chemical binding events on the gate electrode, for example, the SET can act as an electrometer amplifying the chemical state of the gate electrode. If the gate electrode is in contact with a buffer solution, the I_dV_g characteristics of the device change depending on the pH value of the solution, making SET devices potentially useful as pH sensors [16, 17].

2- **Detection of Streptavidin**: Streptavidin is a protein commonly utilized in the detection of various biomolecules due to its formation of a strong bond with biotin and its resulting functionalization on a metallic or semiconducting electrode for biosensing. This type of sensor is commonly prepared by coupling the biotin to the surface of a gate insulator for a transistor-like sensing mechanism. The reaction of streptavidin to the biotinylated surface causes a positive shift in the I_dV_g characteristics of a SET device [17] that enables the detection of a charge change as a result of biomolecule binding events.

1.1 Metallic Devices

Single electron transistors are one of the candidates as an alternative to conventional transistors. These devices have low power consumption, small dimensions of 50 nm and below, and a fundamentally different transport mechanism that can result in fast response times and allows a potentially higher density of components on ICs [18]. Unlike traditional

transistors, SET devices work based on electron tunneling through insulating layers. The devices are comprised of metallic or semiconducting islands between source and drain electrodes, and separated by thin insulating barriers. If an electron has enough energy, it may tunnel from one island to the next, till it reaches the other electrode [10].

A simple single electron transistor has three electrodes, and in its simplest form, a single nanometer-sized metallic island, as shown in Fig. 1.1 The island is coupled to the electrodes via capacitances. The tunnel junctions have widths on the order of couple of nanometers. Ideally, there should be no electron tunneling to the gate electrode.

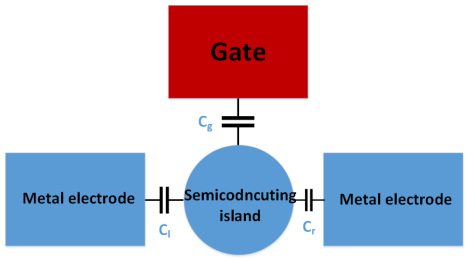

Figure 1.1. Schematic of a SET device with two tunnel junctions, one island and three electrodes. The island couples to the left, right and gate electrodes with capacitances C_l, C_r and C_g, respectively.

Simulating SET devices has been investigated in previous research. The SPICE macro modeling code, for example, utilizes a circuit model of the system built with resistances and capacitances [19]. The governing parameters of the modeled SET devices are defined prior to the circuit analysis of the devices using a physics-based simulation method (such as kinetic Monte Carlo) and the current-voltage characteristic of the device consisting of multiple transistors (typically single island SETs) then depends on the pre-determined parameters and terminal voltages of each transistors. In this model, the coupling between SET devices in series is neglected, which at nanometer dimensions may not be valid [20].

The SPICE macro-modeling can handle more than one SET device, but the interaction between the devices and the Coulomb blockade effect is not taken into account, making the application of the SPICE macro-modeling tool very limited.

Predicting the *IV c*haracteristic of metallic SET devices based on the so-called "orthodox theory" and electron tunneling rates can be performed with methods such as the Master Equation method [21, 22] or the kinetic Monte Carlo (KMC) simulation method [23]. The Master Equation method utilizes a matrix of transition probabilities multiplied into a vector of state occupancies to compute the net currents passing through the junctions. However, since the number of possible transitions and states is infinite, the most important ones must be identified, depending on energy scales of the system, to iteratively solve for the steady state solution of the charge and current transport. This method has been used widely in the past for two-junction (one island) systems; however, in case of more than two junctions in a system (multiple islands), the complexity of the Master Equation method becomes inefficient if the number of possible states makes the matrix too large [22]. The KMC method is more effective in balancing the model of complex transport configurations with efficient computational methodology [22, 24].

The MITS program is a KMC-based algorithm developed by Savaikar et al. [23, 25], that extended the capability of other KMC-based algorithms, such as SIMON [26, 27] and MOSES [22], by reconsidering some of the model's approximations. However, MITS is not applicable to semiconducting materials, as it employed many approximations that are only appropriate for metallic islands and electrodes. For example, the transition probability of a junction in MITS is calculated using approximations: 1. The initial energy of all electrons is taken to be at the Fermi energy, and 2. The density of states is continuous (no

band gap) and a constant. In a semiconducting SET these approximation are not appropriate. The work of this dissertation focuses on extending the capability of MITS by taking into account the key features of a semiconductor, namely, density of states, the band gap, and important energy dependence characteristics near the band edges. As may be expected for semiconductors, their presence in SET devices can be expected to have important temperature-dependent effects as compared to metals. In addition, this work explores the conditions and energy scales under which the discreteness of energy levels in very small islands cannot be ignored.

Charge transport in an SET occurs via electron tunneling through the junctions connecting the source and drain electrodes. Predicting the *IV* characteristic of metallic SET devices has been done using a semi-classical approach starting with the assumptions of the so-called "orthodox theory" and appropriate extensions to calculate tunneling rates. Orthodox theory has three major assumptions [10]:

1. The time for electron tunneling across the barrier is negligibly small compared to the time between electron tunneling events.
2. For a system with junction resistances bigger than 6.5 kΩ, co-tunneling can be ignored.
3. The quantization of energy is ignored in the island.

There are typically other approximations that are employed in studies of models with metallic islands, such as a constant density of states and energy-independent transition probabilities, which will be discussed in detail in this section.

If a total excess charge Q is on an island, an extra electron to be added to the island will be repulsed by this net charge. The charging energy (E_{ch}), which is fundamental to the operation of SET devices, is a measure of this repulsion [10], and can be calculated using

the expression

$$E_{ch} = \frac{e^2}{C}\ , \tag{1.1}$$

where C is the island's total capacitance and e is the magnitude of the electron charge.

The single-electron effects are observed as long as the charging energies are much larger than the thermal energy ($E_{ch} > 10k_BT$, where T is the temperature and k_B is the Boltzmann constant). In relatively large islands, the charging energy is negligible at room temperature. However, for nanometer-sized devices (10 nm and less), the charging energies are in order of 0.1 eV, and are comparable to other energy scales in the system for example, the thermal energy at room temperature, so the single-electron effects can be observed [10, 25].

1.1.1 Coulomb Blockade, Coulomb Staircase, and Coulomb Oscillations

Two key features of IV characteristics of SET devices are the so-called Coulomb blockade (and the associated Coulomb staircase) and Coulomb oscillations. For an electron to tunnel through a junction it must have enough energy to overcome the charging energy, otherwise it will be prohibited from tunneling. If the applied source-drain potential, V_{sd}, is inadequate to supply electrons enough energy to overcome the charging energy, tunneling and current flow are this suppressed. This phenomenon is called the Coulomb blockade effect. Figure 1.2 shows a simple schematic of the blockade condition. External energy sources such as, applied biases, (gate or source-drain) or thermal energy can allow electron tunneling by giving electron enough energy to overcome the charging energy [10, 25]. In SET devices at room temperature, the tunnel junction dimensions should be less than 2 nm, in order to balance having a large charging energy with sufficiently high tunneling

probability. Due to large charging energies in these small junctions, relatively large V_{sd} bias potentials on the order of 0.1-1 V are necessary to allow electron tunneling events. The voltage at which electron tunneling is probable through the device and current is non-zero, is known as threshold voltage. In the Coulomb blockade region (where V_{sd} is less than the threshold voltage) modulation of the gate potential can also enable electron tunneling between source and drain. This phenomenon leads to Coulomb oscillations and will be discussed below. We first consider the Coulomb staircase.

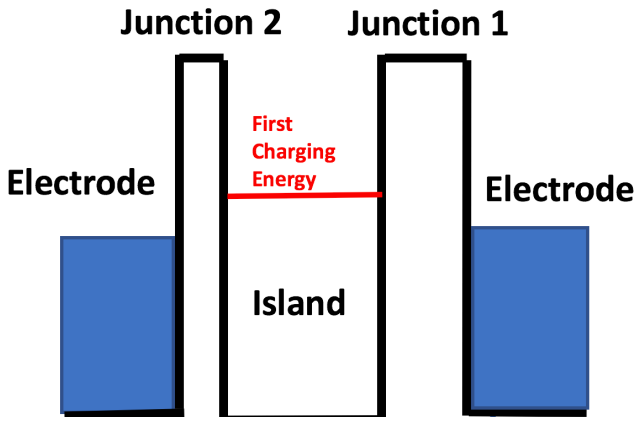

Figure 1.2. Blockade condition under zero bias and low temperatures where electrons up to the Fermi energy of the electrodes do not have enough energy to overcome the charging energy to tunnel to the island.

To understand the Coulomb staircase, consider a simple model of a single island device, in which the island is isolated from the source and drain electrodes by an insulating layer (for example, an oxide), that are called tunnel junctions. The transition probability for an electron to tunnel across a junction depends on properties of the junction and the electron's energy. Consider a condition under which the transition probability through junction 1 is much smaller than the transition probability through junction 2 (*i.e.*, $T_1 \ll T_2$). Such would

be the case, for example, if the width of junction 1 was greater than that of junction 2. A source-drain bias (V_{sd}) applied to this device causes a potential drop across both junctions. If, based on the capacitances it turns out that $V_{sd.,}$ becomes large enough (which by definition is the source-drain threshold voltage) that electrons can overcome charging energy in junction 2, then tunneling can take place in this junction. Under this condition, after electron tunneling happens in junction 2, the potential of the island changes because of the missing electron so electron tunneling may become favorable in junction 1. However, since $T_1 \ll T_2$ tunneling will occur in much lower rate in junction 1 as compared to junction 2. In this case, junction 1 is the rate limiting factor that sets the current magnitude. No qualitative change happens as V_{sd} is increased until it reaches a point at which electrons can overcome the second changing energy in junction 2. Now there will be current pathways across the device that include this island having charge states of zero and +e, as well as some current pathways that have the island in charge states +e and +2e. The abrupt addition of another current pathway in charge-state phase space (or current paths for short), lead to the second step of the Coulomb staircase. Its position in terms of V_{sd} depends on the charging energy, while the current magnitude depends on the tunneling rates of the junctions at the applied bias. This phenomenon, which is shown in Fig. 1.3 with a simple energy-diagram model, leads to the Coulomb staircase in the IV_{sd} characteristic of the device [25, 28, 29]. In this figure, the left electrode is connected to positive voltage.

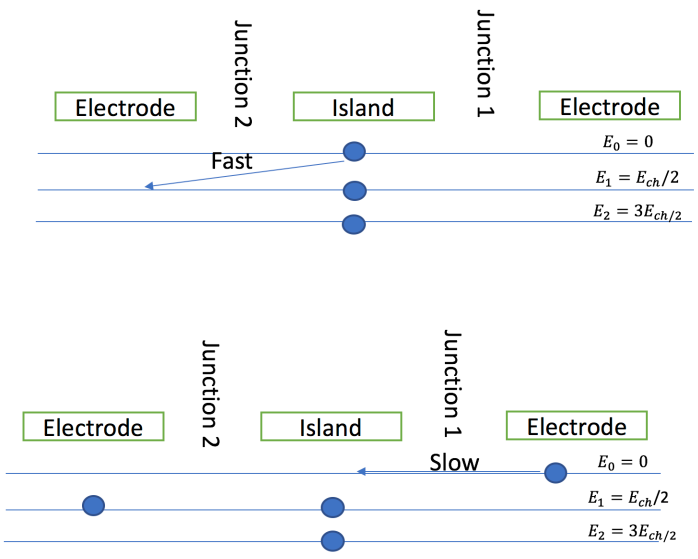

Figure 1.3. Energy diagram of electron tunneling through a SET with a single island where the electron transmission rate is larger in junction 2 than junction 1.

The Coulomb-oscillation phenomenon appears in the current versus gate voltage characteristic [28, 29]. In a single-island device with a gate electrode, under constant and small source-drain bias condition the potential of the island changes by increasing the gate voltage. Upon increasing the gate voltage there will come a point at which electrons will have enough energy to overcome the charging energy at junction 1. The increased potential bias across junction 2 makes subsequent tunneling highly probable at that junction, leading to a net current flow across the device as it is outlined in Fig 1.4 (top). By increasing the gate voltage further, subsequent tunneling across junction 2 decreases due to misalignment of the island's occupied levels with available levels in the left electrode (Fig 1.4. middle). At this point electron tunneling is blocked in junction 1 as well until the gate bias is increased sufficiently to overcome the second charging energy of the island (Fig. 1.4 bottom). At this gate potential the second gate oscillation is observed in the characteristic.

This phenomena repeats further and leads to a periodic variation in source-drain current [30]. This periodic behavior in the current versus gate potential is called the Coulomb oscillation effect. The periodicity in a SET device with a single island can be calculated by:

$$\Delta V_g = \frac{e^2}{C_g}, \tag{1.2}$$

where C_g, is the gate capacitance, and e is the magnitude of the electron charge [29, 30].

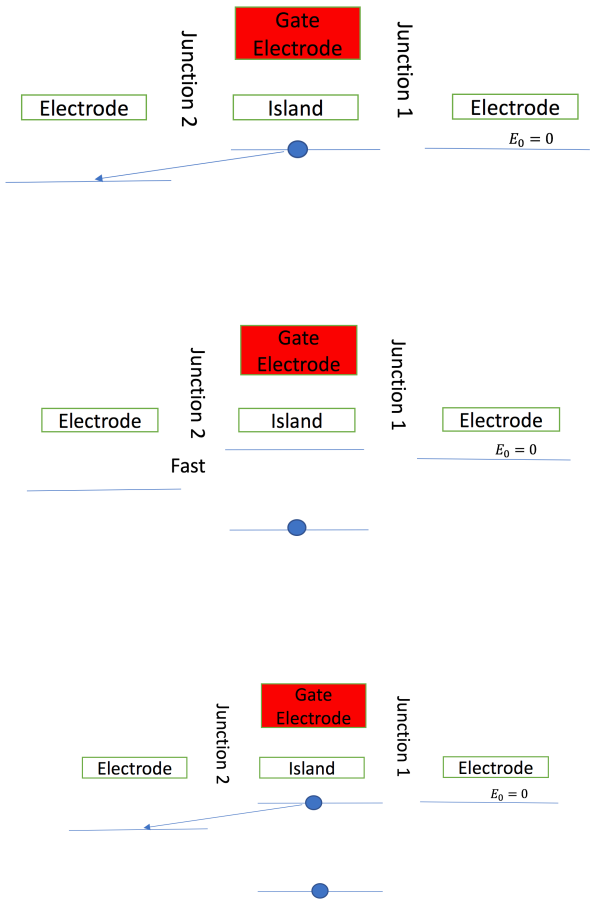

Figure 1.4. Energy diagram of electron tunneling through a SET with a single island where the gate voltage is increasing.

1.1.2 Tunneling Rate

Following work of Savaikar et al. [25], Wasshuber et al. [26, 27] and Amman et al. [31], the general tunneling rate expression inspired by the Fermi golden rule is used in our study. The tunneling rate for an electron across a junction from the initial side with Fermi energy E_i, to the final side with Fermi energy E_f, can be written as [23, 25, 31]:

$$\Gamma_{if} = \int_{-\infty}^{+\infty} \frac{2\pi}{\hbar} |T(E)|^2 D_i(E - E_i) f(E - E_i) D_f\left(E - E_f\right) \times \left[1 - f\left(E - E_f\right)\right] dE \ , \tag{1.3}$$

where

$$f(E) = \left[\exp\left(\frac{E}{k_B T} \right) + 1 \right]^{-1} \tag{1.4}$$

is the Fermi distribution function, E is the electron's energy and $T(E)$ is the tunneling probability. $T(E)$ depends on the electron's effective mass and the properties of the tunneling barrier, such as its shape, width and height [9, 10, 23, 25, 32], and D_i and D_f are the density of states functions in the respective initial and final sides of the barrier. The Fermi function $f(E - E_i)$ gives the probability of the initial state to be occupied with an electron, while $[1 - f(E - E_f)]$ gives the probability of the final state being empty. To calculate the tunneling rate in devices with semiconductor islands, it is the goal of this study to calculate the tunneling rates using appropriate approximations and models for the tunneling probabilities and density-of-states functions, and to explore the subsequent dynamics. In models such as SIMON and MITS for metallic-island devices, several

approximations were used that are appropriate for metal-metal junctions, as outlined below, and which allows for a closed-form solution for this integral.

Following work of Savaikar et al. [23, 25] transition probability across a junction, depends on properties of the junction and initial tunneling energy level. When there is a potential difference across the junction (V_{if}), the barrier height varies over the width of the barrier as shown in Fig. 1.5. If the work functions are much greater than the potential difference across the junction, a constant average value can be used as the height of the barrier. The effect of this approximation has been examined and does not affect the outcome of the algorithm, while it improves the computational time efficiency [23, 25, 33]. A simple model for an electron transition from a metallic island to an electrode is shown in Fig. 1.5. The red arrow denotes the average barrier height *(V_0)* of the trapezoidal energy barrier, d is the junction width and ϕ is the work function of the metals [25, 26, 27].

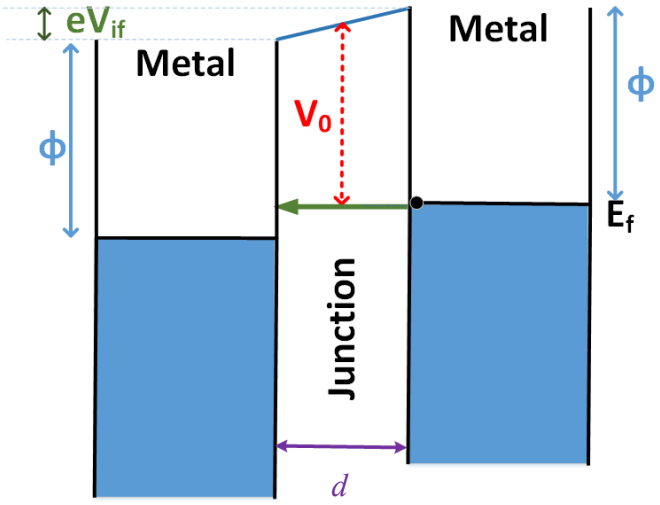

Figure 1.5. Electron tunneling from the middle island (right) to the left electrode when there is a potential difference of V_{if} across the junction. Φ is the work function. The green arrow shows the electron tunneling direction. The blue line denotes the trapezoidal barrier height over the left junction of width (d). The red arrow denotes the average barrier height.

To capture the essential physics we use the well-known results for the model of electron tunneling through a one-dimensional rectangular potential barrier [32]. If the average barrier height is V_o, the probability of the particle being transmitted through the barrier is given by [25, 26, 27]:

$$|T(E)|^2 = \left[1 + \frac{V_0^2 \sinh^2(k_1 d)}{4E(V_0 - E)}\right]^{-1}, \tag{1.5}$$

and

$$k_1 = \frac{\sqrt{2m(V_0 - E)}}{}, \tag{1.6}$$

where E is the electron's energy, V_0 is the barrier height, m is the particle's effective mass, and d is the barrier width. In most prior work the energy of the tunneling electrons are taken to be near the Fermi energy with the simplification that the transition probability is $|T|^2 \sim |T(E_f)|^2$ (note that $|T|^2$ is a function of V_0 which in MITS changes dynamically depending on the potential across the junction.)

For SET devices with more than one island the transition probabilities initiating from metallic materials will be approximated as $|T|^2 \sim |T(E_f)|^2$. In case of SET devices with semiconducting islands the transition probability is approximated depending on the band (conductance and valence) where the tunneling is initiating from and will be explained in details in next chapters.

In metals, the density states of electrons is typically approximated using the free-electron model [34, 35]:

$$D(E) = \left(\frac{8\pi m^{\frac{3}{2}}}{\hbar^3}\right)\sqrt{E}\,, \tag{1.7}$$

where m the electron mass, E is the energy of the electron and $\hbar$ is the reduced Planck constant. In the majority of previous simulation studies, such as the SIMON code by Wasshuber et al. [26, 27] or the MITS algorithm developed by Savaikar et al. [23, 25], the density of states function in (1.7) of the metal electrodes and island are approximated as a constant $D_0 = D(E_f)$, which is the density of states at the Fermi energy [23, 25, 27]. This is satisfactory for simulation of the electron transport in metals since the participating carriers and available states are positioned energetically near the Fermi energy. The density of states in semiconducting materials, however, is not well approximated as a constant, and instead is modeled using a modified parabolic energy-dependent expression, which will be detailed and explored in subsequent chapters.

1.1.3 MITS: KMC based Simulation of Current-Voltage Characteristics of SET Devices

In a single island SET device, the drain is connected to the ground-reference potential, while the gate, and source potentials can be varied. All of the electrodes and the island (or in some cases islands) are coupled via capacitances (Fig. 1.1). In a SET device with one island, under gate and source biases the island's charge state can be written as equation below [25, 31]:

$$Q_m = -ne = C_r(V_m - V_r) + C_l(V_m - V_l) + C_g(V_m - V_g), \tag{1.8}$$

where C_r, C_l and C_g are the right junction capacitance, left junction capacitance and the gate capacitance respectively. V_r , V_l and V_g are the right electrode, left electrode and the gate electrode potentials. V_m is the potential of the island and can be derived as:

$$V_m = \frac{C_l V_l + C_r V_r + C_g V_g - ne}{C_r + C_l + C_g}. \tag{1.9}$$

The potential drop across the middle island (*m*) and left junction (*l*) is given by [25]:

$$V_m = \frac{(C_g + C_r)V_l - C_g V_g + ne}{C_r + C_l + C_g}, \tag{1.10}$$

where *n* is the number of extra electrons on the island. (Note: In this discussion, we are assuming the background charge is zero on the island). In SET devices with more than one island, the charges and potentials are conveniently related by the Maxwell capacitance matrix $\boldsymbol{C}$ according to $\boldsymbol{Q} = \boldsymbol{CV}$, where $\boldsymbol{Q}$ is a vector of island charges, and $\boldsymbol{V}$ is the vector of potentials [33, 36]. The diagonal elements (C_{ii}) are the sum of all capacitances coupled to island *i*, and the off-diagonal elements are negative of the junction capacitances. The capacitances and electrode potentials are all known, while the island potentials are unknown variables that are recalculated after each tunneling event which determines the charge state $\boldsymbol{Q}$ of the system. When an electron tunnels from the middle island "*m*" to the left electrode "*l*", the change in the free energy is given by equation:

$$\Delta W_{ml} = -eV_{ml} + E_{ch} \ , \tag{1.11}$$

where

$$V_{ml} = V_l - V_m \ , \tag{1.12}$$

V_m is the island's potential, V_l is the left electrode's potential and E_{ch} is the charging energy. We consider the time for relaxation of the extra electron to be insignificant compared to the tunneling time and the time between tunneling, so the electron will relax before the

next tunneling event takes place. The geometry of the system, including junction widths and island radii are inputs to this algorithm as are external factors such as temperature and bias voltages. The capacitances can be entered as fixed values or be calculated based on the fixed physical geometry of the system [23, 25, 36]. Since the emphasis of this work is not on geometrical impacts, for simplicity fixed capacitances are assigned to the junctions and the charging energies are calculated based on the capacitances for every junction. If there is more than one island, then the islands' potentials are specified with expressions similar to (1.9), and calculated using the capacitance matrix and the input electrode voltage and the island charge state [23, 25, 27, 36]. In some of the presented work, the capacitance matrix is build using the specific capacitances as presented in the experimental works. If the capacitances are unknown, a simulation tool developed by Banyai that is compatible with our code, can be utilized to calculate matrix capacitances based on geometry of the islands and junctions [23, 36]. This can extend the capability of our simulation tool in the future.

The source and drain potentials are initially taken to be at zero potential. In order to compute the *IV* characteristic, the varying source or gate potential is increased stepwise with a typical increment of 0.01 V. At each voltage step and charge state, tunneling rates are computed and the kinetic Monte Carlo method, as implemented by Savaikar et al. [23, 25], is used to select tunneling events based on these rates. The source-drain current is calculated as the rate that charge reaches the drain electrode. After each tunneling event, the system's charge state, potentials and tunneling rates are updated. The simulation continues until a steady state current reached with satisfactory accuracy (error bars less than 2% of the mean value) [23, 25]. The simulation process flow for this simulation is

given in Fig. 1.6

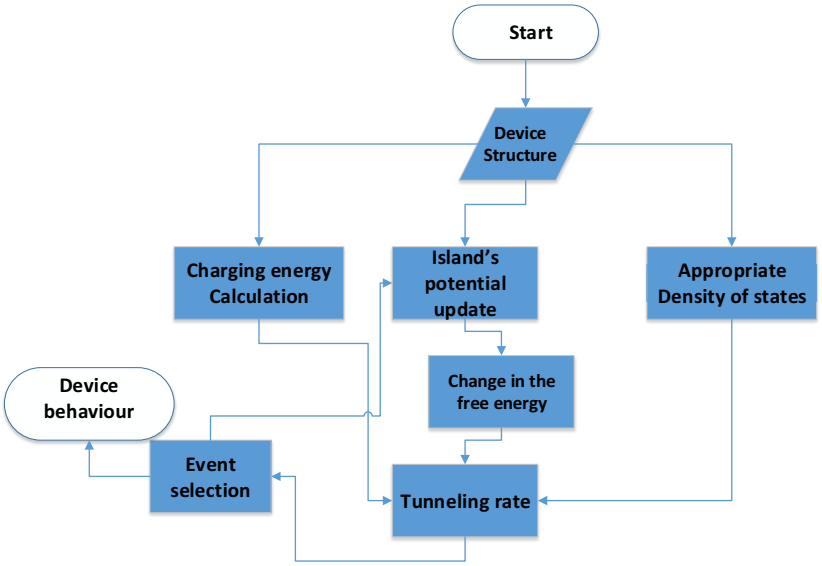

Figure 1.6. Simulation flow diagram of the algorithm used by Savaikar et al. [23] to study the current-voltage (*IV*) characteristic of a system with metallic electrodes and metallic island(s), using kinetic Monte Carlo.

1.2 Metallic versus Semiconducting SET Devices

SET devices have been fabricated using various metallic and semiconductor materials [11, 37-41]. Comparing the functionality of semiconductor and metallic SET devices in several experimental works, shows some unique properties of semiconducting SET. For example, in higher temperature the functionality of SET devices could decrease due to available thermally excited electrons for tunneling. These thermally excited electrons can be filtered using a semiconducting quantum dot [39]. The investigation performed by Acharya [41], shows that the gate controllability in metallic SET devices must improve in order for the device to be useful as a three-terminal electronic device. This work demonstrates improvement of the gate control over the *IV* characteristic of the device,

utilizing silicon semiconductor islands instead of metallic. Experimentally explored semiconducting SET devices, also have shown clearer peak oscillations in IV_g characteristic of the device [38]. In such devices, the height of the peaks is observable and measurable as compared to metallic SET devices in which the Coulomb oscillations at room temperature are complicated and non-measurable.

The energy gap in semiconductor's band structures can be used to control the functionality and behavior of the device in different energy scales. The band gap will also complicate the physics of electron tunneling between semiconducting materials. This dissertation focuses primarily on the study of the *IV* characteristics of semiconducting SET devices by expanding the work of Savaikar et al. [23, 25] and revisiting the approximation used for a metallic device. The size of typical island(s) and junctions in these devices are between 2 and 10 nm. Since a silicon quantum dot with a radius larger than 2 nm has over 890 atoms, using ab initio calculation to predict the behavior of a device with at this size is less time efficient and more complex. While approaching fundamental quantum mechanical limits in energy and carrier transport behavior, semi classical approaches to these quantum islands and devices are still relevant.

1.3 Reference List

[1] H. Amrouch, G. Pahwa, A. D. Gaidhane, J. Henkel, and Y. S. Chauhan, "Negative capacitance transistor to address the fundamental limitations in technology scaling: Processor performance," *IEEE Access*, vol. 6, pp. 52754–52765, 2018.

[2] *Intel Technology and Manufacturing Day in China Showcases 10 nm Updates, FPGA Progress and Industry's First 64-Layer 3D NAND for Data Center*. 2017. Available from: https://newsroom.intel.com/news/intel-technology-manufacturing-day-china/.

[3] G. E. Moore, "Cramming more components onto integrated circuits," *Electronics*, vol. 38, no. 8, 1965.

[4] T. Simonite, "Moore's Law is dead. Now what?" *MIT Technology Review*, May 13, 2016. Available from: https://www.technologyreview.com/s/601441/moores-law-is-dead-now-what/.

[5] Y. Taur, D. A. Buchanan, W. Chen, D. J. Frank, S. E. Ismail, G. A. Sai-Halasz, R. G. Viswanathan, H. C. Wann, S. J. Wind, and H. Wong: "CMOS scaling into the nanometer regime," *Proceedings of the IEEE*, vol. 85, no. 4, p. 486, 1997.

[6] C. Mead, *"Introduction to VLSI Systems,"* Addison-Wesley, Palo Alto, CA, 1979.

[7] J. D. Meindl, *Micropower Circuits*, John Wiley & Sons, Inc., New York, NY, 1969.

[8] J. D. Meindl, "Low Power Microelectronics: Retrospect and Prospect," *Proceeding of the IEEE*, vol. 83, no. 4, pp. 619–635, 1995.

[9] C. Wasshuber, "Recent advances and future prospects in single-electronics," *Proceedings of 2003 Design Automation Conference*, p. 274, 2003.

[10] K. K. Likharev, "Single-electron devices and their applications," *Proceedings of the IEEE*, vol. 87, no. 4, p. 606–632, 1999.

[11] P. S. K. Karre, P. L. Bergstrom, G. Mallick, and S. P. Karna, "Room temperature operational single electron transistor fabricated by focused ion beam deposition," *Journal of Applied Physics*, vol. 102, no 2, p. 024316, 2007.

[12] K. Yano, “Room Temperature Single-Electron Memory,” *IEEE Transaction on Electron Devices*, vol. 41, no. 9, pp.1628–1638, 1999.

[13] O. Kumar and M. Kaur, “Single electron transistors: Applications and problems,” *International Journal of VLSI Design & Communication Systems*, vol. 1, no. 4, 2010, pp. 24–29.

[14] K. A. Walczak, P. L. Bergstrom, and C. R. Friedrich, “Light sensor platform based on the integration of bacteriorhodopsin with a single electron transistor,” *Active and Passive Electronic Components* vol. 2011, p. 586924, 2011.

[15] P. S. K. Karre, M. Acharya, W. R. Knudsen, and P. L. Bergstrom, “Single electron transistor based gas sensing with tungsten nano particles at room temperature,” *IEEE Sensors Journal* vol. 8, pp. 797–802, 2008.

[16] T. Kudo and A. Nakajima, "Highly sensitive ion detection using Si single-electron transistors," *Applied Physics Letters,* vol. 98, no. 12, p. 123705, 2011.

[17] T. Kudo and A. Nakajima, "Biomolecule detection based on Si single-electron transistors for highly sensitive integrated sensors on a single chip," *Applied Physics Letters,* vol. 100, no. 2, p. 023704, 2012.

[18] V. V. Zhirnov, J. A. Hutchby, G. I. Bourianoff, J. E. Brewer, “Emerging research memory and logic technologies,*” IEEE Circuits and Devices Magazine*, vol. 21, no. 3, p. 47–51, 2015.

[19] Y. Yun Seop, H. Sung Woo, and D. Ahn, “Macromodeling of single-electron transistors for efficient circuit simulation,” *IEEE Transactions on Electron Devices,* vol. 46, no. 8, pp. 1667–1671, 1999.

[20] Y. Seop, S. Woo Hwang and D. Ahn, "Macromodeling of single-electron transistors for efficient circuit simulation," *IEEE Transactions on Electron Devices*, vol. 46, no. 8, pp. 1667–1671, 1999.

[21] A. N. Korotkov, R. H. Chen and K. Likharev, "Possible performance of capacitively coupled single-electron transistors in digital circuits*," Journal of Applied Physics,* vol. 78, no. 4, p. 2520–2530, 1995.

[22] F. Willy and Y. Darma, "Modeling and simulation of single electron transistor with master equation approach*," Journal of Physics: Conference Series,* vol. 739, no. 1, p. 012048, 2016.

[23] M. A. Savaikar, D. Banyai, P. L. Bergstrom and J. A. Jaszczak, "Simulation of charge transport in multi-island tunneling devices: Application to disordered one-dimensional systems at low and high biases," *Journal of Applied Physics*, vol. 114, no. 11, p. 114504, 2013.

[24] P. Kumar Sinha and S. Sankaranarayanan, "Single electron transistor and its simulation methods," *International Journal of Engineering Development and Research,* vol. 2, no. 2, p.1402100, pp. 1907–1925, 2014.

[25] M. A. Savaikar, *Stochastic Charge Transport in Multi-Island Single-Electron Tunneling Devices*, Ph.D. Dissertation, Department of Physics, Michigan Technological University, 2013.

[26] C. Wasshuber, H. Kosina, and S. Selberherr, "SIMON-A simulator for single-electron tunnel devices and circuits," *IEEE Transactions on Computer-Aided Design of Integrated Circuits and Systems*, vol. 16, no. 9, pp. 937–944, 1997.

[27] C. Wasshuber, *Computational Single-Electronics (Computational Microelectronics)*. Edited by: *S. Siegfried*, Springer Science & Business Media, p. 278, 2011.

[28] P. U. Vivitasari, Y. Azuma, M. Sakamoto, T. Teranishi and Y. Majima, "Coulomb blockade and Coulomb staircase behavior observed at room temperature," *Material Research Express,* vol. 4, no. 2, 2017.

[29] C. W. J. Beenakker, "Theory of Coulomb-blockade oscillations in the conductance of a quantum dot," *Physical Review B,* vol. 44, no. 4, 1991.

[30] A. A. M. Staring, *Coulomb-blockade oscillations in quantum dots and wires,* Eindhoven: Technische Universiteit Eindhoven, 1992.

[31] R. W. M. Amman, E. Ben-Jacob, P. D. Maker, and R. C. Jaklevic, "Analytic solution for the current-voltage characteristic of two mesoscopic tunnel junctions coupled in series," *Physical Review B,* vol. 43, no. 1, pp. 1146–1149, 1991.

[32] D. J. Griffiths, "The Time Independent Schrödinger Equation," in *Introduction to Quantum Mechanics*, Pearson Prentice Hall, Upper Saddle, NJ, 2004.

[33] J. G. Simmons, "Generalized formula for the electric tunnel effect between similar electrodes separated by a thin insulating film*," Journal of Applied Physics*, vol. 34, no. 6, p. 1793–1803, 1963.

[34] J. Singh, *Semiconductor Devices: Basic Principles*, John Wiley and Sons Inc., New York, NY, 2001.

[35] C. Kittel, *Introduction to Solid State Physics, 8th Edition*, John Wiley and Sons, Inc., New York, NY, 1971.

[36] D. R. Banyai, *Multiscale Examination and Modeling of Electron Transport in Nanoscale Materials and Devices*, Ph.D. Dissertation, Physics Department, Michigan Technological University, 2014.

[37] B. Hao, A. Asthana, P. Hazaveh, P. L. Bergstrom, D. Banyai, M. A. Savaikar, J. A. Jaszczak and Y. K. Yap, "New Flexible Channels for Room Temperature Tunneling Field Effect Transistors," *Scientific Reports,* vol. 6, p. 20293, 2016.

[38] H. Ishikuro and T. Hiramoto, "Quantum mechanical effects in the silicon quantum dot in a single-electron transistor," *Applied Physics Letters*, vol. 71, no. 25, pp. 3691–3693, 1997.

[39] P. Bhadrachalam, R. Subramanian, V. Ray, L. Ma. W. Wang, J. Kim, K. Cho and S. J. Koh, "Energy-filtered cold electron transport at room temperature," *Nature Communication,* vol. 5, no. 4745, 2014.

[40] C. H. Lee, S. Qin, M. A. Savaikar, J. Wang, B. Hao, D. Zhang, D. Banyai, J. A. Jaszczak, K. W. Clark, J.-C. Idrobo, A.-P. Li, Y. K. Yap, "Room-temperature tunneling behavior of boron nitride nanotubes functionalized with gold quantum dots," *Advanced Materials*, vol. 25, no. 33, pp. 4544-4548, 2013.

[41] M. Acharya, *Development of Room Temperature Operating Single Electron Transistor Using FIB Etching and Deposition Technology,* Ph.D. Dissertation, Electrical Engineering Department, Michigan Technological University, 2009.

2 Generalizable Modeling of Charge Transport in Single-Electron Transistor Devices: Application to Thermal Sensitivity in Semiconducting Island Systems

Single-electron devices with semiconducting islands have been fabricated and experimentally demonstrated, but simulation of the transport characteristics requires further development of computationally-efficient methods to more capably demonstrate the physics of the devices. A significant reason for this limited progress is the complexity of the underlying physics of electron tunneling between nanometer-scale semiconducting islands. The calculation of tunneling rates between a semiconductor island and a metallic or a semiconducting electrode is more complex than for tunneling between two metals. In particular, the effects of the band gap and the more complex density of states are examined in this paper. A kinetic Monte Carlo (KMC)-based simulation is developed and applied to calculate the current-voltage characteristics of a semiconducting single-electron transistor (SET) device. Numerical integration is utilized to calculate the tunneling rates. For a semiconducting island, parameters such as the band gap, provide the ability to operate the SET device under different conditions that allow differentiation in the device's sensitivity to temperature. A lower degree of temperature sensitivity can be achieved under a sufficiently high bias potential such that the probability of electron tunneling exists even at low temperatures. Under smaller biases, the primary tunneling is observed only for thermally excited electrons, resulting in a high degree of temperature sensitivity.

2.1 Introduction

For decades now, electronic devices, especially metal oxide semiconductor field effect transistors (MOSFETs), have been decreased in size to enable more highly integrated circuits with greater speed and lower power consumption. Intel displayed 10-nm transistors and claimed it to be the "world's tightest transistor" [1]. As electronic devices scale to dimensions where quantum mechanical behavior begins to dominate device characteristics near room temperature, the understanding of the transport of carriers across junctions and in quantum-electronic tunneling-based structures becomes yet more important to the ongoing development of the electronics industry. Because tunneling behavior scales to atomic dimensions, there is considerable motivation to better understand carrier transport in semi-random assemblies of quantum-scaled device elements [1, 2]. One testbed device that has served as a basis for exploring the nature of carrier transport in random assemblies of quantum dots is the single-electron transistor (SET). SETs have been explored for high-density, ultra-low power electronics, for highly sensitive electrometer devices [3], and for charge transfer sensing for applications such as photon detection [4], gas and chemical [5], or biochemical sensing [6]. The understanding of the transport of carriers across junctions in quantum-electronic tunneling-based structures requires algorithms to predict and simulate the behavior of such devices. Ab initio calculations are capable of accurate modeling of the physics, but are computationally prohibitive given the nanometer scales represented in the systems of interest here. On the other hand, semi-classical physics modeling must be carefully evaluated to account for dimensions that induce quantum mechanical behavior at these scales.

Algorithms based on Master Equation methods or kinetic Monte Carlo (KMC) simulations are the two primary approaches that are used to predict electron tunneling through SET devices and simulate their current-voltage characteristics [7]. Master-Equation approaches [8] utilize transition probabilities and state occupation probabilities to generate a set of coupled differential rate equations that are calculate the system dynamics, including steady-state current-voltage characteristics. Applying this method to a single-island SET device is very efficient; however, the resulting set of rate equations quickly becomes intractable for efficient computation as the number of islands increases or as the number of possible charge states on the islands that must be considered (e.g. at higher biases) increases [7, 8]. One of the main challenges for existing modeling frameworks that is common to both Master Equation and KMC approaches is that a closed form solution of the tunneling rate integral has been utilized. For non-trivial band structure this integral generally does not have a closed-form solution unless extreme and inaccurate approximations are employed. These methods have other limitations, such as using constant junction resistances. The KMC method, although computationally more expensive, is capable of simulating SET devices with longer chains of islands compared to Master-Equation approaches. We have thus chosen the KMC approach to simulate the characteristic of multiple-island devices, by extending the MITS code, a KMC-based simulation tool developed by Savaikar et al. [9, 10] which has expanded and addressed limitations of previously developed KMC tools such as SIMON [11, 12], but has been limited to simulation of metallic islands. A third simulation tool, the SPICE macro-modeling [13], can simulate the quasi-static lumped-element model of single electron circuits where the interconnections between SET devices are large compared to the SET

junctions, ensuring that they are capacitively independent of each other. The SPICE framework does not, however, take into account the dynamics of the tunneling transport with charge state and temperature that is fundamental to the underlying physics of the device. This method is useful and time efficient for well-characterized conditions for temperature and input biases.

SET devices have been experimentally fabricated with metallic and semiconducting materials (see for example, [14-18]). These experimental investigations have shown that there are advantages to utilizing semiconducting islands as compared to metallic-island SET devices. One of the particularly interesting practical examples is thermal filtering, where excited electrons can be blocked from participating in tunneling events utilizing energy gaps in semiconducting materials' density of states [18]. Semiconductors SET devices show clearer Coulomb oscillations (see Section II) and gate controllability as compared to metallic SET devices. For example, the gate control in semiconducting SET devices was experimentally examined by Acharya et al. [16] and showed improvement compared to metallic SET devices. Clear Coulomb-oscillation peaks have also been experimentally demonstrated for a semiconducting SET device by H. Ishikuro and T. Hiramoto [17].

This study is focused on developing an algorithm that may better predict the transport characteristics of a tunneling device with a semiconducting island over temperature and terminal biases, and compare the functionality of semiconducting and metallic SET devices. The radius of islands in these devices is typically no smaller than 2.5 nm. Since a silicon island with a radius larger than 2.5 nm incorporates over 800 atoms, using *ab initio* methods to predict the behavior of the device would be quite complex and computationally

unfeasible. For radii larger than 2.5 nm, discretization of the island can be ignored [27]. Electron tunneling becomes relevant for junction widths below 1nm. Following the work of Likharev [3], the semi-classical approach to tunneling for predicting the current-voltage characteristics of the SET is based on so-called "orthodox theory" and is commonly performed by the KMC method. Orthodox theory has three assumptions: 1- time for electron tunneling is negligible compare to other time scales in the system; 2- only one electron tunneling event happens at a time and co-tunneling is ignored; and 3- the quantization of energy is ignored in the island [3]. Different algorithms have been developed based on the KMC method [7, 9, 10], including SIMON [11, 12] and MITS [9, 10], to predict electron transport in multi-junction devices. However, these generally have limitations in regard to predicting the behavior of SETs with semiconductor device elements. The MITS simulator was developed, in particular, by Savaikar et al. to predict the current flow through multiple-metallic-island transport devices [9, 10], and added some advantages as compared to SIMON, such as calculating the transition probabilities as a function of energy instead of approximating them as a constant. In this work we revisit some approximations, such as constant density of states used by MITS and SIMON, and extend MITS, so it is capable of simulating semiconducting SET devices.

A primary challenge in this study is properly calculating the tunneling rates between the nanometer-size semiconductor island and the electrodes, with reasonable approximations based on the electrical and geometrical characteristics of the system. The models, theory and approximations, such as for the density of states and the tunneling probabilities, that are required to calculate tunneling rates across the junctions are reviewed in Section II. In Section III, we briefly review the kinetic Monte Carlo algorithm used to

predict the current-voltage characteristics of SET devices. Section IV is dedicated to different test cases that verified the validity and relevance of the introduced model. In Section V the unique properties of a SET with a semiconducting island and its potential applications are introduced and explored

2.2 Theory and Background

The current-voltage (*IV*) characteristics of a multi-junction single-electron device depend on electron tunneling rates across each junction. For tunneling to proceed, electrons must have enough energy, from external biases or temperature, to overcome the charging energy, $E_{ch} \equiv e^2/C$ [3], where C is the island's total capacitance and e is the magnitude of the electron charge). For nanometer-sized islands, the charging energy may be relatively large, such that under small biases and at lower temperatures, electron tunneling is suppressed. This phenomenon is called the Coulomb blockade effect [3, 19, 20]. Under a large enough potential bias, known as the threshold voltage, electron tunneling becomes possible, and current can flow between the source and drain electrodes.

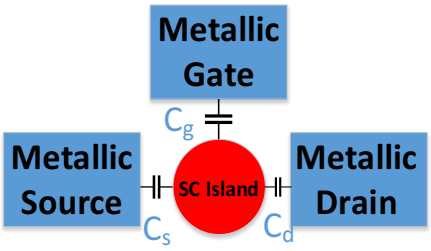

Figure 2.1. Circuit schematic of a SET system with a semiconducting nano island and three electrodes. The capacitance between the drain and the island is marked as C_d, the capacitance between the drain and the island is marked as C_s and the capacitance between the gate and the island is marked as C_g.

We start by considering a simple form of a SET with three electrodes and one semiconducting nanometer-sized island that is separated from the metallic electrodes by dielectric barriers, shown in Fig. 2.1. The gate, source and drain are capacitively coupled to the island. Ideally, the gate electrode should carry no current. Charge transport in an SET occurs via electron tunneling through the junctions connecting the source and drain electrodes. The model has a source and drain junction of 0.5 nm and 1.0 nm, junction capacitances of 0.8 aF and 0.5 aF respectively, and an island radius of 3 nm. The gate electrode provides control of the trans-conductance of the device between the source and drain electrodes, resulting in a true three-terminal electronic device capable of integration in more complex system configurations. The dielectric insulator between the gate electrode and the island would be designed to minimize the probability of tunneling to the gate, in order to keep the gate current low. Simplifications and approximations may be required to calculate the rate of tunneling between a semiconductor and a metal. In this section, we focus on modeling the tunneling rates to and from the island, with appropriate simplifications, with a goal of providing results that both give insights into the device operation, and with the desired accuracy. Changing the potential of the island by the gate potential could enhance or inhibit electron tunneling. When the island's potential changes sufficiently to overcome the discrete charging energy levels, electron tunneling occurs and causes a periodic variation in source-drain current [3, 19, 20] called Coulomb oscillations. The periodicity in a SET device with a single island is given by $\Delta V_{\mathrm{g}} = \frac{e^2}{C_{\mathrm{g}}}$, where C_{g} is the gate capacitance [3, 20].

2.2.1 Tunneling Rate

Following the work of Savaikar et al. [9, 10], and Amman et al. [21], the tunneling rate across a junction can be calculated using the general semi-classical equation which was inspired by Fermi-golden rule. Equation (2.1) shows the tunneling rate between the middle island (*i*) and the left electrode (*f*) of a SET device, for an electron with energy *E* as:

$$\Gamma_{if} = \int_{l1}^{l2} \frac{2\pi}{\hbar} |T(E)|^2 D_i(E)\, f(E - E_i) D_f\left(E - \Delta W_{if}\right) \times \left[1 - f\left(E - E_i - \Delta W_{if}\right)\right] dE \,, \tag{2.1}$$

where

$$\Delta W_{if} = -eV_{if} + E_{ch} \tag{2.2}$$

is the change in free energy of the system upon tunneling across a junction from the initial to the final states. E_i is the Fermi energy of the initial side of the tunneling junction, and D_i and D_f are the density of states functions for the initial and final states of the tunneling electron, respectively. *f(E)* is the Fermi-Dirac distribution function, and *T(E)* is the tunneling probability. Integral limits l_1 and l_2 are $-\infty$ and $+\infty$, respectively; however, in our model finite integral limits are dynamically calculated depending on the applied potentials and tunneling barrier characteristics to improve computational efficiency [9, 10].

2.2.2 Transition Probability

The transition probability depends on properties of the junction, and following work of Savaikar el al. [9, 10], we consider the potential barrier to be a simple rectangular barrier. If there is a potential difference across the junction (V_{if}), the barrier height is changing over the width of the barrier. This changing barrier height depends on the work function of materials across the junction. If the work functions are much larger than the potential

difference across the junction, then the barrier height can be approximated as a constant of the average height over the width. The effect of this approximation is trivial on the outcome of the algorithm and improves the computational efficiency [9, 12, 22].

A simple model for electron transition from the valence band of the island to the metallic electrode is shown in Fig. 2.2, illustrating the relative energy levels of the semiconducting island *(f)* and metal electrode *(i)* with a potential difference *(V_{if})* across the junction. For tunneling that proceeds from the semiconducting island, the average effective barrier height *(V_0)* is calculated according to [9, 10]:

$$V_0 = \frac{\phi_{sc} + \phi_{sc} - eV_{if}}{2} = \phi_{sc} - \frac{eV_{if}}{2} \quad , \tag{2.3}$$

where ϕ_{sc} represents the electron affinity in the island's conduction band or valence band. Using the model of electron tunneling through a one-dimensional rectangular barrier, the single-electron tunneling probability can be approximated as:

$$\left|T(E)\right|^2 = \left[1 + \frac{V_0^2 \sinh^2(k_1 d)}{4E(V_0 - E)}\right]^{-1}, \tag{2.4}$$

where

$$k_1 = \frac{\sqrt{2m(V_0 - E)}}{\hbar} \tag{2.5}$$

E is the electron's energy, eV_0 is the barrier height, and d is the barrier width [23]. For the sake of efficiency in calculating transition probability, we approximate the initial energy of an electron tunneling from the island to be the energy of the appropriate conduction- or valence-band edge; i.e., an electron tunneling from the conduction band is taken to have $E = E_C$ in (4) and (5), and likewise an electron tunneling from the valence band is taken to

have $E = E_V$ in (4) and (5).

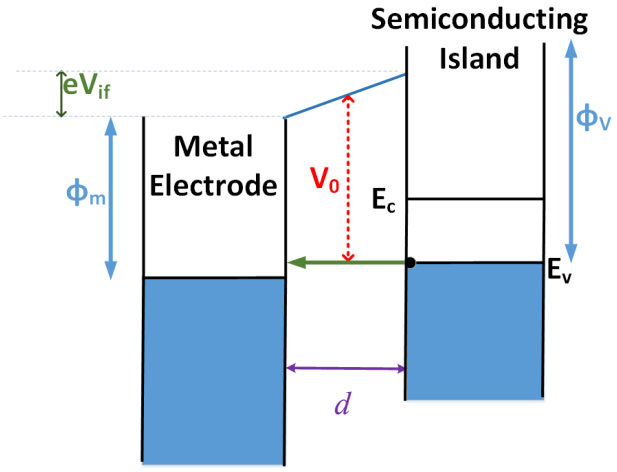

Figure 2.2. Electron tunneling from the middle island's valence band to the left electrode when there is a potential difference of V_{if} across the junction. The green arrow shows the electron tunneling direction. The red arrow denotes the average barrier height over the left junction width (d). ϕ_V and ϕ_m are electron's work function of the valence band and metal respectively.

2.2.3 Density of States

The density of states (DOS) depends on the electronic properties of the material and its geometry, and may take on a complicated form. For metals the density states of electrons which are energetically located near Fermi energy, is approximated using the free-electron model [24, 25]. In majority of previous theoretical studies, such as those using the SIMON code by Wasshuber et al. [11, 12] or the MITS algorithm developed by Savaikar et al. [9, 10], the density of states of the metal electrodes is approximated as a constant $D_0 = D(E_F)$, which is the density of states at the Fermi energy of the metal. This is generally appropriate as a model for electron transport in metals since the participating carriers and available

levels are positioned energetically near the Fermi energy of the material. Semiconductor band structures, however, are not easily described by analytic formula, although approximations can be utilized to develop an expression sufficiently accurate to employ in the tunneling rate equation (1) [26]. The energy separation between discrete energy levels due to quantum confinement effects depends on the size of the nanometer-scale material [27]. If the energy spacing is much smaller than the charging energy ($\Delta E \ll E_{\mathrm{ch}}$) or thermal energy then the energy levels may be considered continuous [27]. The model presented is applied to islands 2.5 nm or larger, which allows us to model the closely spaced discrete energy levels of the quantum island as a continuous energy band, as is used in semi-classical approximations in semiconductor physics. Using the parabolic approximation to model electron's density of states in semiconductors might be timely effective or appropriate for electrons with low kinetic energy but is unable to accurately model the DOS of electrons with higher kinetic energy. At higher energy levels, the DOS of semiconducting materials is more accurately modeled by the non-parabolic approximation. In a semiconductor with an energy gap the modified-parabolic-approximation density-of-states equation can be written as [28, 29]:

$$D(E) = \frac{\sqrt{2}(m_{\mathrm{c}}^{*})^{\frac{3}{2}}\sqrt{(|E - E_{\mathrm{sc}}| + \alpha_{\mathrm{sc}}(E - E_{\mathrm{c}})^{2})}(1 + 2\alpha_{\mathrm{sc}}|E - E_{\mathrm{sc}}|)}{\pi^{2}\hbar^{3}}, \tag{2.6}$$

where

$$\alpha_{\mathrm{sc}} = \frac{1}{E_{\mathrm{g}}}\left(1 - \frac{m_{\mathrm{sc}}^{*}}{m}\right)^{2}, \tag{2.7}$$

m is the free electron mass, m_{sc}^{*} is are the effective mass of electron in the conduction band or valence band, E_{g} is the energy gap, E_{sc} is the edge of the conduction band or the valence band and $\hbar$ is the reduced Planck constant.

A comparison between the non-parabolic density-of-states approximation, parabolic density of state approximation and full-band density of states calculations from [29] shows that the non-parabolic approximation is more accurate at higher energy levels. We can conclude from the comparison that when energy states at 0.5 eV above the conduction band edge or further (0.5 eV below the valence band edge or further), are involved in the tunneling, then the non-parabolic model is required as a more accurate approximation [30, 31]. It should be noted that depending on the applied potential, temperature, and the energy levels which are participating in tunneling, the parabolic approximation may be sufficiently accurate, improving the computational efficiency of the modeling. If the energy levels that are participating in the tunneling are in the window of 1 eV around the Fermi energy, then the parabolic model is a valid approximation. If the temperature and applied potential causes higher energy states to participate in the tunneling events, one needs to take into account the non-parabolic approximation to improve accuracy.

2.3 Numerical Calculation

The drain electrode is connected to the ground and is used as a reference in this study to be at zero potential. The lowest energy level of the drain to be set at 0, the Fermi energy of intrinsic silicon is set to 5.5 eV at equilibrium, and the electron affinity of silicon to be 4.05 eV. Therefore, we consider the highest energy level participating in the tunneling to be at 9.27 eV (~10 eV). Replacing the terms associated with our system as outlined above into (1), the governing equation for the tunneling probability does not have a closed form solution. Thus, (1) is evaluated numerically using the built-in *integral* function in MATLAB, with integration limits that are dynamically calculated based on potential

difference across the junction, with respect to the highest (10 eV) and the lowest (0) allowed energy levels and thermal energies of the system. The series of simulations to construct an *IV* characteristic are started at a potential bias of zero volts, and increased step by step in increments of 0.01 V in each subsequent simulation. The KMC method is used to select a tunneling event, after which the time interval is advanced, and the charge state of the system is updated. After each tunneling event, the potential across the junctions and integral limits re-calculated, and new tunneling rates are re-estimated. This is repeated until a steady-state current converges with error bars less than 2% of the mean value.

2.4 Results: Test Cases

In this section test cases are investigated to demonstrate the robustness of the algorithm, and basic effects of the assumptions made for the model. The test cases are designed to inspect the behavior of the device by changing the key parameters. For each test case, the voltage increment (either gate or source-drain voltage) is set at 0.01 V. A minimum of 10,000 Monte Carlo steps are performed for each voltage increment.

2.4.1 Test I: Coulomb Staircase of a SET Device with Metallic Electrodes and a Semiconducting Island

The first test case is dedicated to studying threshold voltage and the Coulomb staircase effect in the IV_{sd} characteristic. The first fundamental difference between devices with a semiconductor versus a metallic island becomes clear: A larger threshold voltage is required for the semiconducting island due to its band gap. At low temperature, electron tunneling occurs when the input biases are able to supply enough energy for electrons to overcome not only the charging energy but to also sufficiently shift the energy levels across the band gap to allow for alignment of the available energy levels in the density of states.

Following Equation (9) of Amman et al. [29] the threshold voltage of a SET device is given by:

$$V_{sd} = \left[\frac{e^2}{2(C_1 + C_2)}(2n + 1) + \frac{E_{BG}}{2}\right]\left[\frac{(C_1 + C_2)}{eC_2}\right], \tag{2.8}$$

where the first term comes from the charging energy and the second term is the additional shift required by the band gap (E_{BG}). With E_{BG} = 1 eV, and the junction capacitances of 0.8 aF and 0.5 aF, the first threshold voltage is 1.06 V as demonstrated in Fig. 2.3, and in good agreement with the (2.8). Subsequent steps in the IV_{sd} characteristic are effectively washed out by the relatively high bias voltage (Fig. 2.3), as compared to metallic-island devices, where the threshold potential can be much smaller. Nevertheless the characteristic gives indications of a step-like behavior at 1.23 V and 1.43 V, also in good agreement in prediction of (2.8). The steps are more rounded and show notable increases in the slope after each step, as compared to what is observed near the threshold for metallic SETs. This behavior is due to the effect of the band gap in the semiconductor SET, which leads to a significantly larger V_{th} than that in metal SETs. Beyond V_{th}, the device now operates at a relatively high bias that leads to higher tunneling probabilities and increasingly more operating tunneling channels (sequences of tunneling events across the device with potentially different charge states for the island in the process). Similarly, high biases also tend to render the Coulomb steps to appear less discernable in metallic SETs [9].

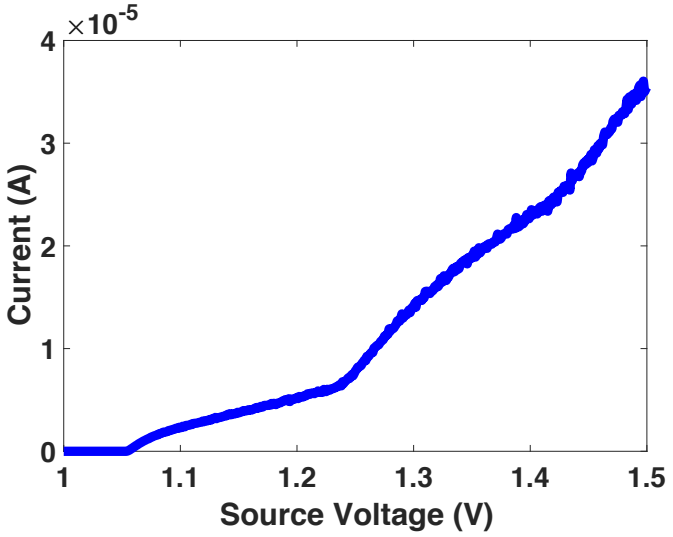

Figure 2.3. The current versus source-drain voltage (IV_{sd}) characteristic of SET with one semiconducting island, at the temperature of 0.1 K and under zero gate bias. Number of MC cycles = 20,000 for each source-drain voltage.

2.4.2 Test II: Impact of Gate Capacitance on IV_g Characteristics on a SET Device with Metallic Electrodes and a Semiconducting Island

The gate current-gate voltage (IV_g) characteristic of a SET for a single-island device is expected to have periodic oscillations (Coulomb oscillations), as described in Section II. If the quantum discreteness of energy levels due to small island size in the model is ignored, the periodicity in potential depends only on the gate capacitance as e/C_g [3, 19, 20]. The current versus gate-voltage (IV_g) characteristic is plotted in Fig. 2.4, for a device at 154 K with source and drain capacitances of 0.8 aF and 0.5 aF, respectively, as discussed in [17]. The current-gate voltage characteristic has been modeled using two gate capacitance values. The Coulomb-oscillation period is halved as the gate capacitance doubles, as expected. This confirms that the algorithm is modeling the gate effect properly.

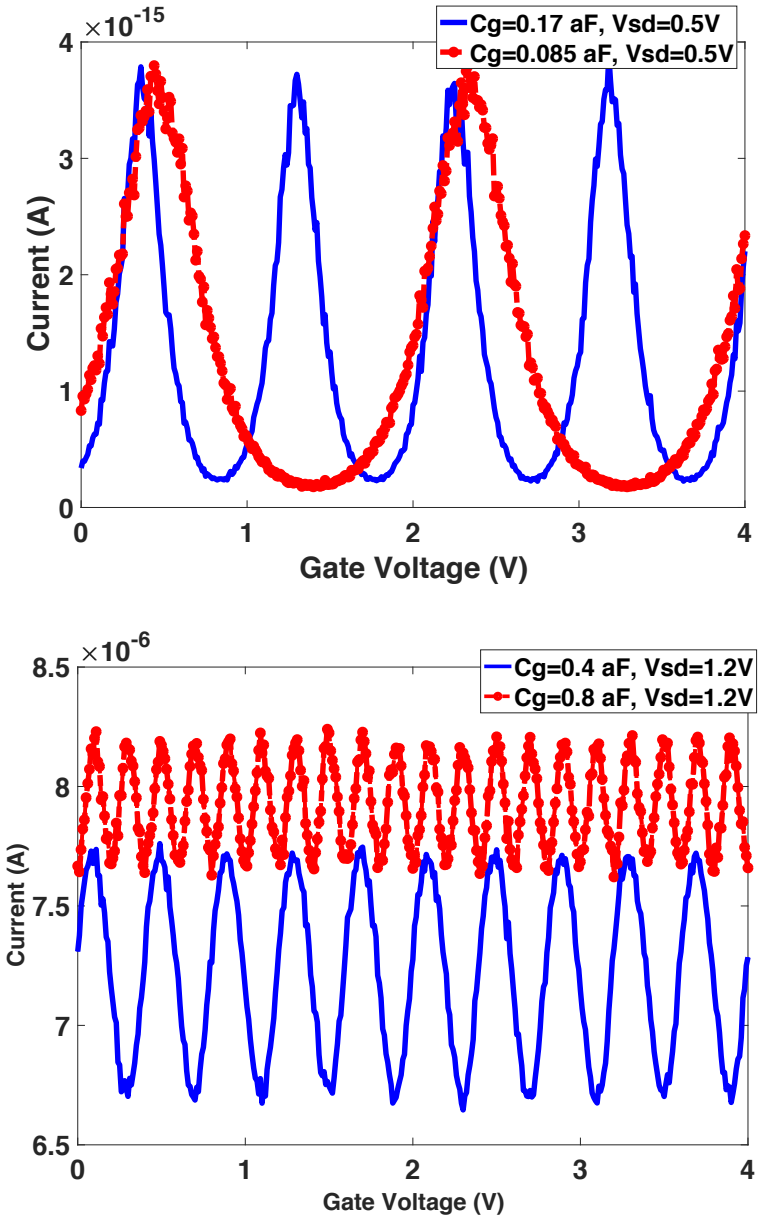

Figure 2.4. Top: Coulomb-oscillation characteristics of a SET with one semiconducting island for two different gate capacitances, one twice that of the other. Simulations were conducted at T = 154 K. Top: source-drain potential V_{sd} = 0.5 V; Bottom: V_{sd} = 1.2 V. Number of MC cycles = 20,000 at each gate voltage.

Figure 2.4 (bottom) shows the current-gate voltage (IV_g) characteristic at 154 K and a higher V_{sd} for two gate capacitance values, of 0.4 aF and 0.8 aF, which are appropriately

scaled to capture the Coulomb oscillations in higher V_{sd}. The Coulomb-oscillation period is halved as the gate capacitance doubles. The periodicity only depends on (e/C_g), as expected, and changing the range of gate capacitances and the input bias does not affect the periodicity. The current magnitude in the SET device increases by increasing the V_{sd}, also as expected. As can be observed in Fig. 2.4 (bottom), changing the gate capacitance from 0.4 aF to 0.8 aF changes the magnitude of the current as well. As these capacitances are comparable to the junction capacitances (0.8 aF and 0.5 aF), the change of 0.4 aF decreases the charging energy resulting in larger current magnitude.

The increase in the magnitude of the current (comparing Fig. 2.4 top and bottom) is dramatic and will be discussed in the next section.

2.4.3 Test III: Impact of Junction widths on IV_g Characteristics on a SET Device with Metallic Electrodes and as Semiconducting Island

The third test case used to demonstrate the relevance of the modeling method is related to the geometry of the system. As mentioned in Section II: Theory and Background, the transition probability depends strongly on the junction width (D). In a series of simulations where the junction widths are proportionally increased while maintaining a fixed ratio, the peak current follows the predicted inverse $\sinh^2(k_1 D)$ proportionality in (2.4) as shown in Fig. 2.5.

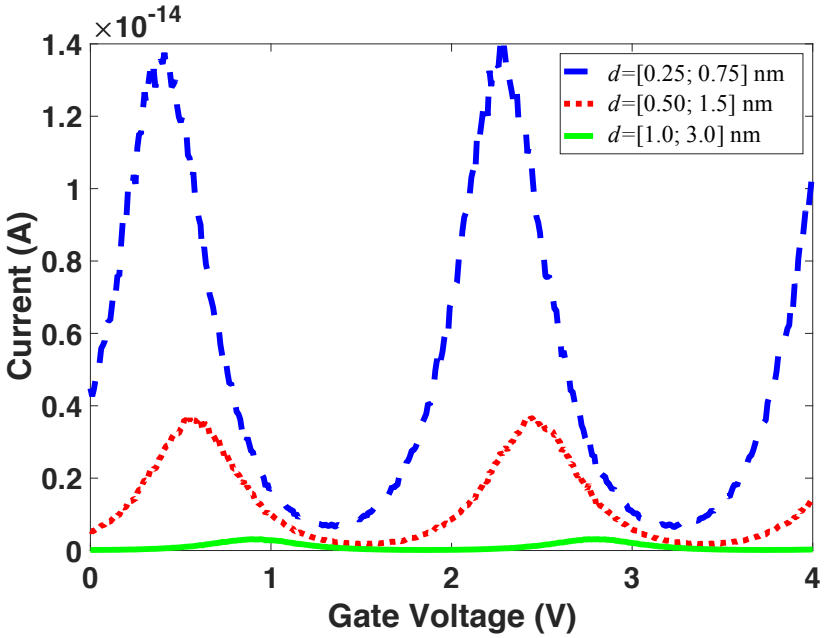

Figure 2.5. The gate-voltage characteristics for three devices with different pairs of junction widths, *d*. Asymmetric junction widths for left and right junctions are scaled by a fixed factor of two in each of the three cases. Here, T = 154 K. Number of MC cycles = 20,000 for each gate potential.

2.5 Results: SET Application and Discussion

To explore the unique aspects of a SET with a semiconducting island, we next study the temperature sensitivity of SET devices with a constant source-drain voltage. We also examine the impact of the island's band gap on the device's performance.

2.5.1 Temperature Dependence: Metallic Electrodes and a Semiconducting Island

In a SET with a semiconducting island, sensitivity of the *IV* characteristics on temperature is found have different regimes, depending on the relative positions of the electrode Fermi levels relative to the band edges of the island. If, for example, under suitable bias conditions there is a path (sequence of probable tunneling events) for electrons

to tunnel from near the Fermi energy of the right electrode to the conduction band of the semiconducting island, followed by tunneling from the valence band of the island to the left electrode, then the effect of temperature on the behavior of the SET should be relatively small, since thermally excited electrons or holes are not necessary for tunneling to be possible. This is illustrated schematically in Fig. 2.6. As an example, for a suitable bias condition under a 1.2 V input source-drain bias and $V_g = 0$, the island's potential rises to approximately 0.6 V, which is greater than half of the band gap. This opens probable paths for electrons in the slower (wider) junction to tunnel from the right electrode to the available states of the conduction band of the island. Furthermore, the valence band of the middle island is aligned with energies close to the Fermi level of the left electrode in the faster (narrower) junction. For this condition, the current remains on the same order of magnitude as demonstrated in Fig. 2.7, showing that as the temperature is increased by almost a factor of 4, from 77 K to 300 K, there is only a relatively small temperature sensitivity, with the peak current increasing by a factor of approximately 10%. The overall magnitude increased but the overall amplitude of the Coulomb oscillations decreases as the temperature increases when the thermal energy becomes of the same order of magnitude as the charging energy.

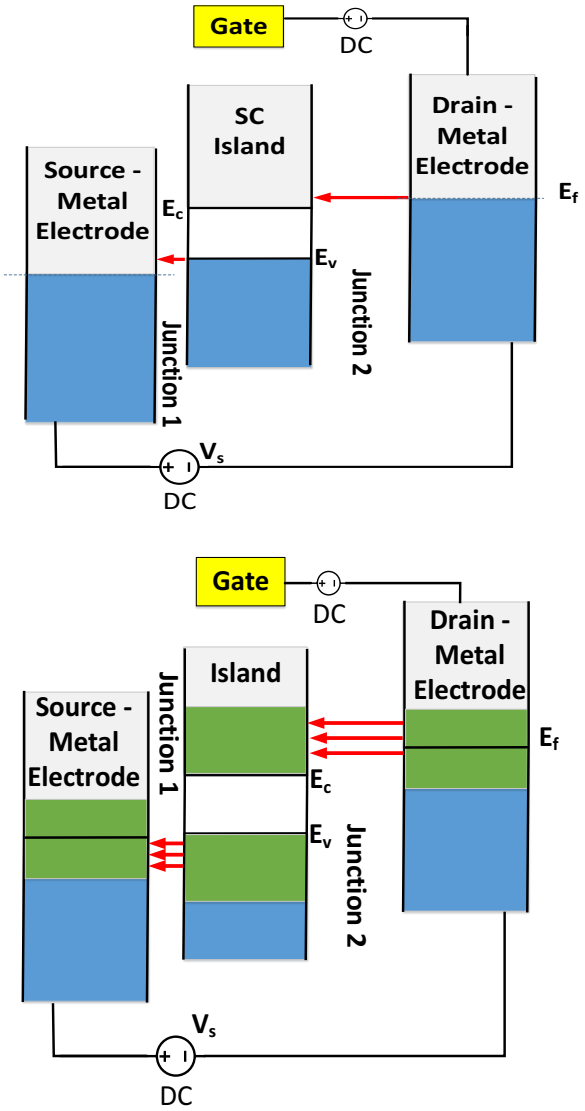

Figure 2.6. Schematic energy-level diagram of a system with two metallic electrodes and a semiconducting island with the band gap of 1eV. Under a source-drain voltage of 1.2 V and a gate potential of 3.9 V, the island's potential is 0.6 V, and the Fermi level of the right electrode overlaps the conduction band. The valence band of the island is aligned with energy levels of the left metal electrode's Fermi level so there is a clear path for electron tunneling through the device. Top: system at $T = 0$ K. Bottom: The system at $T > 0$. Blue represents the filled states, grey represents the empty states and green represents the partially occupied states.

In a regime with a probable electron tunneling path (Fig. 2.6), as is observed in Fig. 2.8, increasing the input voltage leads to a increase in the magnitude of the current. As long as the input voltage is in a range that allows for the convenient electron path to exist, then we have a device which characteristic can be controlled by V_{sd}, and is not drastically sensitive to temperature, which is a unique and potentially valuable feature of the semiconductor-island device. The characteristic at the higher source input voltage of 1.4 V is noisier as a result of there being a wider range of probable tunneling events. At the higher source bias, there are additional available states to tunnel to and additional available states to tunnel from. This increase in the range of potential transitions results in greater number of tunneling events that can participate, and therefore unless a larger number of KMC cycles are employed, the data appear nosier.

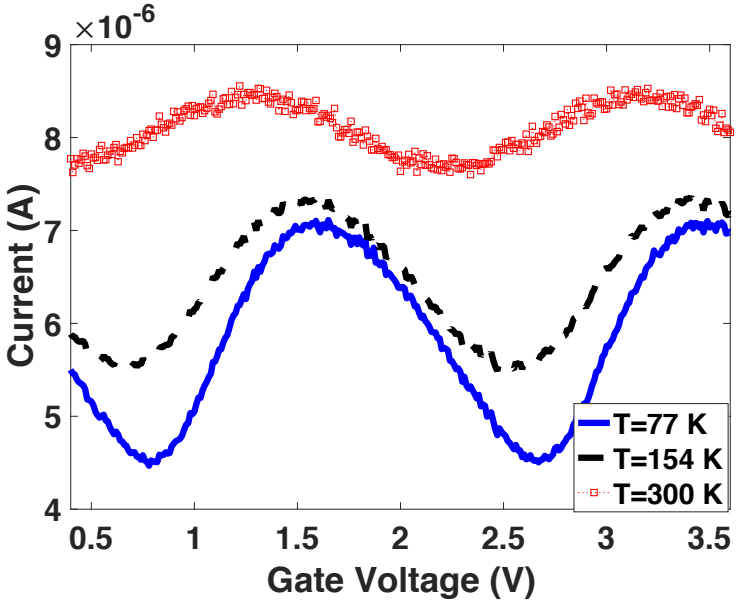

Figure 2.7. The current-gate voltage characteristic for a constant source-drain voltage (V_{sd}) of 1.2 V for temperatures of 77 K, 154 K, and 300 K. These characteristics are weakly temperature dependent. Number of MC cycles = 40,000 for each gate voltage.

A different regime for temperature sensitivity can be observed for cases in which the source-drain potential is relatively small, such the Fermi energy of the right electrode is now aligned within the island's band gap. In this case, as schematically shown in Fig. 2.9, tunneling is impeded at the right electrode except at high enough temperatures such that thermally excited electrons in the right electrode can tunnel to the island's conduction band. The occupancy of energy levels that are involved in tunneling is strongly temperature sensitive and when the input biases of the system are low, the thermally excited electrons are those that primarily participate in tunneling and generate the current flow through the device. Therefore, we can observe a strong temperature effect on the current-gate voltage characteristic of the device. As observed in the simple model in Fig. 2.9, the electron-tunneling path is mostly consisting of partially occupied state due to thermal excitation of electrons. The current magnitude increases over four orders of magnitude as the temperature increases from 154 K to 300 K, as is demonstrated in Fig. 2.10.

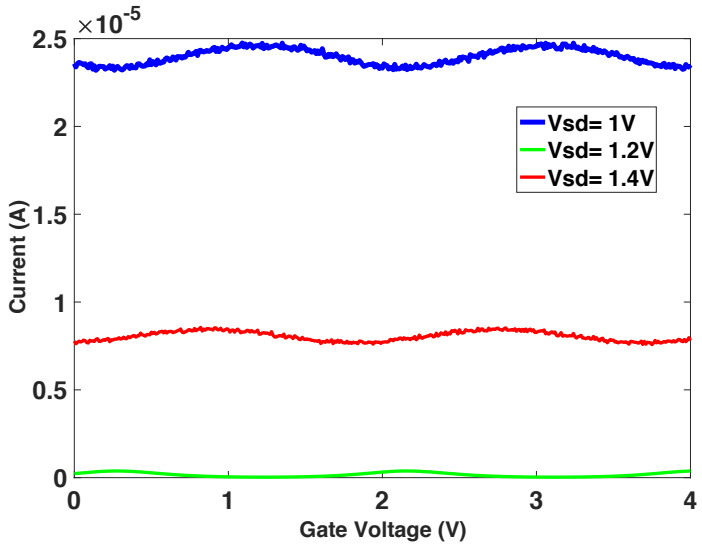

Figure 2.8. The current-gate voltage characteristics of SET model for three different input voltages (V_{sd} = 1, 1.2 and 1.4 V). The temperature is kept constant at 154 K. Number of MC cycles = 20,000 for each gate voltage.

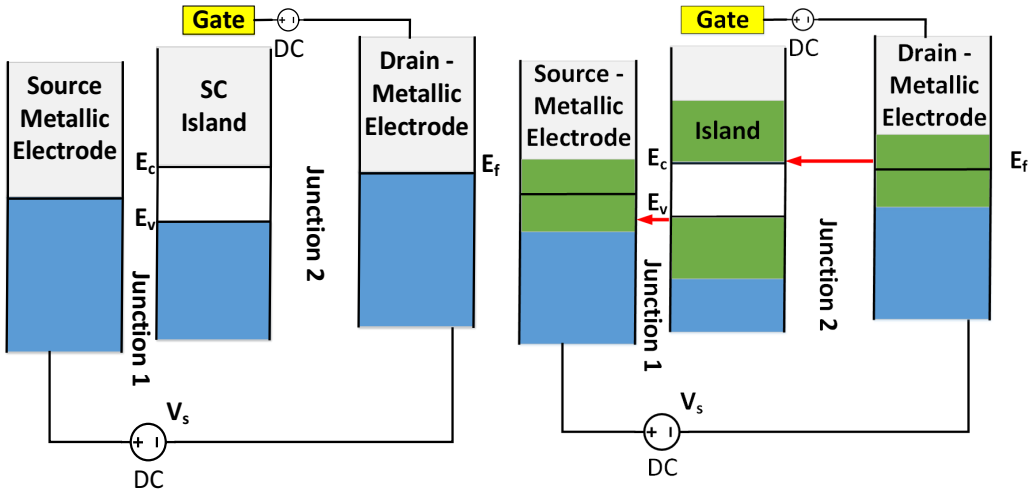

Figure 2.9. The energy-level diagram model of a system with two metal electrodes and a semiconducting island where the island potential is 0.2 V and V_{sd} = 0.5 V. The potential difference of across each of the junctions is not sufficient for the drain's Fermi energy to be aligned with the conduction or valence bands. Left: system at $T = 0$, there is no electron tunneling path. Right: The system at $T > 0$, illustrating a thermally-enabled tunneling path. Blue represents the filled states, grey represents the empty states and green represents the partially occupied states.

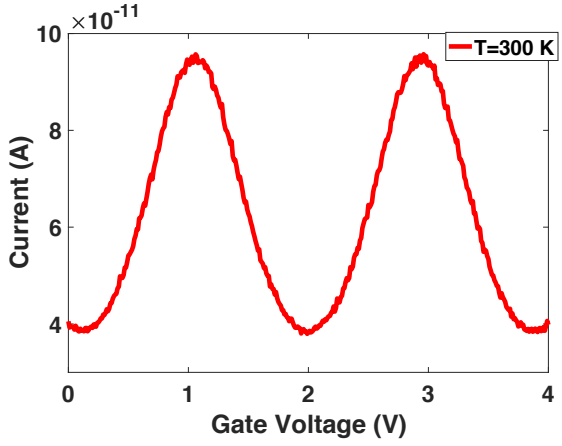

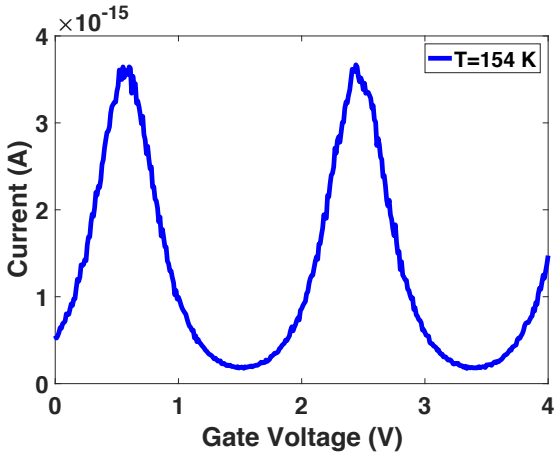

Figure 2.10. The current-gate voltage characteristic for a constant source drain voltage (V_{sd}) of 0.5 V for two different temperatures Top: T = 300 K, number of MC cycles = 40,000 per gate voltage. Bottom: T = 154 K, number of MC cycles = 20,000 per gate voltage.

2.5.2 Semiconducting electrodes and semiconducting island

Because of the techniques used to fabricate semiconducting island(s) there are sometimes positioned between semiconducting electrodes rather than metallic electrodes. This type of semiconducting SET geometry is investigated in this section. The *IV* characteristics of such a device are similar the case of a metal-semiconductor-metal SET, but in different energy regimes. In particular, the input potential bias must be higher to compensate for energy gap in both of the electrodes.

If under higher source-drain bias, then the valence band on the initial tunneling side is aligned with the available states in the conduction band of the island on final side, then a convenient path for electrons exists, as shown in schematic in Fig. 2.11. The Coulomb oscillations are observed under 2.5 V source-drain voltage as demonstrated in Fig. 2.12.

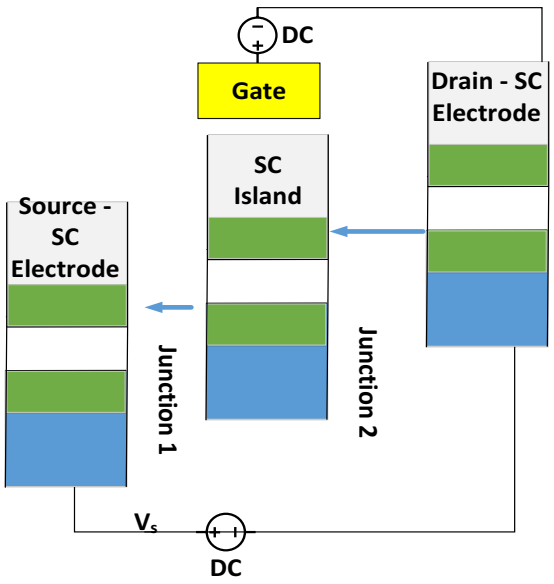

Figure 2.11. Energy-level diagram of a system with two semiconducting electrodes and a semiconducting island. Under a source-drain voltage of 2.5 V and a gate voltage of 3.9 V, the island's potential is around 1 V (predicted from the simulation). The system is at $T > 0$: Blue represents the filled states, grey represents the nearly empty states and green represents the partially occupied states.

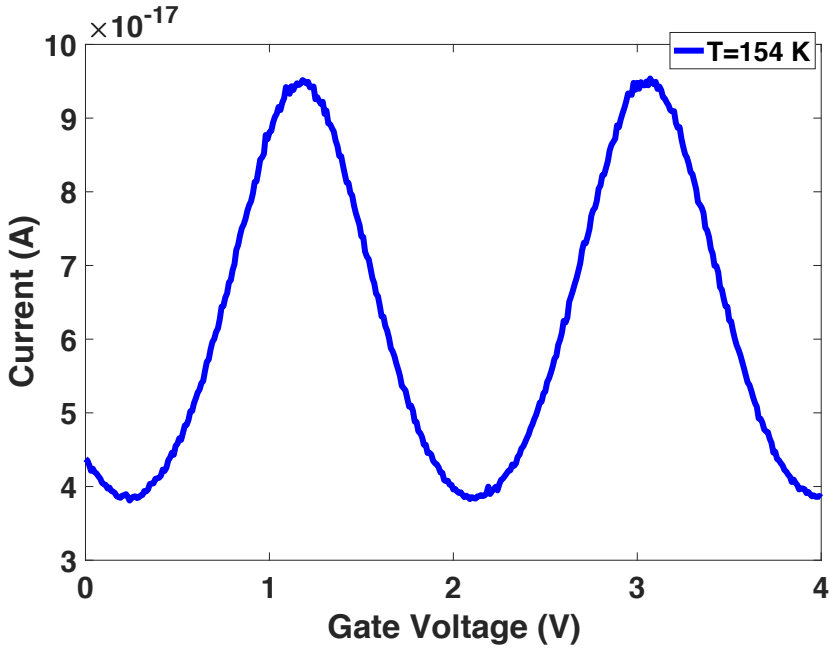

Figure 2.12. The current-gate voltage characteristic of a SET with semiconducting electrodes and island under a constant source drain voltage (V_{sd}) of 2.5 V. Number of MC cycles = 40,000 per gate potential.

2.5.3 Impact of the Band Gap

To explore the advantages of using a semiconducting material versus metal (Fig. 2.13), we have studied the effect of the band gap of 1 eV on the gate IV_g characteristic of the nanometer-scale SET device, with a constant source-drain voltage of 1.4 V. In a device with zero band gap, the probability of electron tunneling from multiple paths is higher due to the wider energy window. As a result, there are smaller fluctuations and more well-defined oscillations observed in the characteristic in the case of the larger band-gap energy, as is shown in Fig. 2.14. As expected, the smaller band gap relates to a greater possibility for electrons to tunnel, so the current magnitude is significantly larger.

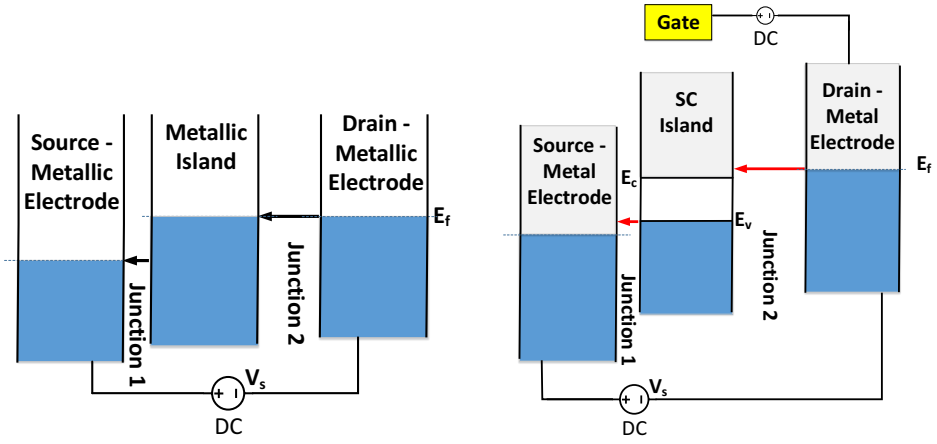

Figure 2.13. Left: The energy level diagram model of a system with two metal electrodes and a metallic island (zero band gap). Right: The energy level diagram model of a system with two metal electrodes and a semiconducting island with band gap of 1 eV.

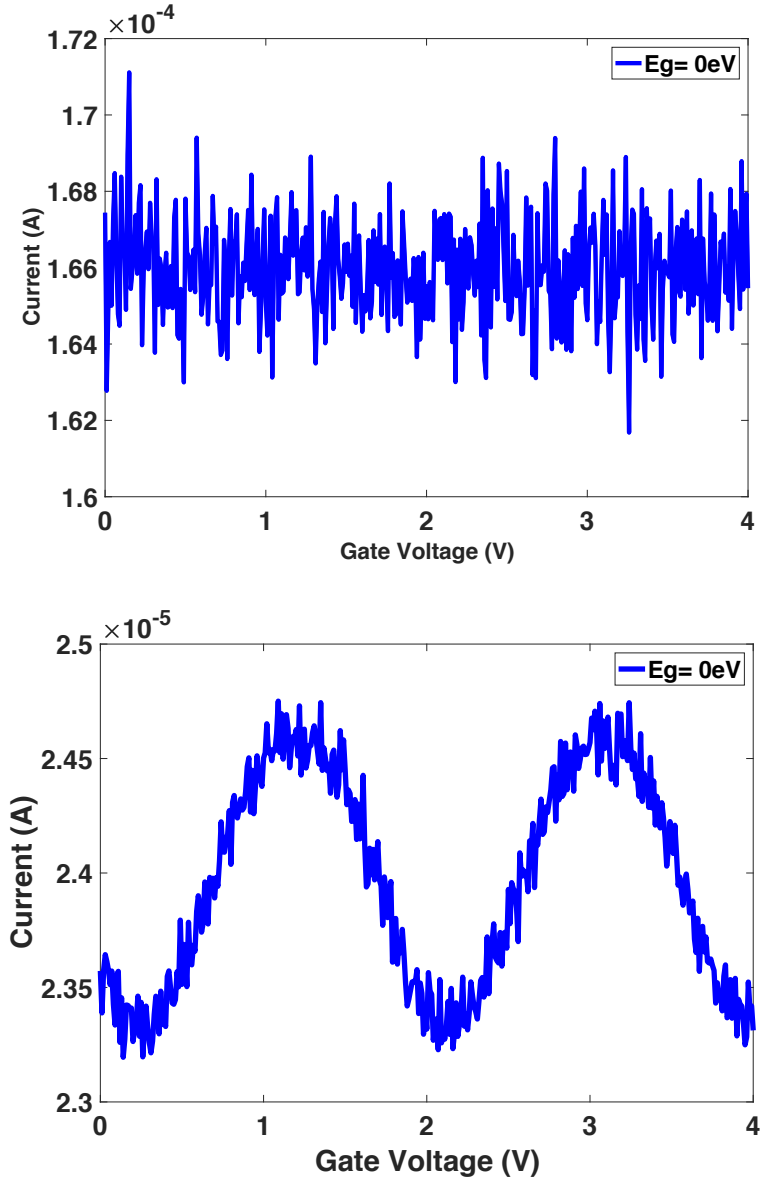

Figure 2.14. Current-gate voltage characteristics of a SET with V_{sd} = 1.4 V and T = 154 K. Top: The current-gate voltage characteristics of SET model with zero band gap. Bottom: The current-gate voltage characteristics of SET model with band gap 1 eV. Number of MC cycles = 40,000 per gate potential.

2.6 Conclusion

In this study, a simulation tool is developed to predict the current-voltage characteristics of SET devices with nanometer-scale semiconducting islands. The tool can

be used for modeling single electron device transport with one or more semiconducting islands with metallic or semiconducting electrodes. Although this work presents results for devices with one island, studies of the characteristics of devices with multiple islands is are also underway and will be presented in future work. A key capability of the tool is the numerical calculation of the tunneling rate across junctions, which allows more realistic modeling of electron transport in materials with complicated band structures.

The characteristics of single-island semiconductor SET devices are studied as a function of the externally controlled parameters, such as the electrode potential and temperature, as well as the internal parameters such as coupling capacitances (impacting the charging energy and degree of gate control), the magnitude of the band gap, and junction widths.

The temperature sensitivity of the IV_g characteristics is an interesting feature of semiconducting SETs that depends on the source-drain bias. For example, when the main electron tunneling path (from valence band to the conduction band) is blocked by the band gap, such as for $eV_{sd} < E_{BG}$, the impact of temperature on the number of electrons participating in tunneling is high, therefore the temperature sensitivity of the device is significant. The sensitivity of the IV_g characteristics to temperature is relatively weak, however, when a significant path for electron tunneling has been opened by an appropriate choice of source-drain potential, such as for $eV_{sd} > E_{BG}$. It was observed that when a higher source-drain potential is applied to the system (> 1 V), the current increases significantly as compared to 0.5 V. In this regime, there is a convenient path for electrons to tunnel (from the electrode to the island's conduction band) so the temperature has only a secondary effect on the magnitude of the current, and the temperature sensitivity is

diminished. The ability to control the degree of temperature sensitivity with input bias utilizing the band gap, is a unique characteristic of the semiconducting SET devices compared to metallic devices.

The gate potential can enhance or inhibit electron tunneling between source and drain, employing the band gap. It is observed that the impact of a band gap in a SET's semiconducting island on the visibility of the Coulomb oscillations is drastic comparing to a metallic SET under same bias condition and temperature where the oscillations are indiscernible. If the electrodes in the SET device are semiconducting as well, the Coulomb-oscillation peaks can be also observed, but the bias conditions under which conductance can be observed will be higher in this case compare to metallic electrodes, due to the electrodes' band gaps.

The improved definition of the Coulomb oscillations, external bias-based control of its temperature sensitivity, and improved gate control over a wide input bias range of the semiconducting single electron device, makes this an interesting candidate for future functional device applications where electrometer-scale charge transport measurements with controllable high or low temperature sensitivity are required.

2.7 Reference List

[1] *Intel Technology and Manufacturing Day in China Showcases 10 nm Updates, FPGA Progress and Industry's First 64-Layer 3D NAND for Data Center*. 2017, Available from: https://newsroom.intel.com/news/intel-technology-manufacturing-day-china/.

[2] A. Shilov, *Samsung and TSMC Roadmaps: 8 and 6 nm Added, Looking at 22ULP and 12FFC*. 2017; Available from: https://www.anandtech.com/show/11337/samsung-and-tsmc-roadmaps-12-nm-8-nm-and-6-nm-added.

[3] K. Likharev, "Single-electron devices and their applications," *Proceedings of the IEEE*, vol. 87, no. 4, pp. 606–632, 1999.

[4] K. A. Walczak, P. L. Bergstrom, and C. R. Friedrich, "Light sensor platform based on the integration of bacteriorhodopsin with a single electron transistor," *Active and Passive Electronic Components* vol. 2011, p. 586924, 2011.

[5] P. S. K. Karre, M. Acharya, W. R. Knudsen, and P. L. Bergstrom, "Single Electron Transistor based Gas Sensing with Tungsten Nano Particles at Room Temperature," *IEEE Sensors Journal,* vol. 8, pp. 797–802, 2008.

[6] T. Kudo and A. Nakajima, "Biomolecule detection based on Si single-electron transistors for highly sensitive integrated sensors on a single chip," *Applied Physics Letters,* vol. 100, no. 2, p. 023704, 2012.

[7] P. K. Sinha and S. Sankaranarayanan, "Single Electron Transistor and its Simulation methods," *International Journal of Engineering Development and Research,* vol. 2, no. 2, p.1402100, pp. 1907–1925, 2014.

[8] F. Willy and Y. Darma, "Modeling and simulation of single electron transistor with master equation approach," *Journal of Physics: Conference Series,* vol. 739, no. 1, p. 012048, 2016.

[9] M. A. Savaikar D. Banyai, P. L. Bergstrom and J. A. Jaszczak,., "Simulation of charge transport in multi-island tunneling devices: Application to disordered one-

dimensional systems at low and high biases," *Journal of Applied Physics,* vol. 114, no. 11, p. 114504, 2013.

[10] M. A. Savaikar, *Stochastic charge transport in multi-island single-electron tunneling devices*, Ph.D. dissertation. Department of Physics, Michigan Technological University, 2013.

[11] C. Wasshuber, H. Kosina, and S. Selberherr, "SIMON-A simulator for single-electron tunnel devices and circuits," *IEEE Transactions on Computer-Aided Design of Integrated Circuits and Systems*, vol. 16, no. 9, pp. 937–944, 1997.

[12] C. Wasshuber, *Computational Single-Electronics (Computational Microelectronics),* Edited by: S. Siegfried, Springer Science & Business Media, 2011, p. 278.

[13] Y. Yun Seop, H. Sung Woo, and D. Ahn, "Macromodeling of single-electron transistors for efficient circuit simulation," *IEEE Transactions on Electron Devices,* vol. 46, no. 8, pp. 1667–1671, 1999.

[14] C. H. Lee, S. Qin, M. A. Savaikar, J. Wang, B. Hao, D. Zhang, D. Banyai, J. A. Jaszczak, K. W. Clark, J.-C. Idrobo, A.-P. Li, Y. K. Yap, "Room-temperature tunneling behavior of boron nitride nanotubes functionalized with gold quantum dots," *Advanced Materials*, vol. 25, no. 33, pp. 4544-4548, 2013.

[15] B. Hao, A. Asthana, P. Hazaveh, P. L. Bergstrom, D. Banyai, M. A. Savaikar, J. A. Jaszczak and Y. K. Yap, "New Flexible Channels for Room Temperature Tunneling Field Effect Transistors," *Scientific Reports,* vol. 6, p. 20293, 2016.

[16] M. Acharya, *Development of Room Temperature Operating Single Electron Transistor Using FIB Etching and Deposition Technology,* Ph.D. Dissertation, Electrical Engineering Department, Michigan Technological University, 2009.

[17] H. Ishikuro and T. Hiramoto, "Quantum mechanical effects in the silicon quantum dot in a single-electron transistor," *Applied Physics Letters*, vol. *71*, no. 25, pp. 3691–3693, 1997.

[18] P. Bhadrachalam, R. Subramanian, V. Ray, L.-C. Ma, W. Wang, J. Kim, K. Cho and S. J. Koh, "Energy-filtered cold electron transport at room temperature," *Nature Communications,* vol. 5, p. 4745, 2014.

[19] L. I. Glazman and V. Chandrasekhar, "Coulomb Blockade Oscillations in a Double-Dot System," *Europhysics Letters,* vol. 19, no. 7, pp. 623–628, 1992.

[20] A. A. M. Staring, *Coulomb-blockade oscillations in quantum dots and wires,* Eindhoven: Technische Universiteit Eindhoven, Philips Research Laboratories Eindhoven, 1992.

[21] M. Amman, R. Wilkins., E. Ben-Jacob, P. D. Maker, and R. C. Jaklevic, "Analytic solution for the current-voltage characteristic of two mesoscopic tunnel junctions coupled in series," *Physical Review B*, vol. 43, no. 1, pp. 1146–1149, 1991.

[22] J. G. Simmons, "Generalized formula for the electric tunnel effect between similar electrodes separated by a thin insulating film," *Journal of Applied Physics*, Vol. 34, no. 6, pp. 1793–1803, 1963.

[23] D. J. Griffiths, "The Time Independent Schrödinger Equation," in *Introduction to Quantum Mechanics*, Pearson Prentice Hall, Upper Saddle, NJ, 2004.

[24] J. Singh, “Electronic levels in semiconductors,” in *Semiconductor devices: basic principles*, John Wiley and Sons, Inc., New York, NY, 2001.

[25] C. Kittel, “Energy bands,” in *Introduction to Solid State Physics, 8th Edition*, John Wiley and Sons, Inc., New York, NY, 1971.

[26] M. Grundmann, “Band structure” in *The Physics of Semiconductors,* New York, NY, Springer, 2010.

[27] P. Hapala, K. Kůsová, I. Pelant and P. Jelínek, “Theoretical analysis of electronic band structure of 2- to 3-nm Si nanocrystals,” *Physical Review B*, vol. 87, no. 19, p. 195420, 2013.

[28] V. Ariel-Altschul, E. Finkman, and G. Bahir, “Approximations for carrier density in nonparabolic semiconductors,” *IEEE Transactions on Electron Devices*, vol. 39, no. 6, pp. 1312–1316, 1992.

[29] J. Maassen, C. Jeong, A. Baraskar, M. Rodwell and M. Lundstrom, “Full band calculations of the intrinsic lower limit of contact resistivity,” *Applied Physics Letters,* vol. 102, no. 11, p. 111605, 2013.

[30] E. Pop, R.W. Dutoon and E. Goodson, “Analytic band Monte Carlo model for electron transport in Si including acoustic and optical phonon dispersion,” *Journal of Applied Physics,* vol. 96, no. 4, 2004.

[31] A. H. Wilson, “The Theory of Electronic Semi-Conductors,” *Proceedings of the Royal Society of London, A: Mathematical, Physical and Engineering Sciences*, vol. 133, no. 822, pp. 458–491, 1931.

3 Efficient Physics-based Modeling of a Representative Semiconducting Quantum Dot Single Electron Device

This chapter has been published as a conference paper and is used with permission, from: P. K. Hazaveh, P. L. Bergstrom, and J. A. Jaszczak, "Efficient Physics-based Modeling of a Representative Semiconducting Quantum Dot Single Electron Device," *IEEE 17th International Conference on Nanotechnology (IEEE NANO 2017)*, pp. 739 – 744, 2017.

In this work, we study electron transport modeling of a semiconducting quantum dot interacting with metal electrodes. The modeling utilizes a physics-based kinetic Monte Carlo algorithm to balance accuracy with improved calculation speed, applied to the transport characteristic of a reported experimental Single Electron Transistor (SET) device with semiconducting silicon islands. We introduce an efficient numerical integration method to accurately calculate the electron tunneling rates for all allowable transitions, then apply kinetic Monte Carlo methods to simulate the electronic transport properties of the device. The method accounts for non-constant density of states and transition probabilities, and parasitic field -effect device coupling. A series of test cases have been introduced to demonstrate the relevance of the model. Two test cases explore the physical properties of the SET to confirm the proper modeling of gate, drain, source capacitances and junction widths. A third test is designed to explore the temperature sensitivity of a SET with a semiconducting island, where the results show an interesting possibility to control the temperature sensitivity of the system through the applied biases. This behavior is not

possible in metallic SET systems. The final test shows that the methodology models a representative experimental three terminal silicon single electron device with a coupled parasitic field effect transistor at low to moderate source-drain biases. The test demonstrates that the complex and aperiodic behavior of the Coulomb oscillations in the experimental device over temperature and bias cannot be fully characterized by the modeled physics of the SET or the nanoscaled MOSFET.

3.1 Introduction

As devices approach fundamentally quantum mechanical dimensions, coupled semi classical modeling solutions may still be applied even for critical dimensions down to approximately 2 nm [1]. Unlike *ab initio* methods, which cannot provide a timely solution for systems of this scale, semiclassical methods can model quantum-tunneling-based devices efficiently and rapidly where care is taken in minimizing parametric assumptions for interesting complex materials. In single electron devices with quantum dots (QDs) larger than 2 nm, if the band structure of the material and electron tunneling behavior are incorporated, more accurate transport models are possible for systems with arbitrary geometries [1, 2]

In this study, we utilize a kinetic Monte Carlo (KMC) based algorithm to simulate the current-voltage characteristic of a device with a semiconducting quantum dot and two electrodes. Master Equation approaches for calculating currents have been developed for single-island systems [3]. However, since such approaches have not been developed for multiple-island devices, we have chosen the KMC method to enable scalable system modeling in the future.

This simulator considers the physics and geometry of the system to model electron transport throughout a single dot device. To broaden the applicability of the model to devices of different types of materials, we have reevaluated many of the simplifying assumptions typically utilized by previous authors for metallic systems [1–4].

3.2 Method

The most general form for the electron tunneling rate from one energy level to another is extracted from the Fermi golden rule:

$$\Gamma_{if} = \int_{l1}^{l2} \frac{2\pi}{\hbar} |T(E)|^2 D_i(E) f(E - E_i) \times D_f\left(E - \Delta W_{if}\right)\left[1 - f\left(E - E_i - \Delta W_{if}\right)\right] dE, \tag{3.1}$$

where E_i is the Fermi energy of the initial side, D_i and D_f are the density of states functions for the initial and final states of electron, respectively. *f(E)* is the Fermi-Dirac distribution function, *T(E)* is the transition probability and ΔW_{if} is the change in the free energy of the system when a tunneling occurs across the junction from the initial to the final energy level. Limits (l_1, l_2) of the tunneling rate integral are dynamically adjusted depending on the potential difference across the junction and the highest and lowest level that can participate in tunneling.

Introducing a potential difference, V_{if}, across a junction causes the electron energy states of one side of the junction to shift by eV_{if} with respect to the other side. In addition, a small island capacitance leads to a large charging energy, E_{ch}, which also effects the change in the free energy of the system over a tunneling event, as given by [2]

$$\Delta W_{if} = -eV_{if} + E_{ch}. \tag{3.2}$$

The probability of the particle being transmitted through the barrier, $T(E)$, can be approximated by the Wentzel–Kramers–Brillouin (WKB) method [5]. There are two approximations made to calculate this probability. First, the barrier height varies over the width of the barrier. To simplify the integration, we treat the barrier as a rectangular barrier whose height is dynamically calculated (dependent upon qV_{if}) as the average height over the width. Second, for a given barrier height, we evaluate $T(E)$ at either the conduction or valence band edges. This is in contrast to previous studies for electron tunneling initiating from a metal, where the transition probability from all the energy levels is considered constant, $T(E_f)$ [1, 4]. We have verified this approximation has improved integration time with minimal impact on the tunneling rates. For example, the transition probability from the edge of the conduction band can be calculated as

$$|T_c|^2 \sim |T(E_c)|^2 = 1 \Big/ \left(1 + \frac{V_0^2 \sinh^2(k_i d)}{4E_C(V_o - E_c)}\right), \tag{3.3}$$

where E_c is the edge of the conduction band, k_i is the wave number in the first region, V_o is the average barrier height and d is the junction width [6].

In (3.1), D_i and D_j are functions of energy. In most previous theoretical work such as in the SIMON code by Wasshuber and Selberherr [4] and in MITS by Savaikar, et al. [1], the density of states for metals has been approximated as the density of states at the Fermi energy, which is an energy independent constant, $D(E_f)$, given by (3.4):

$$D(E_f) = \left(\frac{8\pi m^{3/2}}{\hbar^3}\right)\sqrt{E_f}\,. \tag{3.4}$$

This is an appropriate approximation for metals, since the participating carriers and available states are positioned energetically near the Fermi energy of the material. For

materials with more complex band structures, the density of states should not be approximated as a constant value. The complexity of the density of states approximation for the relevant band structure impacts the model complexity significantly. However, the method described allows for more appropriate choice of functions to describe the density of states for both conduction and valence bands. However, the impact of direct versus indirect bandgaps in semiconductors has not been implemented in the model. Rather, a direct bandgap semiconductor band structure with a parabolic or modified parabolic approximation is chosen. When the energy of the charge carrier diverges significantly from the minimum energy of the band, the parabolic approximation loses its accuracy in representing the band structure. At higher biases, electrons with higher energy levels will participate in tunneling in our system. In order to use the analytical band model for higher energy levels, a modified parabolic term is added in the energy model [7,8]. The modified parabolic approximation for the density of states is given by

$$D(E) = \frac{\sqrt{2}(m^*)^{\frac{3}{2}}\sqrt{(E + \alpha E^2)}(1 + 2\alpha E)}{\pi^2\hbar^3}, \tag{3.5}$$

where

$$\alpha = \frac{1}{E_g}\left(1 - \frac{m^*}{m_0}\right)^2, \tag{3.6}$$

where m^* is the effective mass in the related band (m_c^* for conduction band and m_v^* for valence band), m_0 is the free electron mass, and E_g is the band gap energy.

Replacing the density of states with a parabolic or modified parabolic model results in a tunneling rate integral (3.1) that cannot be easily solved in closed form. In this model framework, we solve this integral numerically and dynamically determine finite integration

limits. This method broadly enables future study of electron transport for idealized metal and semiconductor QD materials represented by complicated band structures, including more complex topologies with multiple QD and mixed materials. In this demonstration of the method, we assume a simple two-junction device with 3 metallic electrodes and a semiconductor quantum dot (island) as shown in Fig. 3.1 to provide a relevant test case. To take into account the band gap of the semiconductor in the tunneling rate equation, each tunneling rate is divided into two integrals. For example, in the first junction (between middle island and the left electrode) the tunneling rate from right to left (middle island to the left electrode) is the probability of electron tunneling from the conduction band of the island to the metal and the probability of electron tunneling from the valence band to the metal. Each electron tunneling event is chosen using KMC based on the calculated rates. The potential differences across the junctions and the integral limits are updated after each transition. This method is repeated until convergence to a steady state current [1].

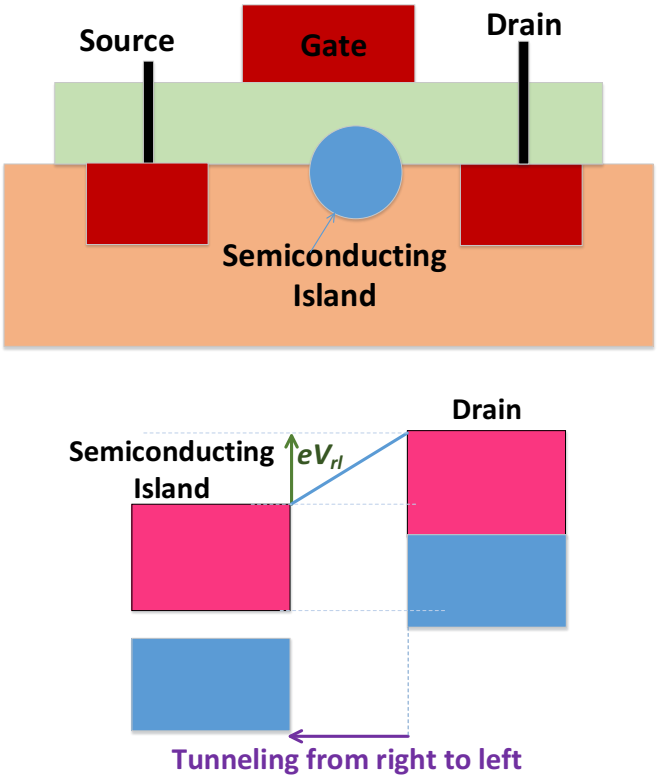

Figure 3.1. Top: Model Single Electron Device topology with three metal electrodes and a semiconductor island. Bottom: Cartoon of the QD-drain junction under an applied bias, eV_{rl}, showing a probable tunneling path from occupied states in the metal electrode to the semiconductor island conduction band. The blue represents valence or filled energy states, and the red represents conduction or available unfilled energy states over the range of potential energies considered in the model.

3.3 A Model device in a Nano-Scaled Point-Contact Metal-Oxide-Semiconductor Field Effect Transistor

In order to explore the applicability and limitations of the model framework with an experimental device, an interesting nano-scaled point contact MOSFET device by Ishikuro and Hiramoto was chosen as an intriguing application [9]. The device technology produced a single semiconducting QD at dimensions small enough for room temperature confinement of electrons on the quantum dot and incorporated a sufficient data set to study.

The device was fabricated in a *p*–type silicon on the oxide (SOI) substrate. The quantum dot and tunneling barriers are fabricated by electron beam lithography at dimensions below 10 nm. The semiconducting QD was formed in a nanoscaled top *p*–type silicon layer with narrow channels defined between source, QD, and drain to ultimately form the narrow tunneling barriers necessary in a single electron device through oxidation. The device demonstrates both Coulomb blockade behavior in the current-voltage characteristic and Coulomb oscillations with a gate potential. The device demonstrates a relatively low temperature sensitivity in the current. However, it exhibits an increasing baseline current drift with temperature. Also, the Coulomb oscillations exhibit a change in periodicity with gate bias. In what follows, test cases are utilized to establish the general validity of the model, after which the application of the model to the nanoscaled point-contact MOSFET is explored.

3.4 Model Results Using a Test Case

In order to demonstrate relevance of the modeling method for this device, three test cases are investigated to explore the validity of the assumptions and approximations made in the model. These tests examine the response of the device to variations in critical device parameters, such as charging energy and coupling capacitances to the QD, temperature, and gate effects. For each test case, the voltage increment (either gate or source-drain voltage) is set at 0.01V, and a minimum of 10,000 Monte Carlo steps are performed for each voltage increment.

3.4.1 Test I: Impact of Gate Capacitance

In a SET with a single island, when the source-drain potential is kept constant and small, the gate voltage-current characteristic of this device should demonstrate periodic oscillations, known as Coulomb oscillations. The period depends on the gate capacitance (e/C_g) and the discreetness of the energy levels on the island [10]. Since the modeled QD diameters are larger than 2 nm, the discreetness of energy levels is ignored in the model [11]. The current-gate voltage (I_dV_g) characteristic is plotted in Fig. 3.2, for estimated source and drain junctions of 0.5 nm and 1.5 nm, respectively, based on source and drain capacitances of 0.8 aF and 0.5 aF, respectively, and an island radius of 3 nm, as given by [9]. The current-gate voltage characteristic has been modeled at two gate capacitances. The Coulomb oscillation period reduces by half as the gate capacitance doubles, as expected. This confirms that the algorithm is modeling the gate effect properly.

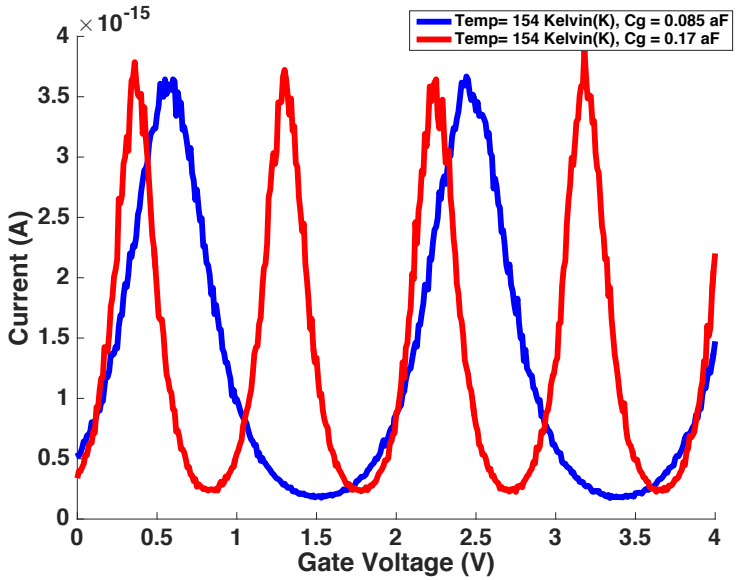

Figure 3.2. Coulomb oscillation characteristics of a SET with one semiconductor QD, for two different gate capacitances. The model was conducted with a source-drain potential (V_{sd}) of 0.5 V, at a temperature of 154 K, for a gate capacitance that doubles from one condition to the next.

3.4.1 Test II: Impact of Charging Energy

The primary effect of decreasing the charging energy is to broaden the width of the Coulomb oscillation peak [12]. It is shown in Fig. 3.2, that this effect results in Coulomb oscillation peaks that are broader and shifted in gate potential. The period of the peaks depends on the gate capacitance, which in this case is kept constant at 0.085 aF. The period for both of the conditions (green and blue) are the same. Because the current is not totally suppressed between the expected Coulomb oscillations for the lower charging energy of 9×10^{-21} J at the tested temperature of 154 K, we observe that the Coulomb blockade is suppressed. This shows that the charging energy plays the expected role in this system and the simulation is capable of properly taking into account the effect of the charging energy. The thermal energy for T = 154 K, is $k_B T = 2\times10^{-21}$ J, where T is the temperature and k_B is the Boltzmann constant. The charging energy of the system related to the blue plot is larger than the thermal energy so a Coulomb blockade is observed. The charging energy of the system related to the green plot is smaller than the thermal energy, so the Coulomb blockade is suppressed.

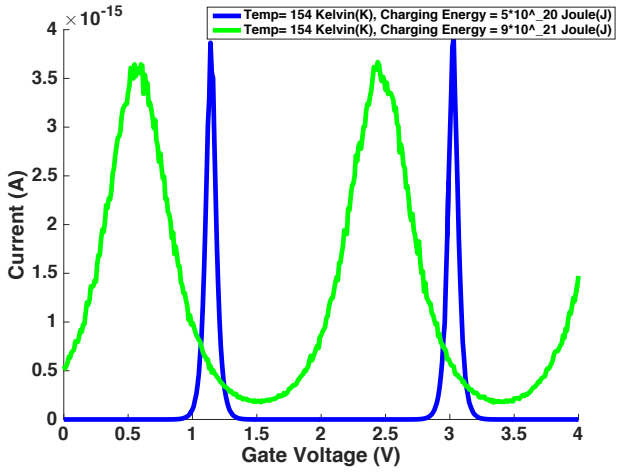

Figure 3.3. Current-Gate Voltage plot for a source-drain potential of 0.5V at 154 K. The plots show two different charging energies. The effect of charging energy shifts and modulates the peak width, and suppresses the Coulomb blockade for the smaller charging energy tested.

3.4.1 Test III: Impact of Geometry on the Transition Probability

The second test to demonstrate the relevance of the modeling method is related to the geometry of the system. As mentioned in the "Method" section, the transition probability in (3.3) depends on the geometry of the barrier. The junction width, *d*, plays a primary role in the transition probability. As the junctions proportionally increase in width while maintaining their ratio, the peak current falls as predicted in (3.3) and (3.1) and as shown in Fig. 3.4 below.

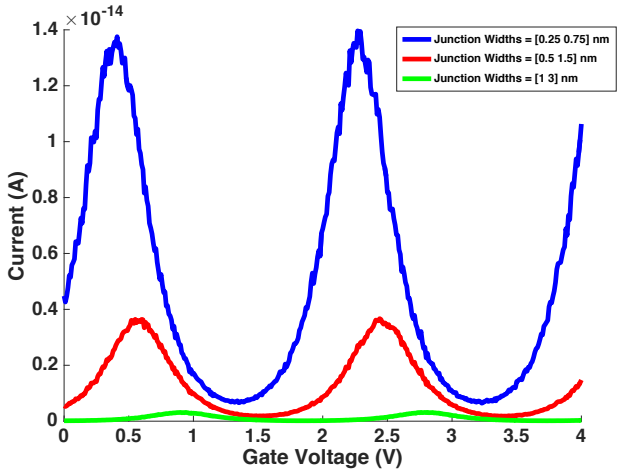

Figure 3.4. The gate voltage characteristic for different junction widths, *d*. As we expect, the peak current reduces as the junction increases in width. To represent the modeled device, assymetric junction widths for left and right junctions are presented, scaled by a factor of two over three conditions at a temperature of 154 K.

3.5 Nano Point-Contact MOSFET Model Application

To explore the terminal and temperature behavior of the current-gate voltage characteristic of the fabricated nano-scaled point contact MOSFET device by Ishikuro and Hiramoto [9], we study the temperature sensitivity of the individual SET device with a constant source-drain voltage and the baseline current of the nano-MOSFET model.

3.5.1 Temperature Dependence

In a SET with a semiconducting island, if there is a path for electrons to tunnel from near the Fermi energy of the right electrode to the conduction band of the semiconducting island, and tunnel from the valence band of the island to the left electrode, then the temperature effect on the SET's behavior is insignificant. This is demonstrated by a simple model outlined in Fig. 3.5 Since the conduction band has many unoccupied energy levels and the valence band has many available electrons, when a higher constant source-drain

voltage is applied to the system (1.2 V instead of 0.5 V), the current increases significantly. At this bias condition, the island's potential rises to 0.6 V, and a significant path opens for electrons in the slower (wider) junction to tunnel from the right electrode to the conduction band of the middle island. Also, the valence band of the middle island is aligned with energies close to the Fermi level of the left electrode in the faster (narrower) junction. For this condition, the current remains in the same order of magnitude as the temperature is changed from 77 K to 300 K, demonstrating a low temperature sensitivity. The Coulomb blockade behavior is increasingly suppressed as the temperature increases since the charging energy is of the same order of magnitude as the thermal energy.

However, if we keep the source drain potential constant but small, so that no convenient electron-tunneling path exists, as shown in the top of Fig. 3.6, we can observe a strong temperature effect on the current-gate voltage characteristic of the device, shown in the bottom of Fig. 3.6 for two temperatures. The current magnitude increases over four orders of magnitude from 154K to 300K. When the biases of the system are low, the thermally excited electrons are those that primarily participate in tunneling and generate the current flow through the device. As observed in the simple model in Fig. 3.6, the electron-tunneling path is from energy levels above the Fermi energy in the right electrode to the island's conduction band and from the islands valence band to the energy levels below the Fermi energy of the left electrode. The occupancy of energy levels that are involved in tunneling is strongly temperature sensitive.

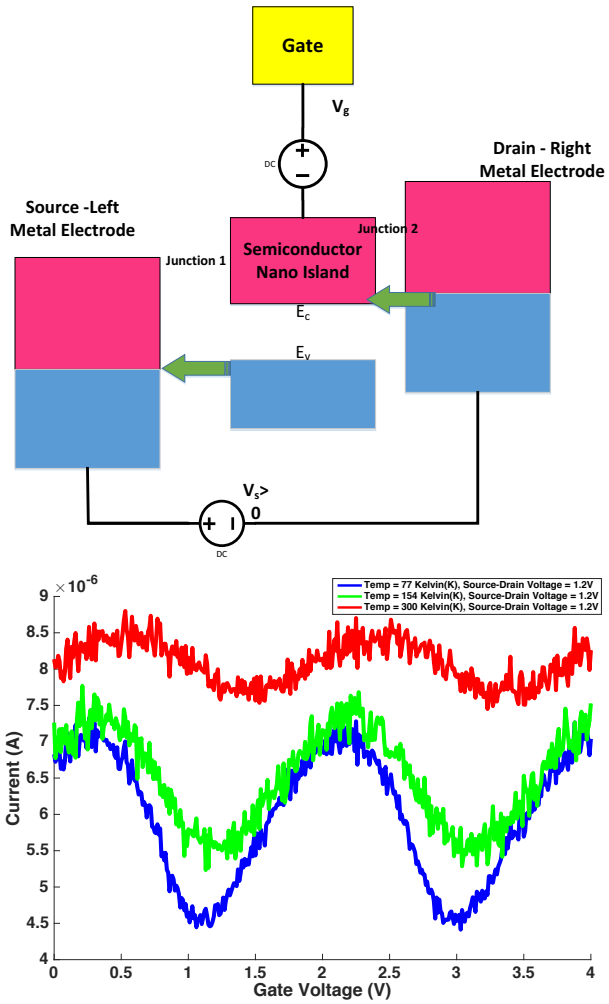

Figure 3.5. Top: The band diagram model of a system with two metal electrodes and a semiconducting island. The islands potential is 0.6V, the source-drain voltage is 1.2 V and the gate voltage is 3.9V. The Fermi level of the right electrode is overlapping the conduction band and the valence band of the island is aligned with energy levels of the left metal electrode's Fermi level. Bottom: The current-gate voltage characteristic for a contant source-drain voltage (V_{sd}) of 1.2 V for temperatures of 77 K, 154 K, and 300 K. These characteristics are weakly temperature dependent.

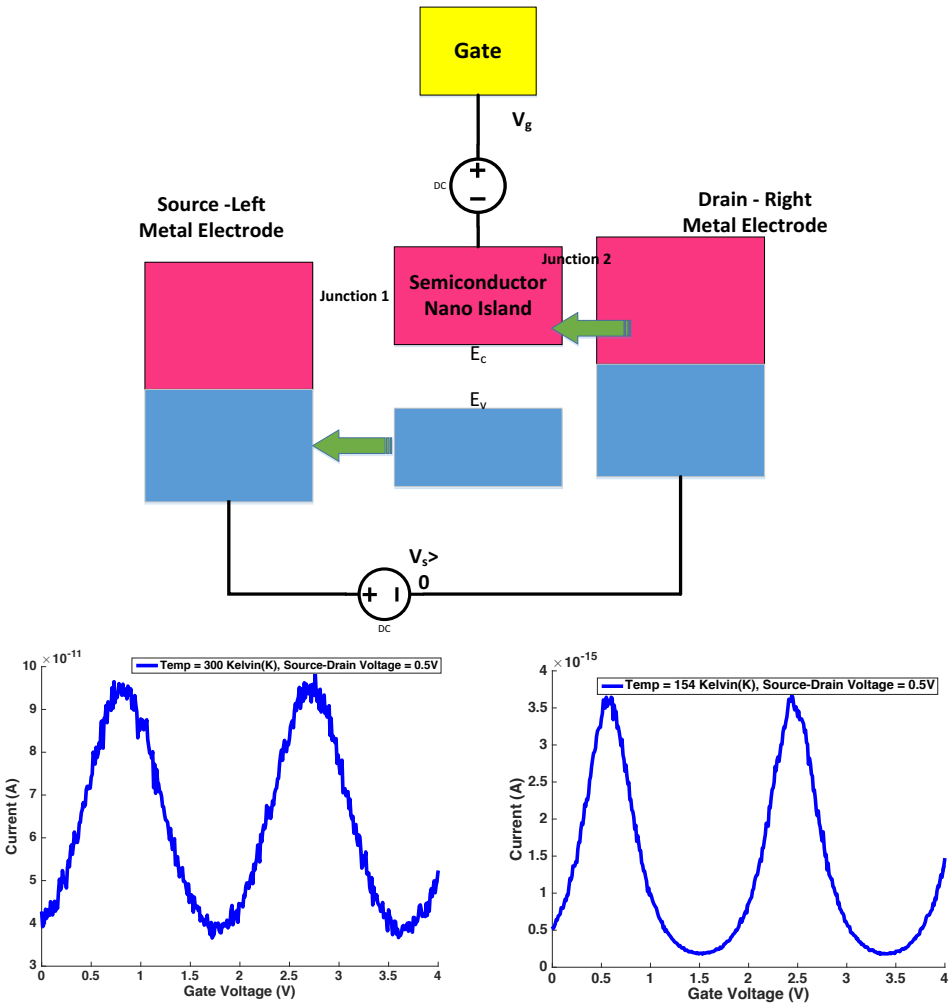

Figure 3.6 Top: The band diagram model of a system with two metal electrodes and the semiconducting island. The QD island potential is 0.2 V and V_{sd} = 0.5 V in this figure. The potential difference of across each of the junctions is not sufficient for the Fermi energy to be aligned with the conduction or valence band. Bottom: The current-gate voltage characteristic for a constant source drain voltage (V_{sd}) of 0.5 V for 2 different temperatures of 154 and 300 K. The current is temperature sensitive and varies over 4 orders of magnitude here.

3.5.2 Baseline Current

Having confirmed the consistency of the method, the interesting temperature behavior of the experimental device along with an exploration of the baseline current drift with

temperature require exploration. The experimental I_dV_g behavior exhibits a total current that appears to be a combination of MOSFET and SET characteristics. Whereas an ideal SET is expected to show a periodic Coulomb oscillation where the current returns to a uniform minimum in the period of oscillation, the experimental *IV* result shows a steady increase in a background current upon which the Coulomb-oscillation is superimposed. The I_d-V_g characteristic of a nanoscale MOSFET is calculated using (3.7)

$$I_D = \frac{W_t}{L_t}\mu_{app}C_{ox}\left(V_{gs} - V_T\right)V_{ds}\ , \tag{7}$$

where W_t and L_t are width and length of the transistor, C_{ox} is the oxide capacitance, μ_{app} is the apparent mobility, V_T is the threshold voltage, V_{gs} is the gate-source voltage, and V_{ds} is the drain-source voltage [13–14]. These parameters are extracted from the experimental device and are shown in Table 3.1 below. The SET characteristic of the device is calculated by the model. Adding the nanoscale MOSFET model represented by (3.7) in parallel with the SET model results in a strong correlation at room temperature between the experimental and modeled behavior, and is shown in Fig. 3.7. The combined current is the sum of the nano-MOSFET and the individual SET currents.

Table 3.1: Extracted nanoscaled MOSFET parameters from [8].

W_t	8 nm
L_t	6 nm
μ_{app}	9.987×10^{-6} m^2/Vs
C_{ox}	1.77×10^{-3} F/m^2
V_T (at 320 K)	0.73 V

The SET parameters in Test I above were chosen so that the resulting total current was on the same order of magnitude of the experimental device and were utilized in this characterization. However, the experimental results are less temperature sensitive for the SET behavior than the physics of the device would indicate. The impact of these differences is discussed below as it relates to the relevance of the modeling method for this device demonstration.

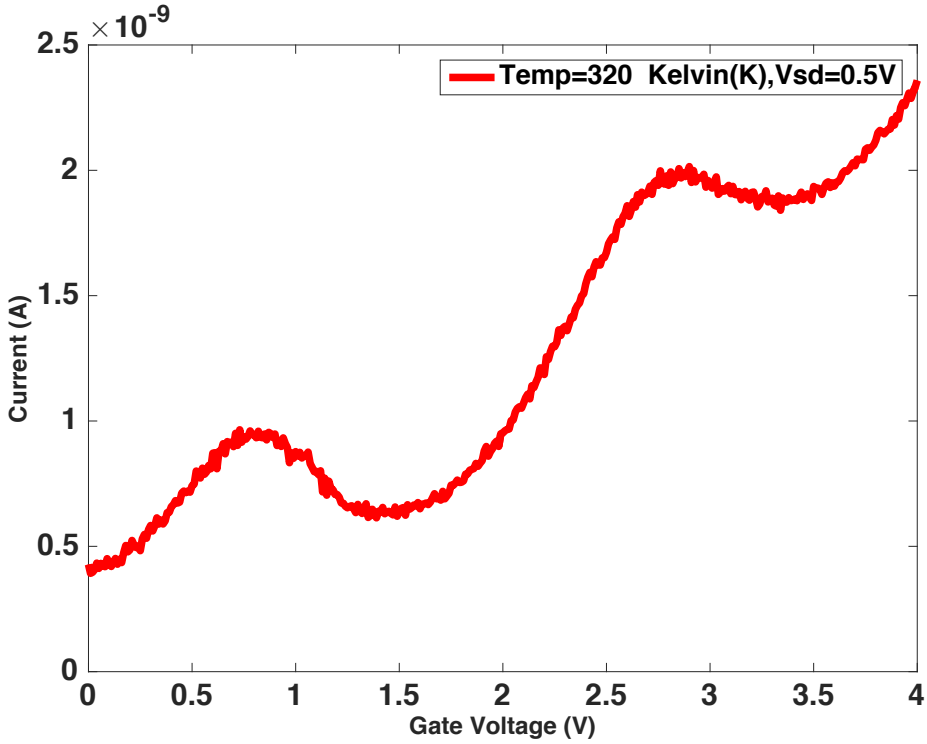

Figure 3.7. Modeled current-gate voltage characteristic of a single electron device in parallel with a nano MOSFET at T = 320 K and a constant source. drain voltage of 0.5 V.

3.6 Discussion and Conclusions

The test cases in this paper have been presented to demonstrate the viability of the modeling framework to explore the behavior of relevant device demonstrations based on the physics of the SET system for QD larger than 2 nm. The proper relationship of the gate

potential, device geometry, and charging energy impact on Coulomb blockade and oscillations have been demonstrated. The sensitivity of the SET output current to temperature was shown to be strongly dependent on terminal potentials and other parameters for the device. Temperature insensitive and strongly temperature sensitive characteristics were observed for the same device under different terminal conditions.

The low temperature sensitivity and weak periodicity of the experimental device by Ishikuro and Hiramoto does not follow what was expect from the physics that support the simulation framework. The temperature sensitivity of the experimental device with the conditions defined in the reference is not as large in magnitude as observed in the modeling under the test conditions. Also, the current oscillation in the experimental device indicates a change in periodicity over gate potential, which cannot be explained by the physics included in the model for the parameters given for the device.

3.6.1 Temperature Sensitivity

The *IV* characteristic of the experimental device over temperature indicates that the temperature sensitivity is relatively weak for the SET behavior. This may indicate that a significant path for electron tunneling has been opened (Fig. 3.5); however, the given parameters and biases do not support this hypothesis. Under these conditions, the model exhibited a strong temperature dependence. However, under different bias conditions, the model did demonstrate a weaker temperature sensitivity. We surmise that the estimated and extracted parameters for the SET device do not fully represent the characteristics for its behavior.

Some strong impacts on the model results would be a change in the charging energy of the QD, the junction capacitances, the formation of multiple quantum dots in the channel, or

the impact of the inversion layer channel formed in a MOSFET device on the geometry or electron confinement of the QD island in the SET. Without additional evidence to confirm these parameters, a more complete model for this device cannot fully represent the thermal behavior of the experimental device.

The ability to control the temperature sensitivity with input biases is a unique characteristic of the semiconducting SETs compared to metallic island devices, being caused and modulated by their energy bandgap. This characteristic represents and interesting behavior to explore for quantum devices in the future.

3.6.2 The Periodicity of Coulomb Oscillation Characteristic

The current-gate voltage characteristic in the experimental device has an oscillatory behavior with a significant variation (up to 30%) in the periodicity with gate potential. The physics of the model presented does not reproduce nonperiodic current oscillations. The island radius is given as 3 nm, which suggests that size induced discreteness in the density of states can be ignored [11]. In such a device, the periodicity of the peaks depends only on the gate capacitance and remains constant for a specific device. Ishikuro and Hiramoto propose, consistent with Zhuang, et al. [10], that the oscillatory variation is based on discrete states in the island. On the other hand, this seems inconsistent with a 3 nm radius, for which we would expect a continuous density of states [11].

3.6.3 Reference List

This chapter is published as a conference paper and reprinted, with permission, from P. K. Hazaveh, P. L. Bergstrom and J. A. Jaszczak, “Efficient physics-based modeling of a

representative semiconducting quantum dot single electron device," *IEEE 17th International Conference on Nanotechnology (IEEE NANO 2017)*, pp. 739 – 744, 2017.

[1] M. A. Savaikar, D. R. Banyai, P. L. Bergstrom, and J. A. Jaszczak, "Simulation of charge transport in multi-island tunneling devices: Application to disordered one-dimensional systems at low and high biases," *Journal of Applied Physics* vol. 114, no. 11, 114504, 2013.

[2] K. K. Likharev, "Single-electron devices and their applications," *Proceedings of the IEEE*, vol. 87, no. 4, pp. 606–632, 1999.

[3] M. Amman, R. Wilkins, E. Ben-Jacob, P. D. Maker, and R. C. Jaklevic, "Analytic solution for the current-voltage characteristic of two mesoscopic tunnel junctions coupled in series," *Physical Review B*, vol. 43, no. 1, 1146, 1991.

[4] C. Wasshuber, H. Kosina, and S. Selberherr, "SIMON-A simulator for single-electron tunnel devices and circuits," *IEEE Transactions on Computer-Aided Design of Integrated Circuits and Systems*, vol. 16, no. 9, pp. 937–944, 1997.

[5] J. G. Simmons, "Generalized formula for the electric tunnel effect between similar electrodes separated by a thin insulating film," *Journal of Applied Physics*, vol. 34, no. 6, pp. 1793–1803, 1963.

[6] M. Grundmann, *The Physics of Semiconductors: An Introduction including Nanophysics and Applications*, 2nd Ed., New York, NY, Springer, DOI: 10.1007/978-3-642-13884-3, 2010.

[7] E. Pop, R. W. Dutton, and K. E. Goodson, "Analytic band Monte Carlo model for electron transport in Si including acoustic and optical phonon dispersion," *Journal of Applied Physics*, vol. 96, no. 9, pp. 4998–5005, 2004.

[8] C. Jacoboni and L. Reggiani, "The Monte Carlo method for the solution of charge transport in semiconductors with applications to covalent materials," *Reviews of Modern Physics*, vol. 55, no. 3, pp. 645–705, 1983.

[9] H. Ishikuro and T. Hiramoto, "Quantum mechanical effects in the silicon quantum dot in a single-electron transistor," *Applied Physics Letters*, vol. 71, no. 25, pp. 3691–3693, 1997.

[10] L. Zhuang, L. Guo, and S. Y. Chou, "Silicon single-electron quantum-dot transistor switch operating at room temperature," *Applied Physics Letters*, vol. 72, no. 10, pp. 1205–1207, 1998.

[11] P. Hapala, K. Kůsová, I. Pelant, and P. Jelínek, "Theoretical analysis of electronic band structure of 2-to 3-nm Si nanocrystals," *Physical Review B*, vol. 87, no. 19, p. 195420, 2013.

[12] L. P. Kouwenhoven, C. M. Marcus, P. L. McEuen, S. Tarucha, R. M. Westervelt, and N. S. Wingreen, "Electron transport in quantum dots," in *Mesoscopic Electron Transport*, pp. 105–214. Springer Netherlands, 1997.

[13] J. Lee, J. H. Lee, I.-Y. Chung, C.-J. Kim, B.-G. Park, D. M. Kim, and D. H. Kim, "Comparative study on energy-efficiencies of single-electron transistor-based binary full adders including non-ideal effects," *IEEE Transactions On Nanotechnology,* vol. 10, no. 5, pp. 1180–1190, 2011.

[14] M. Zilli, D. Esseni, P. Palestri, and L. Selmi, “On the apparent mobility in nanometric n-MOSFETs,” *IEEE Electron Device Letters,* vol. 28, no. 11, pp. 1036–1039, 2007.

4 Impact of Band Gap and Discrete Energy Levels on Temperature Sensitivity of a SET Device

In this chapter, the simulation framework presented in chapter two is utilized to predict electron transport in SET devices with an island with discrete energy levels, based on their electrical properties and energy band structure. In particular, the temperature sensitivity of SET devices with one island is studied and the impact of energy gap and discrete energy levels of the island on device's performance is investigated. For the model studied, the discreteness of energy levels cannot be ignored as the energy spacing between energy levels is comparable to other energy scales of the system, such as the charging energies. The characteristic of a SET with a semiconducting island with discrete energy levels in addition to a band gap is investigated and compared to a continuous-band model metallic island over temperature. This study shows that the band gap and discrete energy levels present in semiconducting quantum dots result in operational conditions which, with proper biases, demonstrates relative temperature insensitivity in the SET devices.

A test case is introduced to test the validity of the simulation framework and assumptions, by simulating the *IV* characteristics of SET devices under different biases and temperatures. A theoretical model is proposed in final section which indicates operating conditions to control the temperature sensitivity of the current-source drain voltage (IV_{sd}) characteristic of the device, utilizing the band gap and a gate electrode. Conditions where electrons with particular thermal energies may be blocked from tunneling by applying a targeted potential to the gate electrode and inhibiting the tunneling probability in the forbidden energy bands, are examined.

4.1 Method

In nanometer-scale SET devices, introducing a bias across the source-drain electrodes, a potential difference falls across each junction (V_{if}) and shifts the electron energy levels on one side of the junction with respect to the other side by eV_{if}. The smaller junctions in SET devices lead to larger charging energies (E_{ch}). In the case of an electron tunneling event, the charging energy changes the free energy of the system. The total change in the free energy of the system for a tunneling event is given by [1]:

$$\Delta W_{if} = -eV_{if} + E_{ch}. \tag{4.1}$$

In this study, we are using the general tunneling rate equation from one level to another, as utilized by Amman et al. [2] and Savaikar et al. [3]:

$$\Gamma_{ij} = \int_{l1}^{l2} \frac{2\pi}{\hbar} |T(E)|^2 D_i(E)\, f(E - E_i) D_f\big(E - \Delta W_{if}\big) \times \big[1 - f\big(E - E_i - \Delta W_{if}\big)\big] dE\,, \tag{4.2}$$

where E_i is the Fermi energy of the initial side, D_i and D_j are the density of states functions for the initial and final states of the electron, respectively. *f(E)* is the Fermi-Dirac distribution function, *T(E)* is the transition probability and ΔW_{if} is the change in the free energy of the system when a tunneling event occurs across the junction from the initial to the final energy state. Integral limits, l_1 and l_2 are dynamically adjusted somewhere between the ground (0) and the electron affinity, depending on the potential difference across the junction. For each band structure model introduced we have replaced terms with proper approximations in the tunneling Eq. 4.2 to calculate the rates. When the rates are known a KMC based algorithm is used to predict the IV_{sd} characteristic of the devices.

4.2 Temperature Dependence of a SET with a Metallic Island

In this section, we explore the temperature sensitivity of a SET device with a metallic island. Two model frameworks have been examined; one of a SET with a metallic island where the energy levels are modeled using the semi classical continuous band model [3], and a second where the island's energy levels are modeled as discrete [2].

4.2.1 Metallic Island: Continuous Band Model

Following work of Savaikar et al. [3] we utilize a model with a metallic island and two metallic electrodes, which is simple enough to examine the effect of discreteness of energy states of the island. Figure 4.1, shows a simple schematic of this device. Under a positive source-drain bias and at zero temperature, the marked tunneling paths in Fig. 4.1 are the probable tunneling paths for electrons with energies close to the Fermi energy. The density of states is modeled using a parabolic continuous band structure [4]. Carriers and available energy levels participating in electron transport for metals are positioned energetically near the Fermi energy, so the density of states of the metal is approximated as a constant, $D(E_f)$, which is the density of states at the Fermi energy [3, 5, 6], and can be calculated using expression below:

$$D(E_f) = \left(\frac{8\pi m^{\frac{3}{2}}}{\hbar^3}\right)\sqrt{E_f}\ , \tag{4.3}$$

where m the electron mass, E_f is the Fermi energy of the right electrode and $\hbar$ is the reduced Planck's constant.

The probability of the particle being transmitted through a rectangular barrier can be approximated as below [5-7]:

$$|T(E)|^2 = \left[1 + \frac{V_0^2 \sinh^2(k_1 d)}{4E(V_0 - E)}\right]^{-1}, \tag{4.4}$$

where

$$k_1 = \frac{\sqrt{2m(V_0 - E)}}{\hbar}, \tag{4.5}$$

E is the electron's initial energy, V_0 is the barrier height and d is the barrier width [8]. For the metallic electrodes, the particle's initial energy state is considered to be the Fermi energy, so the transition probability is reduced to a constant, $|T(E_f)|^2$. Using (4.2) and calculating the tunneling rates, the IV_{sd} characteristic of the metallic SET can be predicted using a KMC based algorithm. Narrow tunnel junctions result in larger charging energies. Under certain positive biases, Coulomb blockade steps are captured in the IV_{sd} characteristic of the metallic SET. Figure 4.2 demonstrates the current steps at T = 0 K. The capacitances are chosen at a scale so that the charging energy and input bias range are comparable in order to clearly capture the Coulomb blockade steps.

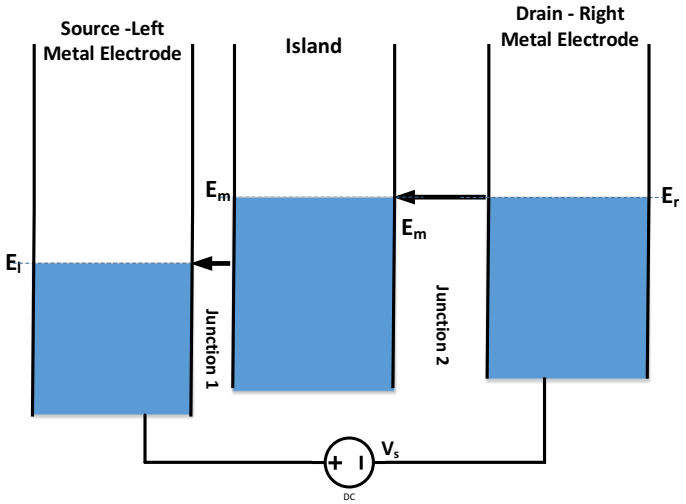

Fig. 4.1. Schematic of a two junction SET with two metallic electrodes and one metallic island, under a positive source-drain bias. This figure shows probable tunneling paths from

occupied states in the metallic electrode/island to the available levels in island/electrodes. The dark blue is marking the full energy bands at zero temperature.

As the source-drain bias increases, electrons gain enough energy to overcome the charging energy so the Coulomb staircase appears in the IV_{sd} characteristics of the device. As the temperature increases the thermally excited electrons start participating in tunneling and the Coulomb steps start fading away. The Coulomb steps disappear at T = 300 K.

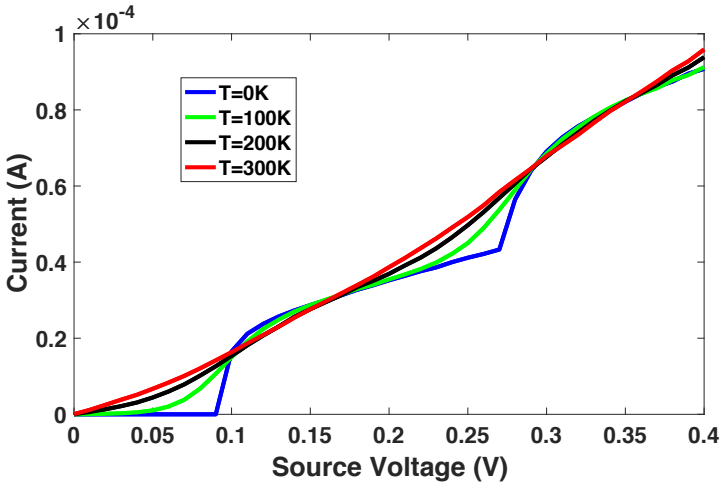

Figure 4.2. The current versus source-drain voltage characteristic of a SET with a metallic island for temperatures of 0, 100 K, 200 K and 300 K. C_1 = 0.5 aF, C_2 = 0.8 aF and number of MC cycles 10,000 for each source-drain voltage.

4.2.2 Island with Discrete Energy Levels

As the size of the island decreases the energy confinement increases. If the spacing between energy levels is comparable to other energy scales in the system, such as the source-drain bias (V_{sd}) and charging energies, then the confinement cannot be ignored and should be considered in calculating tunneling rates; therefore, the continuous band model is no longer suitable [9]. Following the method of Amman et al. [2], we introduce a simple density of states model for discrete energy levels of the island as follows:

$$D\left(E - E_f\right) = D(n\Delta E)\sum_{n=0}^{\infty}\delta(E - E_f - E_o - n\Delta E)\ , \tag{4.6}$$

where ΔE is the energy spacing between the discrete levels, n is the index number of the discrete energy levels, E_0 is the ground state energy and E_f is the Fermi energy of the island. $D(\Delta E)$, is the density of states model for each energy level ($n\Delta E$). Following Amman et al. [2], we consider the discrete energy levels to be of zero energy width and spaced equally apart. Replacing relevant terms in (4.1), the tunneling rate to the island with confined energy levels can be calculated using expression below:

$$T_{ij} = \frac{\Delta E}{e^2 R_{ij}}\sum_{n=0}^{\infty}[(e^{\left[-e\left(V_{ij}\right)+E_{cc}+E_0+n\Delta E\right]}+1)(e^{-(E_0+n\Delta E)}+1)^{-1}, \tag{4.7}$$

where R_{ij} is the junction's resistance, which is calculated dynamically depending on the transition probability, and (V_{ij}) is the potential difference across the junction. The other tunneling rates can be calculated using the same method. If the tunneling rates are known, the current-voltage characteristic of this device under other conditions can be predicted using a KMC based approach.

The transition probability can be calculated using the following energy independent expression [5-7, 13]:

$$\left|T\right|^2 \quad \left|T(E_\alpha)\right|^2 = \left[1+\frac{V_0^2\sinh^2(k_1 d)}{4E(V_0 - E_\alpha)}\right]^{-1}, \tag{4.8}$$

where E_α, is the initial energy state of the electron, k_1 is the wave number, V_o is the average barrier height and d is the junction width. Although the simulation method is capable of calculating the tunneling rate with the transition probability as a function of E, replacing it with a fixed transition probability approximation based on E_α taken either to be the

conduction or the valence band edge energy, as appropriate, improves the time efficiency with negligible error.

All the tunneling rates across the junctions can be calculated under different external and internal factors such as charging energies, input biases and temperature using (4.7). Once the tunneling rates are known, the current-voltage characteristic of this device can be predicted using a KMC based approach. A test case has been designed to test the validity of the simulation model.

The current-voltage characteristic of a SET with an island with discreet energy levels and no band gap is explored as a test case. A simple schematic of this model is outlined in Fig. 4.3, showing the most probable tunneling paths at zero temperature and under positive source-drain bias. The island has discrete energy states of 0.015 eV as was chosen originally by Amman et al. [2]. The density of states of this simple model can be expressed as Eq. 4.6. When a positive bias is applied, Coulomb staircase (the larger step) and current steps which are a result of discrete energy levels available in the island (smaller steps), are both observed at $T = 0$ K, as demonstrated in Fig. 4.4 This result is in agreement with what was observed by Amman et al. [2]. If the thermal energy is greater than the energy spacing, the thermally excited electrons will participate in tunneling events and the discreteness induced steps become indiscernible. The same phenomena modeled at higher temperatures results in the Coulomb staircase to become rounded, as observed in the metallic island case, as thermally excited electrons increase participation in tunneling. The impact of the temperature is studied in more details in section 5.

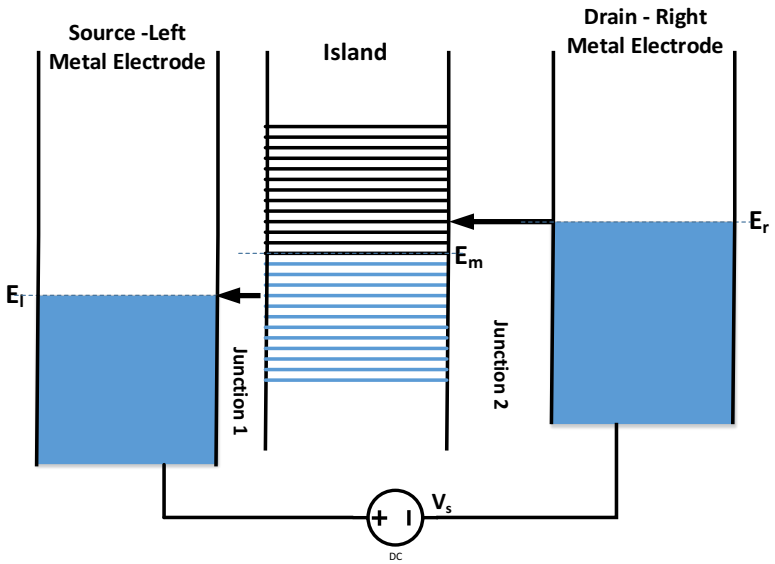

Figure 4.3. Schematic of a source-island-drain junctions under an applied bias, (V_{sd}) showing a probable tunneling path from occupied states in the right metallic electrode to the metallic island's unoccupied discreet energy levels, and, from the island's discrete levels to the left electrode.

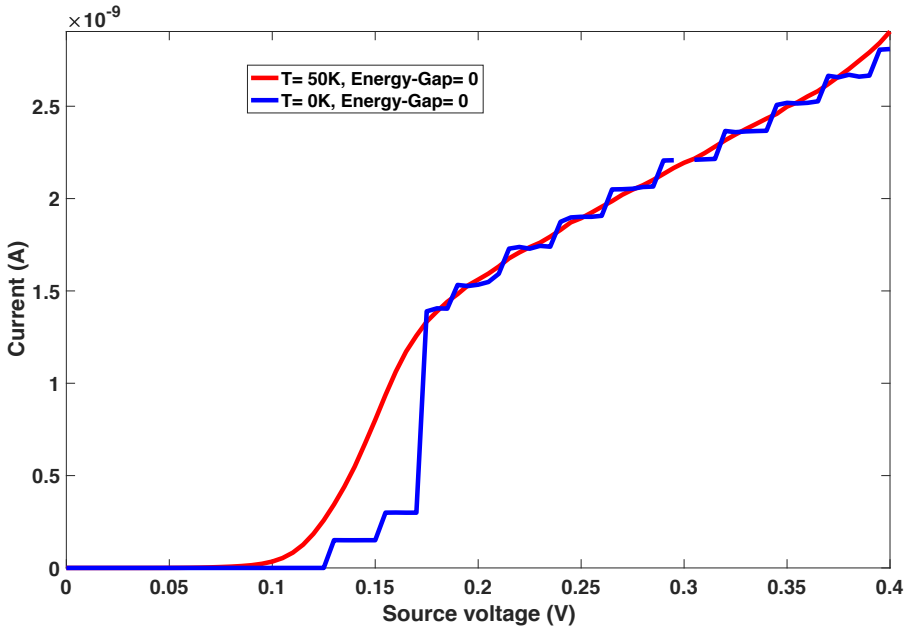

Figure 4.4. The current -Source voltage characteristic of a SET with an island with discrete energy levels of 0.15 eV for temperatures of 0 and 50 K. The discreteness induced steps and Coulomb staircase becomes indiscernible due to the electron tunneling by thermally excited electrons, number of energy levels is 3000 and number of MC cycles is 10,000.

4.3 Results and Discussion

The effect of island's energy gap and the number of available discrete energy levels within the tunneling energy range is explored for the current-voltage characteristic of a SET device. We also propose a theoretical model that can be engineered in the future to control the temperature sensitivity of SET devices.

4.3.1 Impact of the Band Gap on Current-Voltage Characteristic of a SET with a Small Semiconducting Island

The impact of band gap on the current-voltage characteristic of a SET device with a discrete multi-energy-level quantum dot as an island is explored. Figure 4.5 shows a simple schematic for this system. The characteristic exhibits a threshold voltage and discrete induced steps in the current. At zero temperature and zero bias, electrons do not have enough energy to tunnel, if the source-drain voltage increases sufficiently, then electrons can flow through the device and current increases above zero, this is referred to as the threshold voltage. If the band gap increases, the first available energy level in the island is positioned energetically further from the Fermi level of the electrodes so a larger bias is required so electrons can overcome the gap therefore the threshold voltage increases. As demonstrated in Fig. 4.6 for larger band gaps, the threshold voltage increases as we expect, which confirms that our model is capturing the impact of the band gap properly.

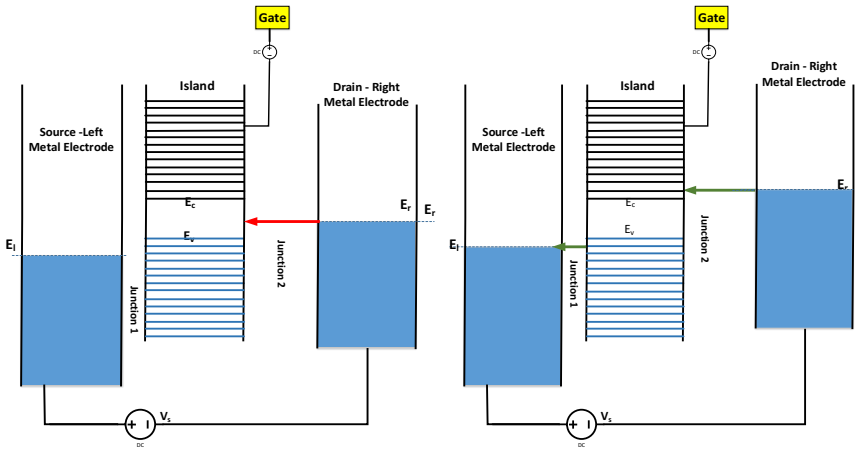

Figure 4.5. Schematic of a SET device under a positive source-drain bias (V_{sd}). The island has a band gap and discrete energy levels. The empty discrete energy levels are outlined in black; the dark blue area represents the fully filled levels at $T = 0$ K. Left: At $T = 0$ K, under small bias conditions, the electron tunneling path from energy states near the Fermi level of the right electrode to the middle island is blocked (red arrow). Right: At $T = 0$ K, under suitable bias conditions, the electron tunneling is facilitated. The green arrow shows an allowed tunneling path.

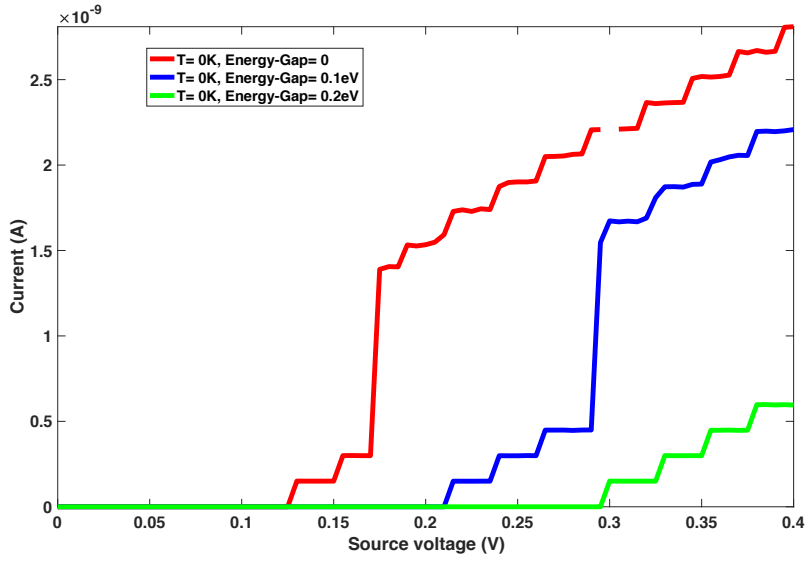

Figure 4.6. The current versus source-drain voltage characteristic of a SET device with a single island at $T = 0$ K for band gaps of 0, 0.1 eV and 0.2 eV, and discrete energy levels (ΔE) of 0.015 eV. $C_1 = 0.5$ aF, C_2=0.8 aF, $C_g = 0.085$ aF, number of energy levels is 3000 and number of MC cycles is 10,000 for each source-drain voltage.

4.3.2 Impact of Number of Energy Levels on the Current-Voltage Characteristic of a SET with a Small Semiconducting Island

In a SET device with one island, as the number of available energy levels in the tunneling energy range decreases, the probability of electron tunneling drops as well. Figure 4.7 shows a simple comparison between two models, one with 8 energy levels available in the tunneling range and one where energy levels are available over the entire tunneling energy range. The current steps observed at low temperatures in Fig. 4.7 are due to the discreteness of energy levels in the island. It is observed that if there are fewer energy levels available in the island, the magnitude of current in the Coulomb oscillation peaks decreases, as expected.

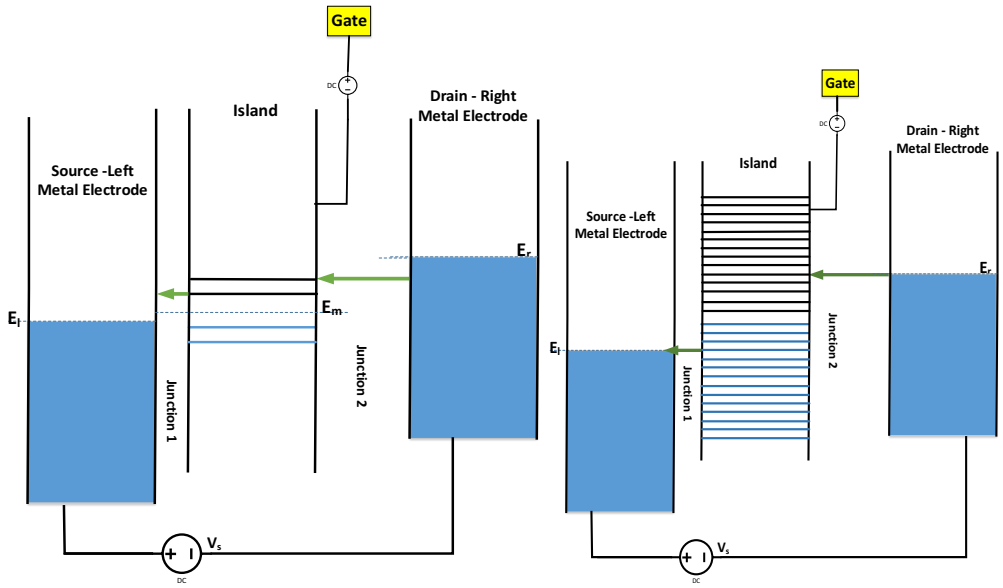

Figure 4.7. Schematic of a SET device with a semiconducting island at $T = 0$ K. The empty energy levels are outlined in black; the dark blue area is a representation of filled levels at $T = 0$ K. Left: Four energy levels are actively participating in tunneling events. Right: Discrete energy levels are available over the entire tunneling energy range.

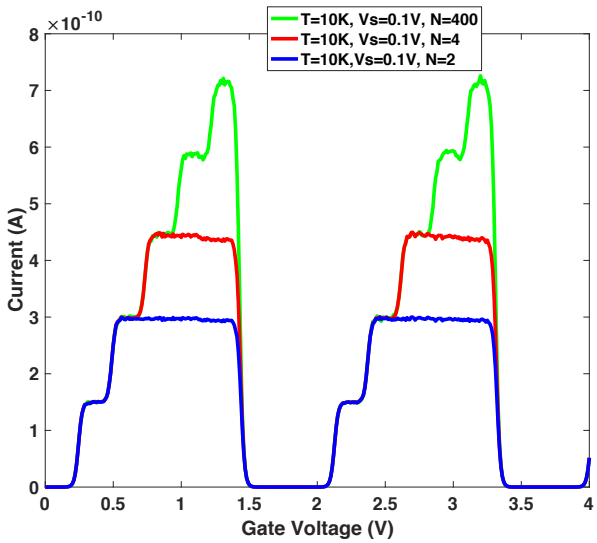

Figure 4.8. The current-gate voltage characteristic of SET devices with discrete energy levels and an energy spacing of $\Delta E = 0.015\text{eV}$, $C_1 = 0.8$ aF, $C_2 = 0.5$ aF, $C_g = 0.085$ aF, number of energy levels is 400 and number of MC cycles is 10,000 for each gate voltage.

4.3.3 Impact of Temperature on the IV_{sd} Characteristic of a SET with a Small Semiconducting Island

We utilize the same simple model as previous section, an island with a band gap of 0.2 eV and discrete energy levels of 0.015 eV to study the impact of increasing the temperature on the IV_{sd} characteristic of the SET device. At lower temperatures under sufficient bias conditions electron tunneling can occur. By increasing the temperature under the same bias conditions, the thermally excited electrons are available to tunnel from higher energy levels, as well as the electrons near the Fermi energy; therefore, the tunneling rates increase. Figure 4.9 is a simple schematic of this model for clarity. As observed in Fig. 4.10, the current steps observed at T = 0 K become indiscernible at T = 50 K, due to participation of thermally excited electrons from higher energy levels in the tunneling events.

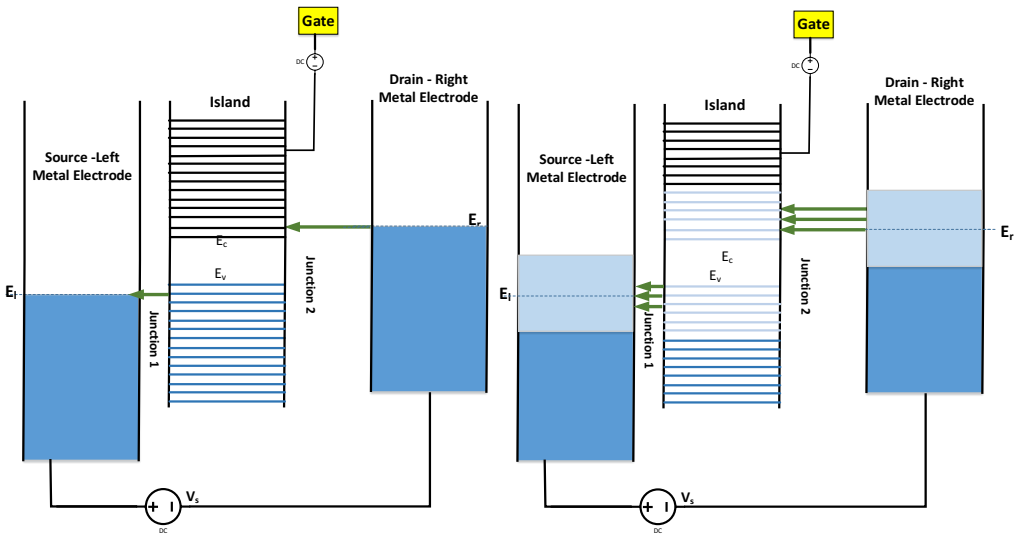

Figure 4.9. Schematic of a SET device under a positive source-drain bias (V_{sd}). The island has a band gap of 0.2 eV and discrete energy levels with 0.015 eV energy spacing. The empty energy levels are outlined in black; the dark blue area represents filled energy levels. The light blue area represents the thermally excited electrons or the available energy levels due to thermal excitation of electrons. Left: At $T = 0$ K, under suitable bias conditions, the electron tunneling is facilitated. Right: At higher temperatures, tunneling is more probable due to the thermally available electron tunneling paths.

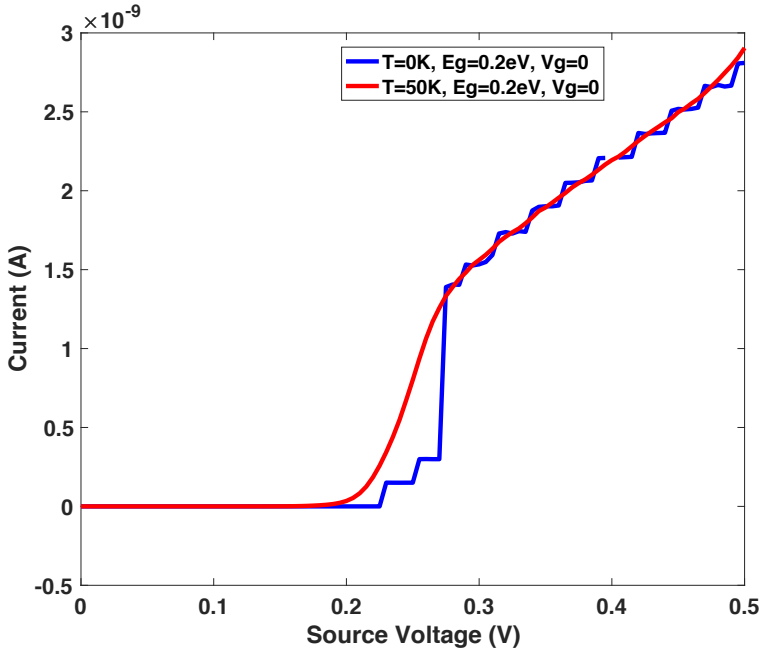

Figure 4.10. The current versus source-drain voltage characteristic of a SET device with a single island, for temperatures of 0 K and 50 K. The island has a band-gap of 0.2 eV, discrete energy levels of 0.015 eV, $C_1 = 0.5$ aF, $C_2 = 0.8$ aF , $C_g = 0.085$ aF and number of MC cycles is 10,000 for each source-drain voltage.

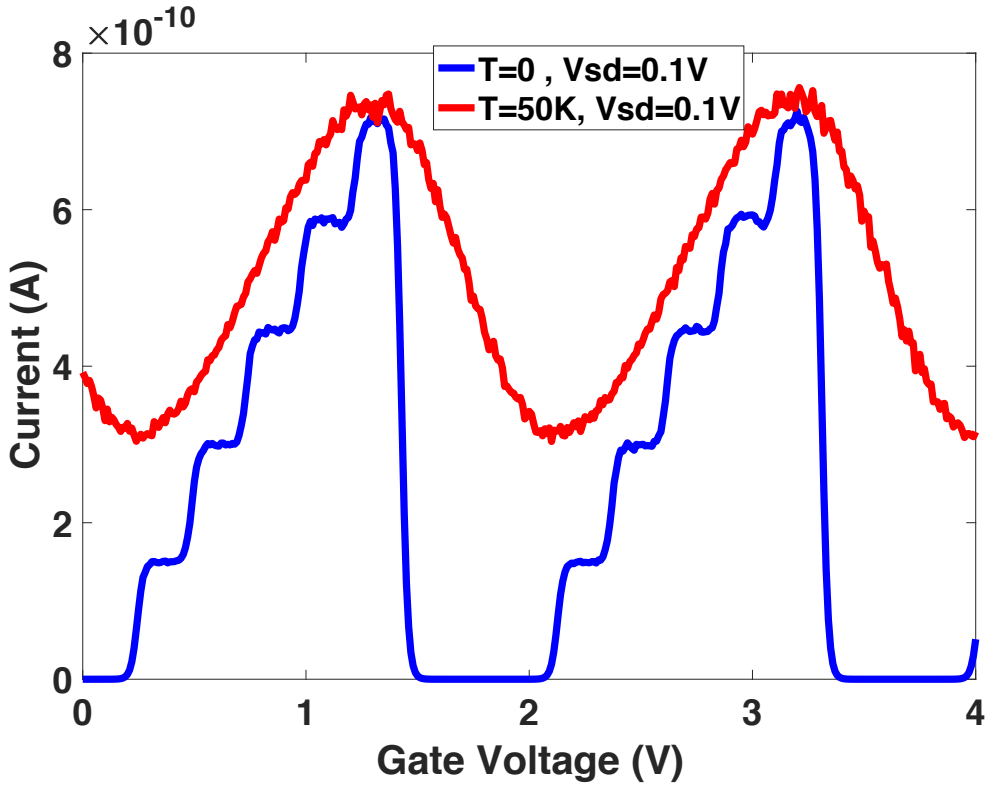

Figure 4.11. The current versus gate voltage characteristic for temperatures of 0 K and 50 K for a SET device with a semiconducting island. The island has a band gap of 0.2 eV, C_1=0.5 aF, C_2=0.8 aF and C_g=0.085 aF, $\Delta E = 0.015$ eV, number of energy levels is 3000 and number of MC cycles is 10,000 for each gate voltage.

The current-gate voltage (IV_g) characteristics of this model is plotted in Fig. 4.11, with a gate capacitance of 0.085 aF, the period of peak oscillations ($\frac{e}{C_g}$) is expected to be 1.88 V [1]. This period is observed in Fig. 4.11. The current steps at lower temperatures are due to the discreteness of the energy levels and are observed as the energy spacing between the levels is comparable to other energy scales in the system. At higher temperature, the thermally excited electrons play a great role in increasing the tunneling probability. Therefore, the minimum current (lower peak) increases and the steps become indiscernible

compared to those observed at lower temperatures. This change in the IV_{sd} characteristic of the device caused by thermally excited electrons is not ideal. For example, the excited electrons can cause a higher current flow through the device therefore the power dissipation increases [10]. Generally speaking for a SET device to be practical the current-voltage characteristics should have a low degree of temperature sensitivity which doesn't jeopardize the functionality of the device. In the next section, we study the impact of discreteness of energy levels and energy gap on temperature sensitivity. We also investigate utilizing discrete energy levels and forbidden energy bands in semiconducting islands to decrease the temperature sensitivity.

4.3.4 Utilizing Band Gap and Confined Energy Levels to Control the Degree of Temperature Sensitivity of a SET

The band gap is one of the unique and useful characteristics of semiconductors. Thermally excited electrons which do not yet have enough energy to overcome the band gap to move to the conduction band and cannot participate in electron tunneling. The band gap also causes higher threshold voltage as was observed before. Applying a potential to the third electrode (gate electrode) can align the energy levels of the island to the tunneling energy range and compensate for the impact of the band gap on the threshold voltage so no higher V_{sd} is needed. To sum up, the band gap blocks thermally excited electrons and gate voltage decreases the threshold voltage caused by the band gap. This reduces the impact of temperature on the current characteristics of the device. Figure 4.12 shows a simple schematic of devices with a semiconducting island with discrete energy levels, one with a band gap, and one without a band gap.

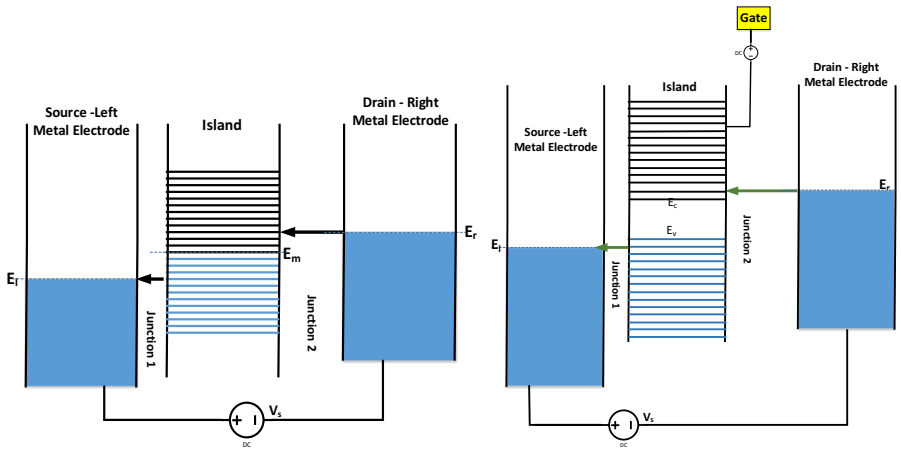

Figure 4.12. Schematic of a SET device under a positive source-drain bias (V_{sd}). The empty energy levels are outlined in black; the dark blue area represents filled energy levels at T = 0 K. Left: The island has no band gap but has discrete energy levels. At T = 0 K, under suitable bias conditions, the electron tunneling is facilitated. Righ: The island has a band gap and discrete energy levels. At $T > 0$, the gate voltage can be utilized to open a path for electrons to tunnel.

At lower temperatures, the energy levels that are shifted close to the Fermi energy of the electrodes are participating in tunneling events. If the energy spacing is comparable to other energy scales in the system, a staircase is observed in IV_{sd} characteristics of the SET device at low enough temperatures. As demonstrated in Fig. 4.14, at higher temperatures the discreteness induced steps become indiscernible as thermally excited electrons are participating in tunneling from higher energy levels. Comparing Figs. 4.13 and 4.14 shows that with band gap and an appropriate gate potential we can prevent the current steps from becoming completely indiscernible by preventing some of the thermally excited electrons to participate in tunneling.

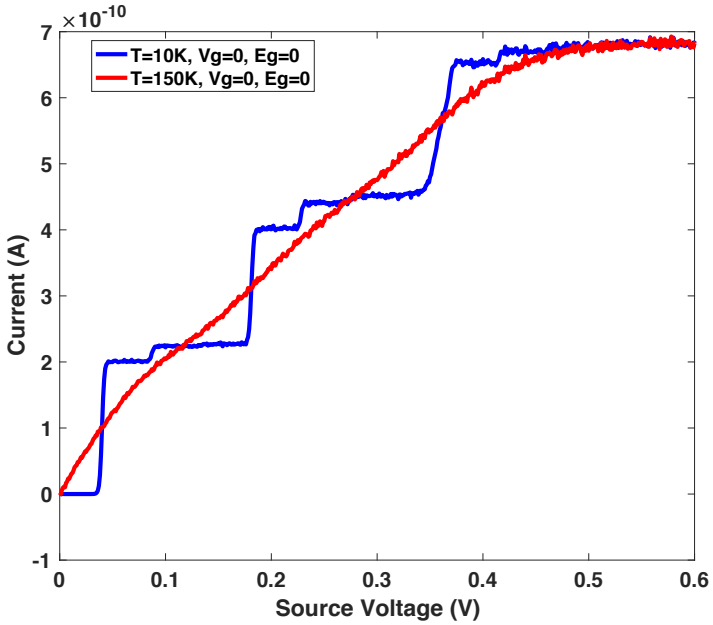

Figure 4.13. The current versus source-drain voltage characteristic of a SET with a semiconducting island. The island has multiple energy levels participating in tunneling, with energy spacing of $\Delta E = 0.015$ eV, $C_1 = 0.85$ aF, $C_2 = 2.9$ aF, $C_g = 0.52$ aF and number of MC cycles is 10,000 for each source-drain voltage.

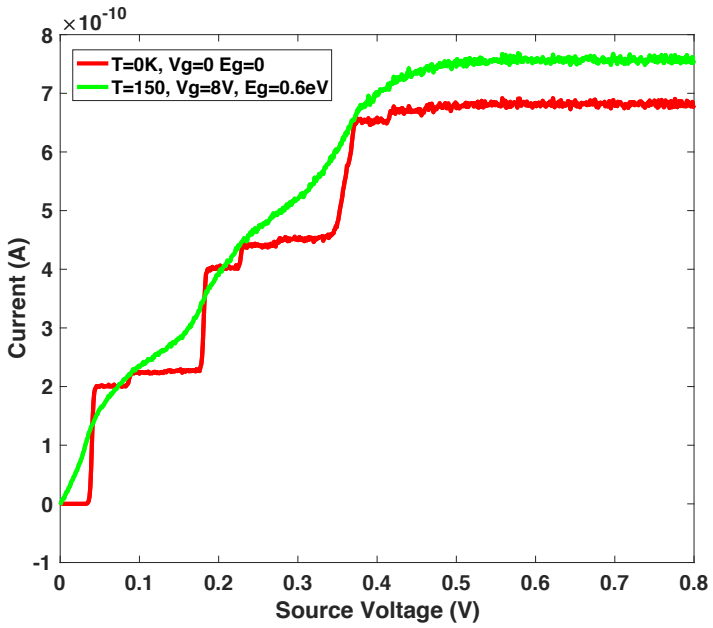

Figure 4.14. The current versus source-drain voltage characteristic of a SET with a semiconducting island for two different gate voltages and band gaps. The island has multiple energy levels (400), with energy spacing $\Delta E = 0.015$ eV, $C_1 = 0.85$ aF, $C_2 = 2.9$ aF, $C_g = 0.52$ aF. The number of MC cycles is 10,000 for each source-drain voltage.

4.3.5 Utilizing a Semiconducting Quantum Dot with Few Energy Levels to Control the Degree of Temperature Sensitivity of a SET

A hypothetical SET device model that has low temperature sensitivity under certain bias conditions is proposed here. In this model, the island has 8 energy levels participating in tunneling events with an energy spacing of 0.015 eV ($\Delta E = 0.015$ eV). Using the band gap and a gate electrode, we introduce regimes in which the temperature sensitivity can be controlled and minimized. Figure 4.15 shows a simple schematic of this model.

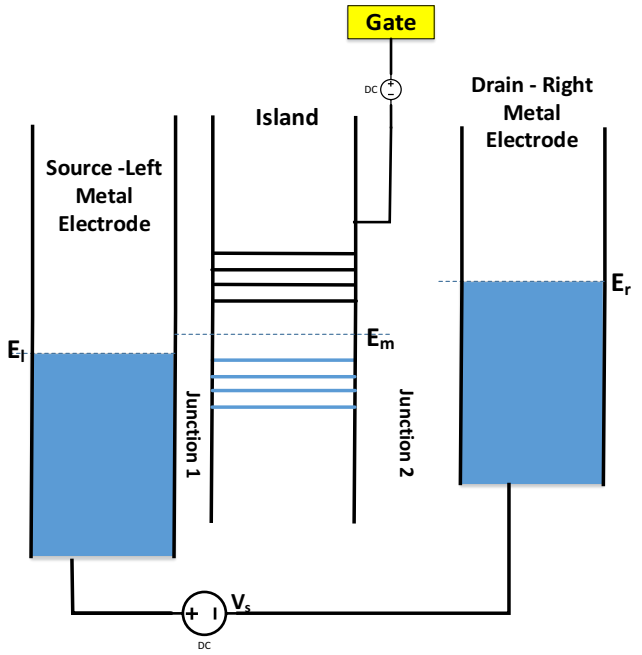

Figure 4.15. Cartoon model of a SET device with three electrodes a semiconducting island with 8 energy levels participating in tunneling events.

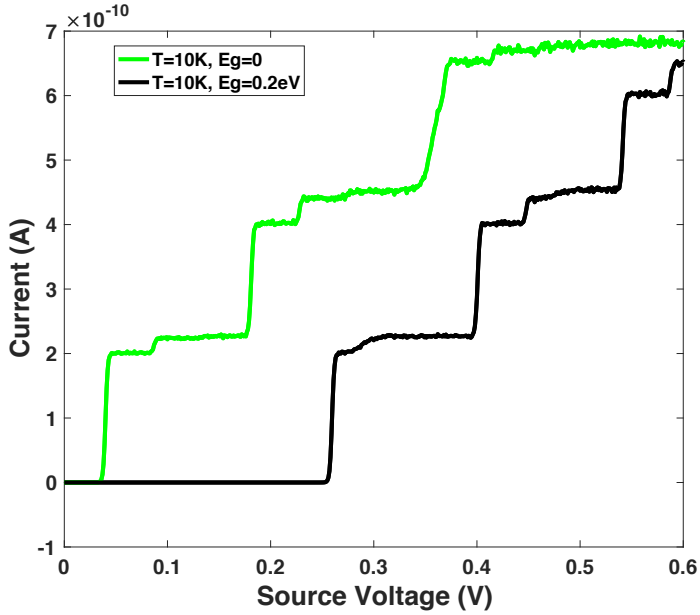

Figure 4.16. IV_{sd} characteristic of a SET with an 8-energy level semiconducting island and energy spacing of $\Delta E = 0.015$ eV for two different bang gaps ($E_g = 0$ and $E_g = 0.2$ eV). $C_1 = 0.85$ aF, $C_2 = 2.9$ aF, $C_g = 0.52$ aF. The number of MC cycles is10,000 for each source-drain voltage.

If there are not many available higher energy levels for thermally excited electrons to excite to, then increasing the temperature does not increase the probability for tunneling events. The gate electrode can be utilized to compensate for larger threshold voltage in devices with a band gap. By applying potential to the gate, energy levels can be shifted close to the Fermi energy of source and drain electrode; therefore, they can participate in electron tunneling.

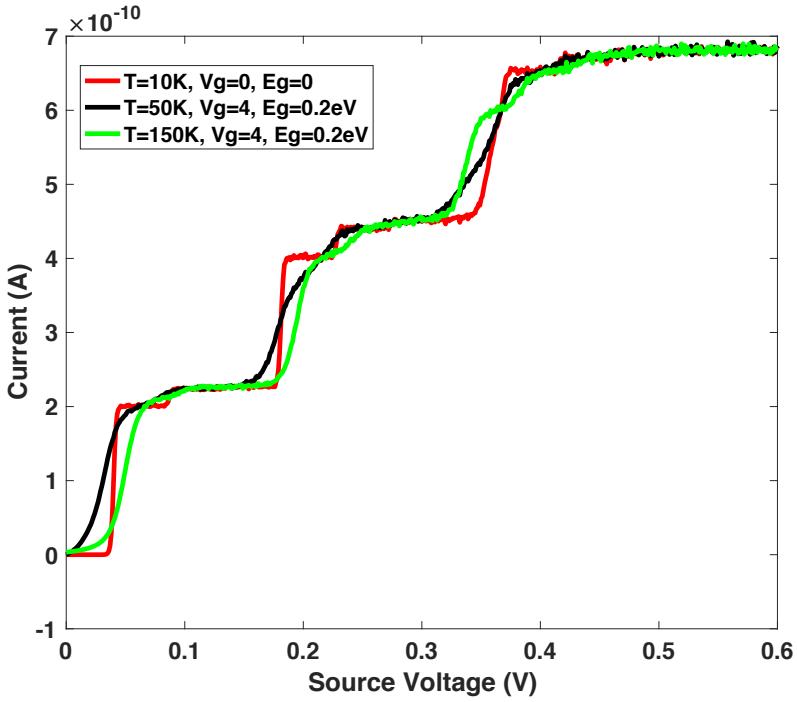

Figure 4.17. The current versus source-drain voltage characteristic of a SET with a semiconducting island for different gate voltages and band gaps. The island has 8 energy levels participating in tunneling, with energy spacing of $\Delta E = 0.015$ eV, $C_1 = 0.85$ aF, $C_2 = 2.9$ aF, C_g=0.52 aF. The number of MC cycles is 10,000 for each source-drain voltage.

The current steps observed in Fig. 4.17 are preserved at $T = 150$ K in a device with an island which has energy gap of 0.2 eV and few energy levels. The gate potential overcomes

the gap to enable electrons from the Fermi energy of the electrodes to tunnel to and from the discrete island.

4.4 Conclusion

In this study, we have explored the properties of SET devices with one island and particularly focused on the impact of temperature on these devices. We demonstrated that a SET with a metallic island is highly temperature sensitive. Increasing the temperature, the current steps which are observed at lower temperatures become indiscernible. For a SET with an island that has narrowly-spaced discrete energy levels, the discreteness induced current steps are is observed at lower temperatures and become indiscernible in higher temperatures. The greater the number of energy levels available to participate in tunneling, the harder it is to block the thermally excited electrons from tunneling.

If there are no higher energy levels available in the island, the thermally excited electrons will not participate in electron tunneling, this makes small semiconductor islands a useful candidate to reduce the degree of temperature sensitivity in SET devices. Utilizing a gate electrode to compensate for the band gap, this device configuration could preserve the steps from becoming indiscernible and lead us to a hypothetical device topology which may be useful in controlling the temperature sensitivity of a SET device, within a range of suitable biasing.

The proposed model is a SET with a quantum dot as the island which has a band gap and only few energy levels available in electron tunneling energy range. This device in higher temperatures functions as a device with an island with no gap and no gate voltage in lower temperatures. The few available levels can be energetically adjusted to the energy

range closer to fermi energy of the electrodes by applying proper gate potential therefore electron tunneling can happen. In higher temperature, the there are no available energy levels therefore electrons have no tunneling path and the device is immune to temperature increase. Comparing this model to a device with a metallic island or semiconducting island with multi energy levels, the current steps in the IV_{sd} characteristics could be preserved. The steps that are detected in higher temperature are well defined in higher temperatures as well (going from 10 K to 150 K). This model is of course theoretical and fabricating an ultra-small semiconductor, with only few energy levels available is fairly difficult.

4.5 Reference List

[1] K. K. Likharev, "Single-electron devices and their applications," *Proceedings of the IEEE*, vol. 87, no. 4, p. 606–632, 1999.

[2] R. W. M. Amman, E. Ben-Jacob, P. D. Maker, and R. C. Jaklevic, "Analytic solution for the current-voltage characteristic of two mesoscopic tunnel junctions coupled in series," *Physical Review B*, vol. 43, 1991.

[3]M. A. Savaikar, D. Banyai, P. L. Bergstrom and J. A. Jaszczak, "Simulation of charge transport in multi-island tunneling devices: Application to disordered one-dimensional systems at low and high biases," *Journal of Applied Physics*, vol. 114, no. 11, p. 114504, 2013.

[4] C. Wasshuber, *Computational Single-Electronics (Computational Microelectronics),* Edited by: S. Siegfried, Springer Science & Business Media, 2011, p. 278.

[5] M. A. Savaikar, *Stochastic Charge Transport in Multi-Island Single-Electron Tunneling Devices*, Ph.D. Dissertation, Physics Department, Michigan Technological University, 2013.

[6] C. Wasshuber, H. Kosina, and S. Selberherr, "SIMON-A simulator for single-electron tunnel devices and circuits," *IEEE Transactions on Computer-Aided Design of Integrated Circuits and Systems*, vol. 16, no. 9, pp. 937–944, 1997.

[7] B. Hao, A. Asthana, P. Hazaveh, P. L. Bergstrom, D. Banyai, M. A. Savaikar, J. A. Jaszczak and Y. K. Yap , "New Flexible Channels for Room Temperature Tunneling Field Effect Transistors,*" Scientific Reports,* vol. 6, p. 20293*,* 2016.

[8] D. J. Griffiths, "The Time Independent Schrödinger Equation," in *Introduction to Quantum Mechanics*, Pearson Prentice Hall, Upper Saddle NJ, 2004.

[9] P. Hapala, K. Kůsová, I. Pelant and P. Jelínek, "Theoretical analysis of electronic band structure of 2- to 3-nm Si nanocrystals," *Physical Review B*, vol. 87, no. 19, p. 195420, 2013.

[10] P. Bhadrachalam, R. Subramanian, V. Ray, L. Ma. W. Wang, J. Kim, K. Cho and S.J. Koh, "Energy-filtered cold electron transport at room temperature," *Nature Communication,* vol. 5, no. 4745, 2014.

[11] E. M. Conwell, M.O. Vassell, "High-Field Transport in pnp- Type GaAs," *Physical Review*, vol. 166, no. 3, p. 797–821, 1968.

[12] M. Grundmann, *The Physics of Semiconductors: An Introduction including Nanophysics and Applications*, 2nd Ed., New York, NY, Springer, DOI: 10.1007/978-3-642-13884-3, 2010

[13] C. Jacoboni, L. Reggiani, “The Monte Carlo method for the solution of charge transport in semiconductors with applications to covalent materials,” *Reviews of Modern Physics*, vol. 55, no. 3, p. 645–705, 1983.

5 Simulation of Charge Transport in Multi-Island Tunneling Devices: Application to Disordered One-Dimensional Systems at Low Temperature

Some figures and text are reprinted, with permission, from P. K. Hazaveh, P. L. Bergstrom, and J. A. Jaszczak, "Modeling of gate effects on electron transport in a single-electron transistor with two semiconducting islands between two semiconducting electrodes," *Proceedings of the IEEE 13th Nano Materials and Devices Conference (NMDC 2018),* 13–17 October 2018, Portland, OR, pp. 459–452.

In this chapter, we introduce an algorithm to predict the current-voltage (*IV)* characteristic of double-island single electron transistors (SETs) under different bias voltages and temperatures varying form 10 K to 300 K. The main focuses of this study are: 1-Predicting Coulomb oscillations in the IV_g (gate voltage versus current) characteristics, 2-Exploring the effect of temperature and gate-capacitances coupling the islands to the gate in a SET with two semiconducting islands, 3-Investigating the impact of discrete energy levels in the band structure of an island. This study employs recently developed simulation tools, based on semi-classical modeling of tunneling rates and kinetic Monte Carlo simulation, to calculate electron tunneling rates between semiconductor quantum dot islands. In a double dot SET the islands are coupled together and predicting the peak placements in IV_g characteristics is not possible unless in extreme coupling cases. A simulation tool is necessary for predicting the IV_g characteristic of such a device. It is demonstrated that different gate capacitances coupling gate electrode to islands with different band structures results in enhancing or blocking electron tunneling paths therefore increasing or decreasing slope in IV_g characteristics.

5.1 Introduction

The ability to fit more components on integrated circuits is one of the primary motivations behind studying quantum electronic devices. With active elements (tunneling islands) at the scale of nanometers, single electron transistors (SETs) are promising for future low power logic units and high density integrated systems [1]. The small island sizes and junction widths, and therefore the associated large charging energies, allow such devices to operate at room temperature [2] in principle. At these small sizes the charging energies cannot be ignored. SET devices with semiconducting islands have demonstrated behaviors in experimental studies that are motivating for engineering applications. One of the examples is filtering thermally excited electrons from participating in electron tunneling using confined energy states [3]. Another examples is the gate control and clear Coulomb blockade oscillation in semiconducting SET devices which was experimentally examined by Acharya et al. [4]. The experimentally explored semiconducting SET by H. Ishikuro and T. Hiramoto [5], shows some unique behavior such as clear Coulomb oscillation peaks and a baseline current.

We have extended capabilities of MITS developed by Savaikar et al. [6], to simulate Semiconducting SET devices. We have started with a simple model shown in Fig. 5.1. Consist of two islands and three electrodes. C_1, C_2 and C_3 are junction capacitances and the islands are coupled to the gate electrode by C_{g1} and C_{g2}.

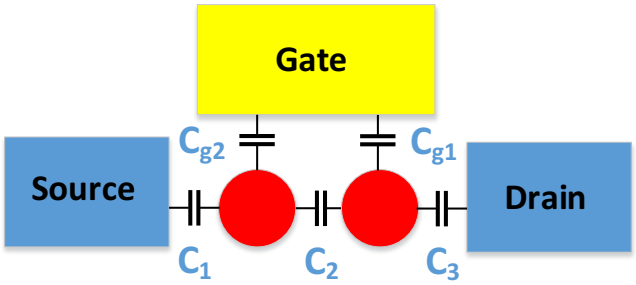

Figure 5.1. Circuit schematic of a SET device with three electrodes and two islands.

5.2 Method

Following work of Amman et al. [7] and Savaikar et al. [6], general tunneling rates can be computed according to:

$$\Gamma_{if} = \int_{l1}^{l2} \frac{2\pi}{\hbar} |T(E)|^2 D_i(E) f(E - E_i) \times \tag{5.1}$$

$$D_f(E - \Delta W_{if})[1 - f(E - E_i - \Delta W_{if})]dE,$$

where

$$\Delta W_{if} = -eV_{if} + E_{ch}, \tag{5.2}$$

is the change in free energy of the system due to the tunneling event [2], E_i is the Fermi energy of the initial side of the tunneling junction, and D_i and D_f are the density-of-states functions for the initial and final states of the junction, respectively. *f(E)* is the Fermi-Dirac distribution function, *T(E)* is the transition probability. The charging energy, E_{ch}, is given by $E_{ch} = \frac{e^2}{C}$, where C is the island's total capacitance and e is the electron's charge [2]. The integration limits l_1 and l_2 are dynamically adjusted for computational efficiency in

our simulations, depending on the potential difference across the junction and the highest and lowest energy levels that can participate in tunneling.

Introducing a potential difference, V_{if}, across a junction, shifts the electron energy states of one side of the junction by eV_{if} with respect to the other side. The potential difference is due, in general, to the combined effects of the charges on the islands and the fixed potential of the source, drain, and gate electrodes. Based on input biases and thermal energies of the system the maximum energy levels that can participate in tunneling events are 10 eV above the Fermi level. Any range less than that has a risk of not considering all the energy levels participating in tunneling events. The integral limits are designed to include the dominant energy ranges participating in tunneling events of each junction and are calculated dynamically based on the junction's potential. This integral does not have a closed form solution for tunneling between semiconducting materials unless with extensive simplifications. We have solved this integral numerically.

5.2.1 Transition Probability

Following MITS by Savaikar et al. [6], we approximate the potential barrier across a junction as having a rectangular shape whose height is given by the average of the approximately trapezoidal barrier. This height dynamically changes in the course of the simulation as it varies with the charge state of the islands. In MITS, the barrier height is calculated as with the approximation that all the electron tunneling events are initiating from energy levels very close to the Fermi energy, which results in an energy independent barrier height. The primary reason for this approximation is to calculate a closed form solution for the tunneling integral. On the other hand, in our simulation, the rate integral is calculated numerically so we maintain an energy dependent transmission probability. The

probability of an electron being transmitted through a rectangular barrier of height (V_o), can be approximated as the energy dependent function below [8-10]:

$$|T(E)|^2 = \left[1 + \frac{V_0^2 \sinh^2(k_1 d)}{4E(V_0 - E)}\right]^{-1}, \tag{5.3}$$

where

$$k_1 = \frac{\sqrt{2m(V_0 - E)}}{\hbar}, \tag{5.4}$$

$$V_0 = \frac{\phi_{sc} + \phi_{sc} - eV_{if}}{2} = \phi_{sc} - \frac{eV_{if}}{2}, \tag{5.5}$$

E is the energy of electron, V_o is the barrier height, d is the barrier (junction) width, m is the electron's mass, ϕ_{sc} represents the electron affinity in the island's conduction band or valence band ($\phi_{sc} = \phi_c$ for the conduction band, and $\phi_{sc} = \phi_V$ for the valence band), and V_{if} is the potential difference *across* the junction. As the energy barrier across the junction is relatively larger than the energy levels of electrons participating in tunneling, under certain biases, the initial energy level of all electrons could be considered the edge of the conduction/valence band. This assumption will improve the time efficiency of the simulation.

5.2.2 Density of States

Carriers and energy levels available to participate in electron transport in metals are positioned energetically near the Fermi energy so the density of states of the metal device elements (electrodes or islands) is commonly approximated as a constant $D_0 = D(E_f)$, which is the density of states at the Fermi energy [9, 10], One of the limitations of previous theoretical work such as in MITS by Savaikar et al. [2, 6, 9] and the SIMON code by

Wasshuber et al. [9, 11], employ a constant density of states approximation evaluated at the Fermi energy. While this approximation is an appropriate for metals at lower biases and temperatures, it is not well suited for semiconductors, which have a band gap and density of states that are not constant at the energies of interest. The energy confinement in semiconductors larger than 2.5nm is much smaller than other energy scales used in this study and can be ignored in this model. For semiconductors larger than 2.5 nm [12]. In this study we have used a continious model for the density of states of the semiconductors larger than 2.5nm that includes not only the band gap, but a modified-parabolic energy dependence of density of states [13, 14]:

$$D(E) = \frac{\sqrt{2}(m_c^*)^{\frac{3}{2}}\sqrt{(|E - E_{\mathrm{sc}}| + \alpha_{\mathrm{sc}}(E - E_c)^2)}(1 + 2\alpha|E - E_{\mathrm{sc}}|)}{\pi^2\hbar^3} \quad , \tag{5.6}$$

where

$$\alpha_{\mathrm{sc}} = \frac{1}{E_g}\left(1 - \frac{m_{\mathrm{sc}}^*}{m}\right)^2 \quad , \tag{5.7}$$

m is the free electron mass, m_{sc}^* is are the effective mass of electron in the conduction band or valence band, E_{g} is the energy gap, E_{sc} is the edge of the conduction band or the valence band and $\hbar$ is the reduced Planck's constant.

As the nominal size of a quantum dot (island) decreases (less than 2.5 nm), the energy spacing increases between its discrete energy levels [44]. If the energy spacing is comparable to other energy scales of the system, modeling the quantum dot with a continuous-band model is no longer an accurate assumption. Following work of Amman et al. [28] we consider energy levels of the first island to be of zero width and spaced equally in this model for simplicity. The relaxation time is still considered negligible

compare to the time between tunneling events. The density of states of this simple model can be expressed as below [28]:

$$D_m(E - E_m) = D_m(n\Delta E) \sum_{n=0}^{\infty} \delta(E - E_m - E_o - n\Delta E), \tag{5.8}$$

where ΔE is the energy spacing between the discrete levels, n is the index of discrete energy levels, E_0 is the ground state energy and E_m is the fermi energy of the island. $D_m(n\Delta E)$ is dynamically calculated using Eq. 5.6.

5.3 Results and Discussion

We are interested in current characteristic of the SET under DC bias. All junctions have the same electrical properties as they all have semiconducting material surrounding them, so the tunneling rate of all of the junctions can be calculated using the same method. When the rates are known based on the potentials across the junctions, then one transition is selected randomly and still based on energy favorable transitions, using the KMC method. After each tunneling event the integral limits and potential drops across each junction are reevaluated. This is repeated at each step until a steady state current is converged with error bars less than 2% of the mean value. For each test case, the voltage increment (either gate or source-drain voltage) is set at 0.01 V, and a minimum of 10,000 Monte Carlo steps were performed for each voltage increment in order to determine *IV* characteristics.

5.3.1 Impact of the Modified Parabolic Density of States

To check the validity of our algorithm, we compare our results for current-versus-gate-voltage (IV_g) characteristics for a metallic double-dot SET with results presented by

Glazman and Chandrasekhar [15]. In their work, the conductance was demonstrated as a function of the gate voltage for two extreme regimes: one where the junction capacitances are much large than the gate capacitances ($C_1 = C_2 = C_3 \gg C_{g1}, C_{g2}$), and one where the gate capacitances are much larger than the junction capacitances ($C_1 = C_2 = C_3 \ll C_{g1}, C_{g2}$). The effect of the modified-parabolic density of states and the band gap on the IV_{gs} characteristics of a SET were also explored.

Figure 5.2. compares the IV_{gs} characteristic of a metallic SET and a semiconducting SET device with same junction and gate capacitances where the junction capacitances are much large than the gate capacitances ($C_1 = C_2 = C_3 \gg C_{g1}, C_{g2}$). For comparative purposes, the band gap in the semiconducting device is taken to be zero so the effect of only the modified parabolic density of states can be observed with no other changes in energy scales. As expected, the magnitude of the current decreases dramatically for the semiconductor model due to the decrease in the number of carriers and available states for tunneling near the Fermi energy as compared to a metallic model. The peak separation and peak widths, which depend on temperature and capacitances, stay the same as the metallic device and are in qualitative agreement with [15]. This test case also serves to validate the numerical integration involved in the calculation of the tunneling rates (5.1) in our algorithm.

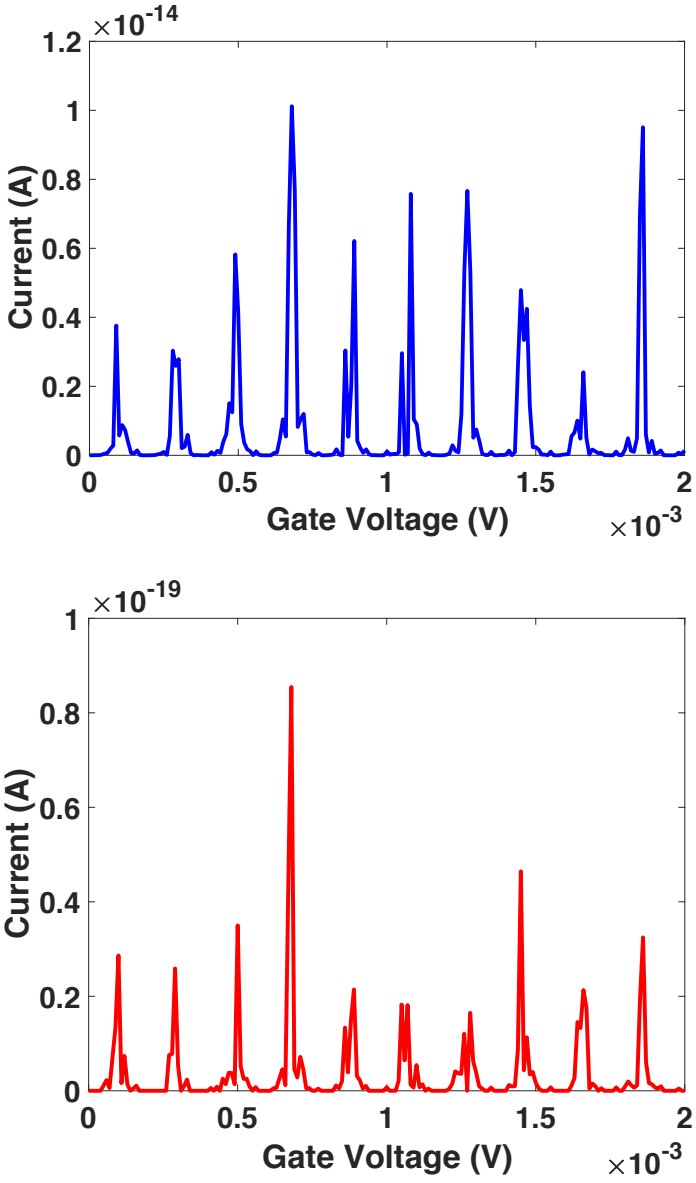

Figure. 5.2. $C_1 = C_2 = C_3 = 11.2$ aF and $C_{g1} = 1.92$ fF, C_{g2}=4.36 fF, $T = 0.01$ K. Top: The IV_{gs} characteristic of a SET with two metallic islands. Bottom: The IV_{gs} characteristic of a SET with two semiconducting islands with modified-parabolic bands but zero band gap. ©2018 IEEE. Reprinted with permission, from P. K. Hazaveh, P. L. Bergstrom, and J. A. Jaszczak, "Modeling of gate effects on electron transport in a single-electron transistor with two semiconducting islands between two semiconducting electrodes," *Proceedings of the IEEE 13th Nano Materials and Devices Conference (IEEE NMDC 2018),* pp. 459 – 462, 2018 [16].

5.3.2 On State Gate Control

In metallic double-island SET devices the gate voltage does not have a significant effect on the source-drain current in "on" state. When the applied source-drain bias reaches the threshold voltage, the number of available electrons and holes in an energy window near Fermi energy across the junction is high, therefore a clear transition path is available for electrons to tunnel, independent of V_g [16]. Semiconducting SET devices, on the other hand, do not have a sea of electrons at the Fermi energy available to tunnel, so the gate plays a significant role in adjusting energy levels available for electron tunneling. As the gate potential increases, the potentials of the islands change in favor of electron tunneling events by overcoming the band gap, charging energies and aligning more available levels with electron-filled levels. Figure 5.3 illustrates that the current is gate controlled at source-drain potentials greater than the Coulomb blockade threshold voltage, demonstrating the impact of bandgap and non-constant density of states for tunneling transitions at energies away from the band edges. In our model at V_{sd} = 4 V, for example, increasing the gate potential by 2 V results in an 11% increase in the current. The observed gate effect in the modeled semiconducting SET device can be compared to a minimal gate effect for an equivalent metallic device [16].

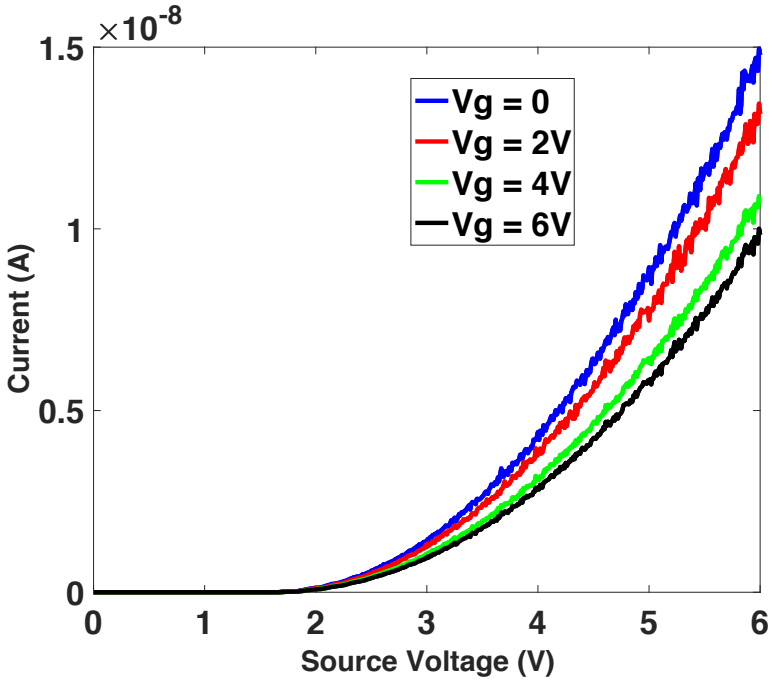

Figure 5.3. The source-drain *IV* characteristics of a SET with two semiconducting islands, two semiconducting electrodes and a gate electrode. $C_1 = 0.8$ aF, $C_2 = C_3 = 0.5$ aF, $C_{g1} = C_{g2} = 2.5$ aF, and $T = 50$ K. ©2018 IEEE. Reprinted with permission, from P. K. Hazaveh, P. L. Bergstrom, and J. A. Jaszczak, "Modeling of gate effects on electron transport in a single-electron transistor with two semiconducting islands between two semiconducting electrodes," *Proceedings of the IEEE 13th Nano Materials and Devices Conference (IEEE NMDC 2018),* pp. 459 – 462, 2018 [16].

5.3.3 Impact of Temperature on *IV* Characteristic of a SET with Continuous Band Structure

As described by Glazman and Chandrasekhar [15], when the junctions' capacitances and the gate capacitances are of comparable magnitudes, the current oscillations as a function of gate voltage are not readily predictable. The energy states of the system after each electron tunneling event depends on potential across the junctions and the charging energies. Predicting the gate-controlled oscillations is not possible at present, except with

KMC-based simulations. We have explored such a system with double semiconducting islands and two semiconducting electrodes in this section. The junction capacitances are equal: $C_1 = C_2 = C_3 = 11.2\ aF$ and gate capacitances are in the same range as junction capacitances: $C_{g1} = 1.92$ aF and $C_{g2} = 4.36$ aF. To make energy scales smaller and the simulations more time effective, all the energy gaps in band structure of semiconductors are considered 0.2 eV. With increasing the temperature, the periodicity of the IV_g characteristics changes as demonstrated in Fig. 5.4.

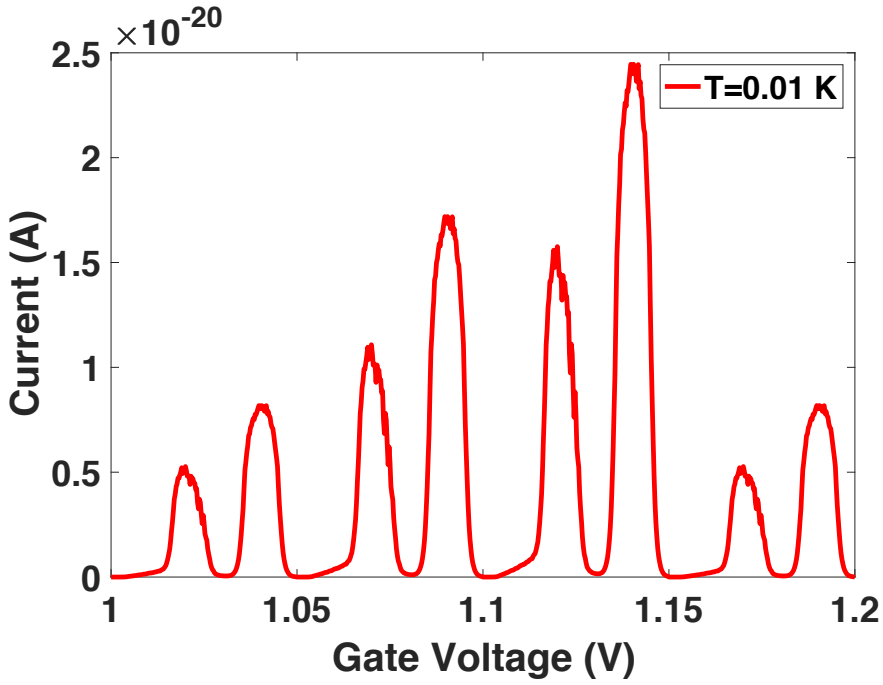

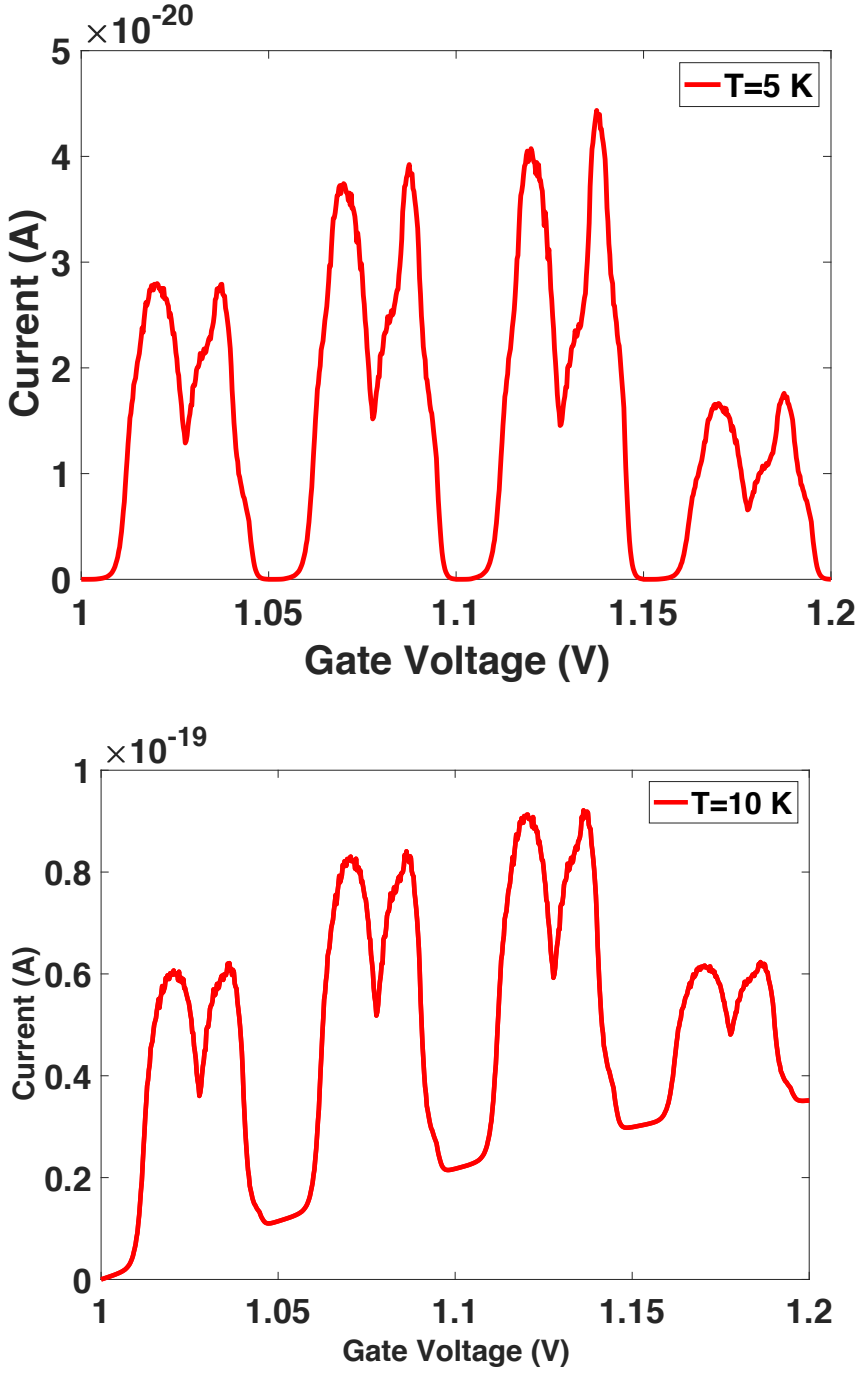

Figure 5.4. The IV_g characteristic of a SET with two semiconducting islands with band gap of 0.2 eV, under 0.1 V source-drain bias and at T = 0.01 K (top), T = 5 K (middle) and T = 10 K (bottom). $C_1 = C_2 = C_3$ = 11.2 aF and C_{g1} = 1.92 aF, C_{g2} = 4.36 aF. Top figure is ©2018 IEEE. Reprinted with permission, from P. K. Hazaveh, P. L. Bergstrom, and J. A.

Jaszczak, “Modeling of gate effects on electron transport in a single-electron transistor with two semiconducting islands between two semiconducting electrodes,” *Proceedings of the IEEE 13th Nano Materials and Devices Conference (IEEE NMDC 2018),* pp. 459 – 462, 2018 [16, 17].

At lower temperatures, if electrons at the edge of the valence band have enough energy to overcome the band gap and charging energies, it is probable for tunneling to occur. If tunneling across at least one of the junctions is energetically blocked, the current drops to zero. Increasing the temperature at this regime results in wider energy range available as the tunneling path for electrons therefore the current flow is maximum for a larger range of gate voltages so the wider peaks are observed. As a result of these available thermally excited electrons, the tunneling path is not blocked as soon as the edge of the bands are aligned with the band gap therefore the current does not fall back to zero. Therefore, multiple peaks observed at T = 0.01 K, in Fig. 5.4. start merging as the temperature increases.

By increasing the source-drain input voltage and/or temperature the tunneling paths for electrons opens up. To capture the temperature effect under higher source-drain input bias we need to look at a wider range of gate voltages which is demonstrated in Fig 5.5 For gate voltages, up to 6 V [17].

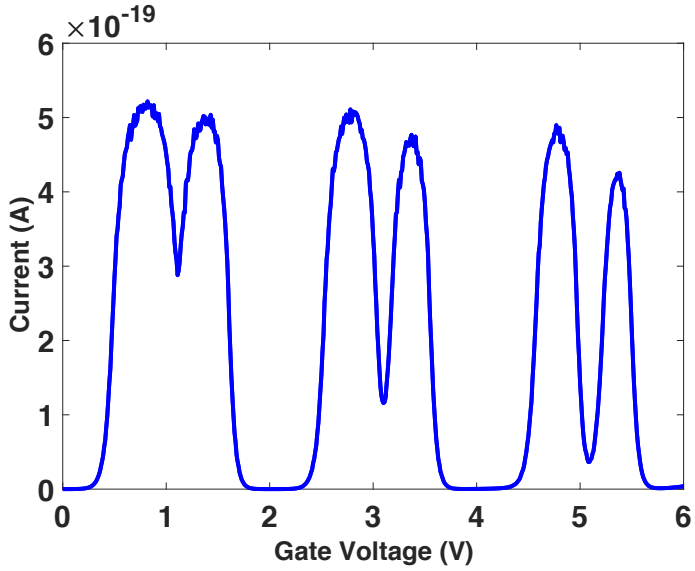

Figure 5.5. The IV_g characteristic of a SET with two semiconducting islands with band gap of 0.2 eV, under 0.5 V source-drain bias and at $T = 0.01$ K. $C_1 = C_2 = C_3 = 11.2$ aF and $C_{g1} = 1.92$ aF, $C_{g2} = 4.36$ aF [17].

At input voltage of 0.5 V, with the gate voltages applied the electrons have enough energy to overcome the charging energies and the band gap therefore electron tunneling is more probable in lower temperatures. As the temperature increases, the tunneling becomes increasingly probable, and the tunneling path never "shuts off" due to the thermally available electrons for tunneling. Therefore, it is expected that the current stay above zero as is observed in Fig. 5.4. On the other hand, when the energy range of electrons participating in tunneling is the narrowest then the current is at a minimum. The tunneling window in which the electron tunneling is probable is controlled by the gate, and as demonstrated in Fig. 5.6, results in Coulomb oscillations [17].

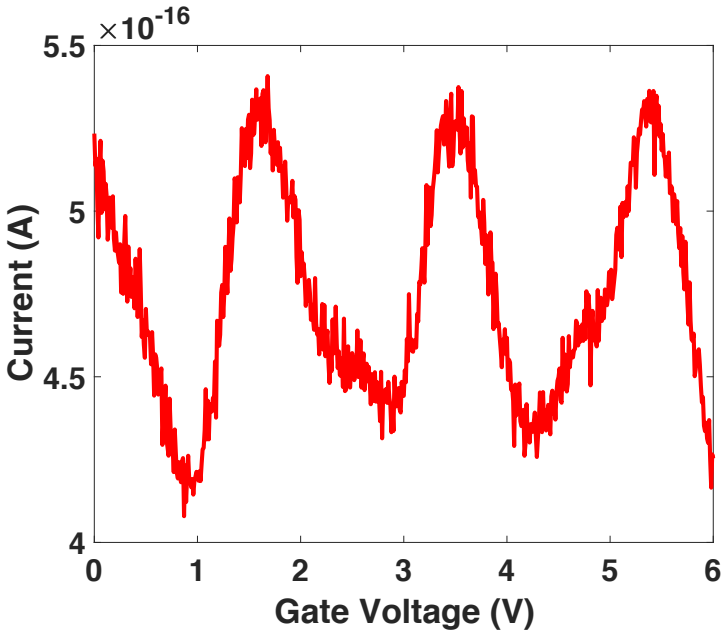

Figure 5.6. The IV_g characteristic of a SET with two semiconducting islands with band gap of 0.2 eV, under 0.5 V source-drain bias and at T = 50 K. $C_1 = C_2 = C_3 = 11.2$ aF, C_{g1} =1.92 aF, and $C_{g2} = 4.36$ aF [17].

5.3.4 Impact of Temperature on *IV* Characteristics of a SET with one Metallic Island and One with Discrete Energy Levels

One of the advantages of our algorithm is that the numerical integration of the tunneling rate allows the application of the calculation to materials with different band structures. In this section, we describe an asymmetric model having two different junctions, metal-metal and metal-semiconductor. In this simple model (Fig. 5.7), the two metallic electrodes and the metallic island are taken to be large enough to have a continuous energy band and an effectively constant density of states near their Fermi energy. On the other hand, the semiconducting island is taken to be small enough such that it has discrete energy levels, following [6], which we take to be separated by 0.015 eV. Experimental research work shows that the discreteness of the energy levels can be captured by choosing a dominant tunneling junction. In previous theoretical work of Amman et al. [7] the Coulomb blockade

steps have been captured in a two junction SET, using the Master equation approach. In this study, we have developed a novel algorithm to capture the current steps representing the discreteness, for a three-junction device. Later this algorithm is used to model electron transport through the device for different temperature and input biases.

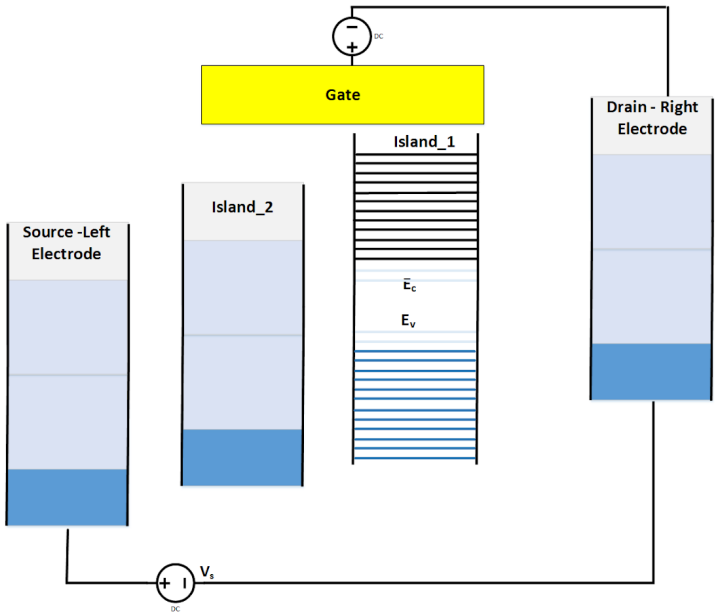

Figure 5.7. The band diagram model of a system with three electrodes and two islands. One island is metallic the other island is a semiconducting quantum dot with discrete energy levels. The dark blue bands are representing the filled valence band. In higher temperatures, the light blue is representing the available electrons and holes due to thermal excitation of some electrons [17].

To explore the temperature impact on the current gate voltage characteristic of a SET with gate capacitances of $C_{g1} = 0.085$ aF, $C_{g2} = 0.17$ aF and $C_{g1} = 0.085$ aF, $C_{g2} = 0.085$ aF are plotted in Fig. 5.8. At T = 10 K there are no electron filled levels of the island, aligned with the empty levels of the metallic island. Increasing the gate voltage facilities alignment of the levels so there is a path for electron to tunnel. But there are many empty levels that could potentially be electron tunneling paths if they are filled. Increasing the

temperature fills those empty levels and as a result a significant increase in conductance can be observed at T = 300K.

There is a surprising feature in *IV* characteristic of this mode, the baseline current which has been observed in some experimental works as well [5]. We can explain this behavior by taking a closer look at the islands' potentials. The tunneling probability from island one (*i1*) to island 2 (*i2*) depends on the potential difference across the junction ($V_{12} = V_{i1} - V_{i2}$). These islands are coupled to the gate via capacitances. If the coupling gate capacitance of the metallic island *(i2*) is larger than the coupling gate capacitance of the island with discrete energy levels (*i1*) (e.g. $C_{\mathrm{g1}} < C_{\mathrm{g2}}$) the change in the gate voltage enhances the probability of electron tunneling by changing V_{12} in favor of electron tunneling. In this case the electron tunneling is enhanced by *i2* (V_{12}) and does not need to wait for the discrete energy levels of *i1* to shift completely. As a result, electron tunneling does not finish one period and starts a new one and a baseline current is observed by increasing the gate potential [17].

In general, in a SET device with two islands coupled to the gate, potential of both sides of the junctions are changing after each tunneling event. If the islands are coupled to the gate with different capacitances, increasing the gate voltage not only changes the islands' potentials but also changes the voltage difference between the islands; With different gate capacitances electron tunneling events from the discrete level islands can be enhanced or blocked (depending on which gate capacitances is larger) by the other island as the gate voltage increases. Comparing to the system with same gate capacitances which change in

the gate voltage does not change the potential difference between the islands ($V_{12} = V_{i1} - V_{i2}$). Therefore, in a system with $C_{g1} = C_{g2} = 0.085$ aF, no baseline current is observed.

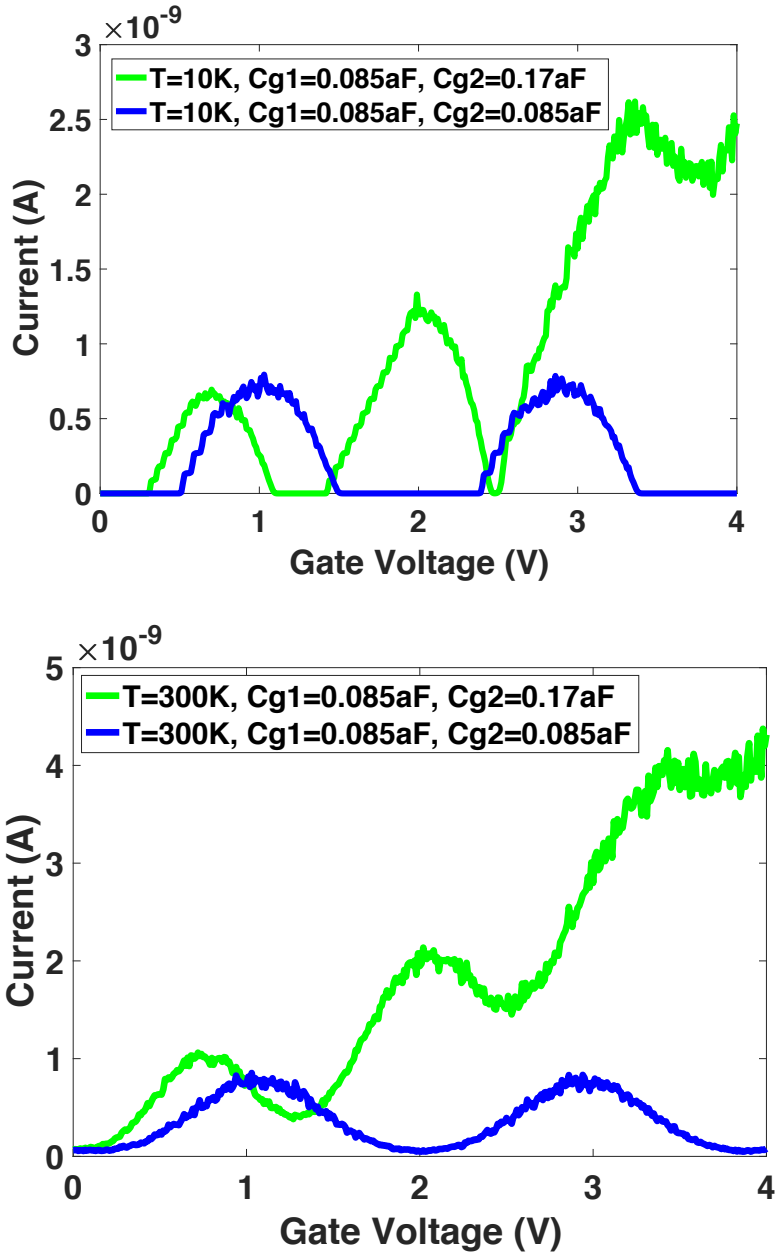

Figure 5.8. The IV_g characteristics of a SET with two islands. One island is metallic and the other island is a semiconducting quantum dot with discrete energy levels of 0.015 eV and $V_{sd} = 0.1$ V. $C_1 = 0.15$ aF, $C_2 = 0.5$ aF, $C_3 = 0.5$ aF. Green: $C_{g1} = C_{g2} = 0.085$ aF. Blue: $C_{g1} = 0.085$ aF, $C_{g2} = 0.17$ aF [17].

If the metallic island is coupled to a gate capacitance larger than the gate capacitance of the semiconductor island ($C_{g1} < C_{g2}$), we observed that increasing the gate voltage changes the potential difference between the floating islands (V_{12}) in favor of electron tunneling; therefore, we should observe the opposite effect if the metallic island (*i2)* is coupled to a smaller capacitance *(*$C_{g1} > C_{g2}$). Examining a model where the gate capacitance of the metallic island is smaller than the gate capacitance of the island with discrete energy levels ($C_{g2} < C_{g1}$) we observe in Fig. 5.9., as expected, the current decreases as this energy level of the metallic islands does not shift as much as the discrete island, and the electron tunneling is blocked from specific energy levels [17].

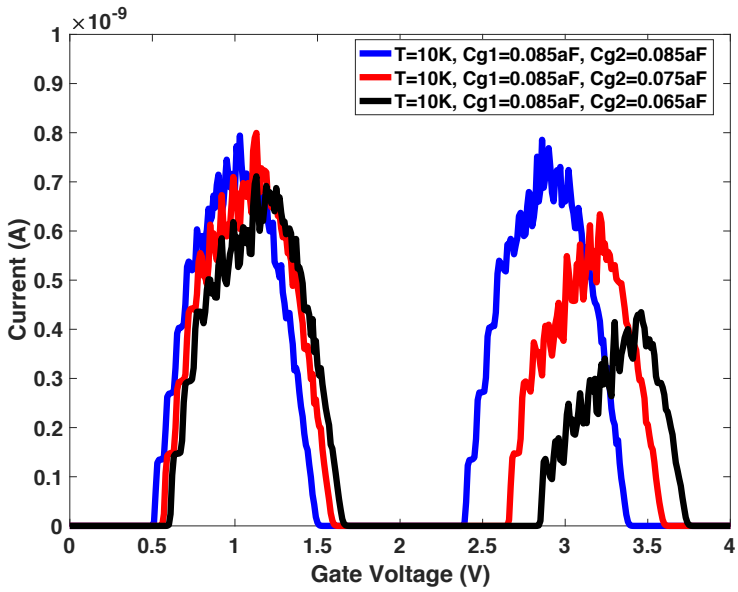

Figure 5.9 The IV_g characteristics of a SET with two islands at T = 10 K. One island is metallic with continuous band model, and the other island is a semiconducting quantum dot with discrete energy levels of 0.015 eV and V_s = 0.1 s. Red: C_1 = 0.15 aF, C_2 = 0.5 aF, C_3 = 0.5 aF. Blue: C_{g1} = 0.085 aF, C_{g2} = 0.085 aF. Red: C_{g1} = 0.085 aF, C_{g2} = 0.075 aF. Black: C_{g1} = 0.085 aF, C_{g2} = 0.065 aF [17].

5.4 Conclusion

The introduced algorithm is a time efficient tool to predict electron tunneling through double island semiconducting SET devices. Our simulation tool allows for the modeling of electron transport between materials with non-trivial band structures such semiconductors or small quantum dots with discrete energy levels.

In a double-island SET, the tunneling probability depends on the potential difference across junctions which depends on multiple parameters such as: charging energy, input bias, gate voltage, gate capacitances. These parameters are intertwined in a double island SET device which makes predicting the exact position of peaks and the period of coulomb oscillation impossible unless using simulation tool.

The effect of temperature, discrete energy levels and gate capacitances on IV_g characteristic of a double island SET with semiconducting materials is explored in this study. As there are more energy-dependent parameters involved in the band structure of a semiconductor island (such as the band gap), using them to control the temperature sensitivity is possible.

Our simulation tool is capable of taking into account the discrete energy levels if their energy spacing is comparable to other energies in the system. One of the surprising features observed in a SET with two types of islands (one metallic and one semiconducting with discrete levels) was the base line current. Further investigation was pursued and it was concluded that the different capacitance coupling islands to the gate plays a role in facilitating or blocking electrons paths from one the islands to the other, resulting in different current-voltage characteristics.

5.5 Reference List

[1] K. Uchida, “Single-Electron Transistors and Circuits for Future Ubiquitous Computing Applications,” *IEEE Proceedings of the 32nd European Solid-State Circuits Conference*, pp. 17-20, 2006.

[2] K. K. Likharev, "Single-electron devices and their applications," *Proceedings of the IEEE*, vol. 87, no. 4, pp. 606 – 632, 1999.

[3] P. Bhadrachalam, R. Subramanian, V. Ray, L.-C. Ma, W. Wang, J. Kim, K. Cho and S. J. Koh, “Energy-filtered cold electron transport at room temperature,” *Nature Communications,* vol. 5, p. 4745, 2014.

[4] M. Acharya, “Development of Room Temperature Operating Single Electron Transistor Using FIB Etching and Deposition Technology,” Ph.D. dissertation, Electrical Engineering Department, Michigan Technological University, Houghton, MI, USA, 2009.

[5] H. Ishikuro and T. Hiramoto, "Quantum mechanical effects in the silicon quantum dot in a single-electron transistor," *Applied Physics Letters*, vol. 71, no. 25, pp. 3691-3693, 1997.

[6] M. A. Savaikar, D. Banyai, P. L. Bergstrom and J. A. Jaszczak, “Simulation of charge transport in multi-island tunneling devices: Application to disordered one-dimensional systems at low and high biases,” *Journal of Applied Physics,* vol. 114, no. 11, p. 114504, 2013.

[7] M. Amman, R. Wilkins, E. Ben-Jacob, P. D. Maker, and R. C. Jaklevic, “Analytic solution for the current-voltage characteristic of two mesoscopic tunnel junctions coupled in series,” *Physical Review B*, vol. 43, no. 1, 1991.

[8] B. Hao, A. Asthana, P. Hazaveh, P. L. Bergstrom, D. Banyai, M. A. Savaikar, J. A. Jaszczak and Y. K. Yap, "New Flexible Channels for Room Temperature Tunneling Field Effect Transistors*" Scientific Reports,* vol. 6, p. 20293, 2016.

[9] C. Wasshuber, H. Kosina, and S. Selberherr, "SIMON-A simulator for single-electron tunnel devices and circuits," *IEEE Transactions on Computer-Aided Design of Integrated Circuits and Systems*, vol. 16, no. 9, pp. 937–944, 1997.

[10] M. A. Savaikar, *Stochastic charge transport in multi-island single-electron tunneling devices*, Ph.D. dissertation. Department of Physics, Michigan Technological University, 2013.

[11] C. Wasshuber, *Computational Single-Electronics (Computational Microelectronics),* Edited by: S. Siegfried, Springer Science & Business Media, 2011, p. 278.

[12] P. Hapala, K. Kůsová., I. Pelant, and P. Jelínek, "Theoretical analysis of electronic band structure of 2- to 3-nm Si nanocrystals," *Physical Review B,* vol. 87, no. 19, 2013.

[13] M. Grundmann, "Band structure," in *The Physics of Semiconductors,* Springer, 2010.

[14] V. Ariel-Altschul, E. Finkman, and G. Bahir, "Approximations for carrier density in nonparabolic semiconductors. IEEE Transactions on Electron Devices," *IEEE*, vol. 39, no. 6, pp. 1312-1316, 1992.

[15] L. I. Glazman and V. Chandrasekhar, "Coulomb blockade oscillations in a double-dot system," *Europhysics Letters,* vol. 19, no. 7, 1992.

[16] P. K. Hazaveh, P. L. Bergstrom, and J. A. Jaszczak, "Modeling of gate effects on electron transport in a single-electron transistor with two semiconducting islands between

two semiconducting electrodes," *Proceedings of the IEEE 13th Nano Materials and Devices Conference (IEEE NMDC 2018),* pp. 459 – 462, 2018.

[17] P. K. Hazaveh, P. L. Bergstrom, J. A. Jaszczak, "Modeling of gate effects on electron transport in a single-electron transistor with two semiconducting islands between two semiconducting electrodes," (to be submitted).

6 Conclusion

This work is dedicated to understanding the behavior of electron transport between semiconducting quantum dots, and has led to development of an algorithm to predict the current-voltage behavior of semiconducting single electron transistors under DC biases using accurate, computationally efficient and physically reasonable approximations. A truly three-electrode SET device (source, drain and gate) has been studied, which is suitable for transistor-based applications [1]. The models that have been explored in this work are topologically one-dimensional SET devices that consist of one or two semiconducting islands and three metallic/semiconducting electrodes. The major concentration of this research is exploring the effect of different energy scales involved in the system such as temperature, charging energies, bang gap and input biases on the current-voltage characteristics of the devices.

Single-island SET devices have more well-defined and predictable characteristics compared to multi-island devices, such as a well-defined threshold voltage and Coulomb-oscillation period [2-4]. Therefore, we began this study by exploring the underlying physics of electron tunneling between a device comprised of single semiconducting island and metallic electrodes, which is compared to the behavior of comparable device with a metallic island. Understanding the impact of the band gap and non-trivial band structure is possible in this simple model. The IV_{sd} (drain current versus source-drain voltage characteristics) and IV_g (drain current versus gate voltage characteristics) are demonstrated. This simulation tool reveals the relationships between different complex and coupled energy scales of a semiconducting SET device. After understanding the underlying physics and impact of different energy scales on the behavior of a single-island SET, we moved

forward to simulating the *IV* characteristics of double-island SET devices which have shown interesting behavior in past experimental studies [5].

Exploring semiconducting SET devices shows some similar characteristic to metallic devices and useful features that are unique to semiconductors [6]. Similar to metallic SET devices, the conductance of the semiconducting device is higher for narrower junctions. The small (nm range) islands result in large charging energies under appropriate rate of input voltages, compared to other energy scales and lead to observation of the Coulomb oscillations [3, 6]. It is shown in this study in lower temperatures the band gap as well as charging energies is the deciding factor on the magnitude of the threshold voltage. In the off state (below the threshold voltage), there is no convenient path for electrons to tunnel. Increasing the temperature in this state to the point that an electron's thermal energy (k_BT) is comparable to the energy gap causes thermally excited electrons to participate in tunneling, and conductance is observed. In the on state (above the threshold voltage), thermally excited electrons are not the dominant contributor to the device conductance, so the temperature sensitivity of the device decreases. The ability to control the degree of the temperature sensitivity is one of the unique characteristic of a SET with semiconducting materials.

Features such as the period and peak placement in the Coulomb oscillations can be predicted from the energy state equations in a single island SET device [7]. In a SET device with two (or more) islands, the energy balance for the islands is more complicated, and multiple factors are intertwined [8]. Therefore, predicting the resulting characteristic features in the SET current-voltage characteristics is not possible except when applying approximations in extreme cases (for example, gate capacitances that are much larger than

junction capacitances). In general cases, the developed simulation tool remains the only current method to predict these characteristics.

6.1 The Innovative Continuation

1. A primary development of this work is the further expansion of the MITS simulation tool by Savaikar et al. [3] to implement numerical integration of the tunneling rate equation, which allows the capability of the modeling framework to explore the *IV* characteristics of devices fabricated by materials with complex band structures and energy-dependent tunneling probabilities.
2. We have specifically utilized this tool to explore electron transport in semiconducting-semiconducting, semiconducting-metallic and metallic-metallic tunneling junctions. For the sake of computational time efficiency for islands with size of 2.5-5 nm, the semiconducting band structure is approximated by a simple continuous bottom-of-the-band model (i.e. parabolic shape); and for islands smaller than 2.5 nm, the band structure is modeled with discrete energy levels which have zero width and uniform energy spacing [9]. The capability of the developed tool is not limited to these band models and could be extended to incorporate more complex band structures and more sophisticated tunneling probability factors.
3. Using appropriate approximations [10,11] for the density of states model and incorporating the band gap in simulation improves the applicability of this algorithm, compared to existing simulation tools, for predicting electron transport in semiconducting devices. This enables the exploration of the behavior for a variety of

semiconducting single electron devices as a function of temperature and input bias conditions.

4. In calculating the transition probability, the energy-dependent barrier heights are calculated dynamically, dependent on the potential across the tunneling junction and the initial energy of the electron participating in a tunneling event [3]. For the sake of computational time efficiency for calculating the transition probability related to conduction/valence band, the initial energy of the electrons is considered to be at the edge of the conduction or valence band. This approximation is based on assuming all the electrons participating in tunneling are energetically close to the edge of the bands compare to the electrons' affinity in studied materials. At higher temperature and larger bias voltages where the electrons' energy levels are significantly large compared to the band edge and electron affinity, our numerical calculation is capable of calculating energy-dependent transition probability as required.
5. In our simulation framework, the tunneling rate is not simplified as a closed from solution related to a specific band structure; therefore, the *IV* characteristic of tunneling-based devices with junctions that have different properties such as a SET device which has both semiconductor-semiconductor and semiconductor-metallic junctions is possible.
6. The impact of the band gap and discrete energy levels of semiconducting island in a SET device is investigated and our results show that the energy gap and discrete energy levels present in a semiconducting island can be utilized to control the degree of temperature sensitivity of single-electron transistors. For example, using specific terminal biases, a probable energy path for electrons is available even at lower

temperatures so that increasing the temperature does not significantly impact the magnitude of the current; therefore, the temperature sensitivity of the SET may be reduced. On the other hand, if the applied potentials do not allow a probable tunneling path to exist at lower temperature, then a high temperature sensitivity is observed. The existence of a band gap in the band structure of semiconducting island gives them a unique advantage over metallic SET devices. An exclusive characteristic of a SET with semiconducting islands is the bias dependent temperature sensitivity of the device.

7. In a SET with a semiconducting island larger than 3 nm, under smaller biases, Coulomb blockade steps can be observed in current-voltage characteristics. As the temperature increases, the threshold voltage decreases and steps become indiscernible. We have demonstrated that using a theoretical SET model with a smaller semiconducting island which has few energy levels available for tunneling, can preserve the Coulomb blockade steps from washing out entirely at higher temperatures.
8. In a SET with a single island, the gate capacitance dictates the period of Coulomb blockade peaks in current versus gate-voltage characteristics [4]. In double-island SETs, the period between peaks depends on all capacitances that couple electrodes and islands and energy state of the system which results in often observing non-uniformed peaks and peak placements. The capability to simulate electron transport in a multi-island SET device is an important and necessary tool to predict the non-uniform peaks observed in experimental research, which enables a predictive method to explore and understand experimental device behavior.

6.2 Future Work

The algorithm developed in this study has opened numerous possibilities for future work. However, to increase the capability of the simulation tool, further work is needed. Some particular aspects of this tool which need improvement and potential applications of the introduced simulation tool is listed below:

1. Code Optimization and Documentation

Using numerical calculation to solve the tunneling rate integral dramatically increases the computational time of the new simulation tool compared to algorithms where the tunneling rate integral can be approximated in a closed form solution. Careful optimization of the simulation code should be done by taking advantage of best practices and utilization of optimized numerical integration methods. The simulation code also needs to be carefully documented with comments and references in order to be usable by future investigators in our group. This will make possible the simulation of devices with more islands or with more complex band structures and more accurate accounting of tunneling probabilities.

2. Predicting *IV* characteristics of double-islands single-electron transistors with discrete energy levels

The presented simulation tool can predict the *IV* characteristics of a SET with two semiconducting islands, where at least one of the islands has dimensions greater than ~3 nm and the energy levels therefore can be modeled with a continuous band model for the density of states. As the size of semiconducting islands decreases to reach dimensions smaller than ~3 nm, the spacing between discrete energy levels of the islands increases to the point that they are comparable to the island's charging energy, junction potential energy differences, and possibly the thermal energy. In this case, the discreteness of the energy

levels in the density of states cannot be ignored. Since for electron tunneling to happen, proper biases and charging energies are necessary to allow the alignment of discrete energy levels on both sides of the junction, predicting the capacitances and bias voltages that facilitates electron tunneling between islands with discrete levels with no severe approximations has not yet been developed. Finite-lifetime broadening of the discrete energy levels can be incorporated into the simulation code, however this has not yet been implemented. A modified or alternative simulation tool is required to predict electron tunneling in devices with these types of junctions.

3. Predicting the *IV* characteristic of SET devices with more than 2 islands:

The number of semiconducting islands in our simulations have so far been limited to only one or two islands on a one-dimensional array (single path between source and drain electrodes) primarily due to the computational costs of running the current simulation tool. One of the limitations of fabricating a SET is controlling the position and number of islands between electrodes. To analyze the behavior of experimentally fabricated SET devices and to predict electron transport in SET devices with more than two islands, even along a single path, an improved simulation tool is needed.

4. **Predicting the *IV* characteristic of a two-dimensional semiconducting SET devices**:

Following point 3, predicting the *IV* characteristics in a device comprised of coupled islands in a two-dimensional array- one in which there can be multiple tunneling paths between the source and drain, will require an improved or alternative algorithm. The capacitances between all of the coupled islands and electrodes can be calculated based on an assumed geometry following methods such as that of Banyai [12].

5. Controlling the temperature sensitivity of a semiconducting SET device:

One of the greatest opportunities based on this research is the thermal filtering of electron tunneling by exploring the geometry and energy scales which can facilities the occurrence of the Coulomb blockade at room temperature. The only few discrete energy levels of the island available in desired energy range for electron tunneling can be a practical way to block electrons in higher energy levels to participate in electron tunneling. We have demonstrated that using ultra small semiconducting islands with few energy levels participating in tunneling, can preserve the Coulomb blockade steps from becoming indiscernible. A condition in which the Coulomb blockade steps in current-voltage characteristic of a SET at room temperature is fully maintained, has not yet been achieved. Another example following work of Bhadrachalam et al. [13], is utilizing a quantum size semiconducting material with few available energy levels to filter the thermally excited electrons. The few energy levels available, only allow electrons with lower energy to tunnel to the island [13].

6. Predicting electron transport across junctions with complicated properties

Numerically calculating the tunneling rates in this algorithm makes the simulation tool valuable for researchers to predict electron tunneling between materials with complex band structures and across junctions with complicated properties such as energy dependent barrier heights and different materials across junctions. Asymmetric junctions and different density of states model across a junction lead to more complex tunneling rate integral. Using accurate approximations to solve the integral for a closed form solution is less likely in these cases. Numerically calculating the rates is necessary in such models to account for properties of the junctions accurately.

7. Simulation of photon-SET interaction-based devices:

Photon assisted tunneling in single electron transistors can be predicted by modifying the developed algorithm. One example is “Photon-Pumped Current in an Asymmetric Si SET”, done by Fujiwara et al. [14]. In this experimental work it is observed that photoexcitation generates new high peaks in current-voltage characteristics; and electron-hole recombination generates current drops [14]. Single photon detecting sensors [15] and photon-activated switches in the single-electron transistor [16] are other examples of existing experimental researches that may benefit from the developed simulation tool.

6.3 Reference List

[1] M. Acharya, *Development of Room Temperature Operating Single Electron Transistor Using FIB Etching and Deposition Technology,* Ph.D. Dissertation, Electrical Engineering Department, Michigan Technological University, 2009.

[2] C. Wasshuber, H. Kosina, and S. Selberherr, “SIMON-A simulator for single-electron tunnel devices and circuits,” *IEEE Transactions on Computer-Aided Design of Integrated Circuits and Systems*, vol. 16, no. 9, pp. 937–944, 1997.

[3] M. A. Savaikar, D. Banyai, P. L. Bergstrom and J. A. Jaszczak, “Simulation of charge transport in multi-island tunneling devices: Application to disordered one-dimensional systems at low and high biases,” *Journal of Applied Physics*, vol. 114, no. 11, p. 114504, 2013.

[4] K. K. Likharev, "Single-electron devices and their applications," *Proceedings of the IEEE*, vol. 87, no. 4, pp. 606 – 632, 1999.

[5] H. Ishikuro and T. Hiramoto, "Quantum mechanical effects in the silicon quantum dot in a single-electron transistor," *Applied Physics Letters*, vol. *71*, no. 25, pp. 3691 – 3693, 1997.

[6] P. Hazaveh, P. L. Bergstrom, and J. A. Jaszczak. "Efficient physics-based modeling of a representative semiconducting quantum dot single electron device," *IEEE 17th International Conference on Nanotechnology (IEEE-NANO)*, pp. 739 – 744, 2017.

[7] A. A. M. Staring, *Coulomb-blockade oscillations in quantum dots and wires,* Eindhoven: Technische Universiteit Eindhoven, DOI: 10.6100/IR384910, 1992.

[8] L. I. Glazman and V. Chandrasekhar "Coulomb blockade oscillations in a double-dot system" *Europhysics Letters,* vol. 19, no. 7, 1992.

[9] P. Hapala, K. Kůsová, I. Pelant and P. Jelínek, "Theoretical analysis of electronic band structure of 2- to 3-nm Si nanocrystals," *Physical Review B*, vol. 87, no. 19, p. 195420, 2013.

[10] M. Grundmann, *The Physics of Semiconductors: An Introduction including Nanophysics and Applications*, 2nd Ed., New York, NY, Springer, DOI: 10.1007/978-3-642-13884-3, 2010V.

[11] V. Ariel-Altschul, E. Finkman, and G. Bahir, "Approximations for carrier density in nonparabolic semiconductors. IEEE Transactions on Electron Devices," *IEEE*, vol. 39, no. 6, pp. 1312-1316, 1992.

[12] D. R. Banyai, *Multiscale Examination and Modeling of Electron Transport in Nanoscale Materials and Devices*, Ph.D. Dissertation, Physics Department, Michigan Technological University, 2014.

[13] P. Bhadrachalam, R. Subramanian, V. Ray, L. Ma. W. Wang, J. Kim, K. Cho and S. J. Koh, "Energy-filtered cold electron transport at room temperature," *Nature Communication,* vol. 5, no. 4745, 2014.

[14] A. Fujiwara, Y. Takahashi, and K. Murase, "Observation of single electron-hole recombination and photon-pumped current in an asymmetric Si single-electron transistor," *Physical Review Letters*, vol. 78, no.8, p. 1532-1535, 1997.

[15] M. H. Devoret, and R.J. Schoelkopf, "Amplifying quantum signals with the single-electron transistor," *Nature*, vol. 406, p. 1039, 2000.

[16] J. M. Hergenrother, "Photon-activated switch behavior in the single-electron transistor with a superconducting island," *Physical Review B*, vol. 51, no. 14, p. 9407-9410, 1995.

A Copyright Documentation

The IEEE does not require individuals working on a thesis or dissertation to obtain a formal reuse license, subject to acknowledging the use copyrighted material.

http://www.ieee.org/publications_standards/publications/rights/rights_link.html

The following IEEE copyright/credit notices have been placed prominently in the chapters, references and figure captions, as appropriate:

© 2017 IEEE. Reprinted, with permission, from P. K. Hazaveh, P. L. Bergstrom and J. A. Jaszczak, "Efficient physics-based modeling of a representative semiconducting quantum dot single electron device," *IEEE 17th International Conference on Nanotechnology (IEEE-NANO)*, pp. 739 – 744, 2017.

©2018 IEEE. Reprinted with permission, from P. K. Hazaveh, P. L. Bergstrom, and J. A. Jaszczak, "Modeling of gate effects on electron transport in a single-electron transistor with two semiconducting islands between two semiconducting electrodes," *Proceedings of the IEEE 13th Nano Materials and Devices Conference (IEEE NMDC 2018),* pp. 459 – 462, 2018.